Investigating the Interactions of Fatty Acids, Amyloid Beta & SARS-CoV-2 Spike Protein Fragment

by

Lilian Toma

A thesis

presented to the University of Waterloo

in fulfillment of the

thesis requirement for the degree of

Master of Science

in

Pharmacy

Waterloo, Ontario, Canada, 2023

Author's Declaration

I hereby declare that I am the sole author of this thesis. This is a true copy of the thesis, including any required final revisions, as accepted by my examiners.

I understand that my thesis may be made electronically available to the public.

Abstract

There is no cure for Alzheimer's disease (AD), and the negative implications of having AD were further exacerbated in recent years, as patients with dementia are at the highest risk for mortality upon contracting COVID-19. The amyloid cascade theory postulates that AD is caused by toxic aggregates of amyloid beta (Aβ) peptide. The main objective of this project was to design, synthesize and evaluate a library of fatty acid derivatives based on docosahexaenoic acid (DHA), oleic acid (OA), eicosapentaenoic acid (EPA), linoleic acid (LNA), and α-linolenic acid (ALA) as inhibitors of Aβ42 aggregation. 10 fatty acid derivatives were synthesized, characterized, and evaluated for Aβ42 aggregation inhibition activity using thioflavin T-based Aβ42 aggregation kinetics assays. The methyl ester derivatives were found to be the most promising inhibitors, with the LNA derivative methyl (9*Z*,12*Z*)-octadeca-9,12-dienoate (**2a**) being the most potent (61% inhibition at 25 μM). Transmission electron microscopy (TEM) experiments confirmed the anti-aggregation activity of **2a,** and computational modeling studies suggest that the evaluated fatty acid derivatives bind in a narrow channel at the interface of the N- and C-termini in the Aβ42 pentamer model. Furthermore, the fatty acid derivatives were not toxic to HT22 mouse hippocampal cells (cell viability ~94–104% at 25 μM). Our secondary objective was to evaluate amyloidogenic peptide fragment FKNIDGYFKI derived from the SARS-CoV-2 spike protein for its ability to promote Aβ42 aggregation. Interestingly, the decapeptide was found to inhibit Aβ42 aggregation at all tested concentrations (~37–52%). In summary, thesis outcomes demonstrate that fatty acid derivatives and spike peptide fragment exhibit anti-Aβ42 activity by direct binding and have the potential to be used as novel pharmacological tools to study Aβ aggregation and to design novel therapies to treat AD.

Acknowledgements

I would like to thank the University of Waterloo School of Pharmacy and Faculty of Science, Canadian Institutes of Health Research, and the Government of Ontario for financial support of this project.

Thank you to my supervisor, Dr. Praveen Nekkar Rao, for sharing your kindness, support, empathy and passion for research. You are an inspiration to all your students, and we appreciate the care and guidance you share with each one of us.

I would like to extend my thanks to my committee advisors Dr. Jonathan Blay, Dr. Jeff Nagge, and Dr. Shawn Wettig for your support and direction over the course of this project. Additionally, I would like to express my gratitude to my lab members for their encouragement, guidance, and company. I am so grateful to have met and worked with all of you.

Table of Contents

List of Figures

List of Schemes

List of Tables

List of Abbreviations

Ach = Acetylcholine

Acute respiratory distress syndrome = ARDS

AD = Alzheimer's disease

Aβ = Amyloid beta

AICD = APP intracellular domain

ALA = α-Linolenic acid

ACE2 = Angiotensin converting enzyme 2

APP = Amyloid precursor protein

β-site APP cleaving enzyme 1 = BACE-1

BBB = Blood-brain barrier

C83 = 83-amino acid C-terminal APP fragment

C99 = 99-amino acid C-terminal APP fragment

CCK-8 = Cell counting kit 8

CNS = Central nervous system

COVID-19 = Coronavirus disease 2019

Cryo-EM = Cryogenic electron microscopy

CSF = Cerebrospinal

DHA = Docosahexaenoic acid

DMEM = Dulbecco's modified eagle media

DS = Discovery Studio

EPA = Eicosapentaenoic acid

Envelope protein = E protein

F12 = Ham’s F12

FBS = Fetal bovine serum

HFIP = Hexafluoro-2-propanol

HSV-1 = Herpes simplex virus type 1

LC-MS = Liquid chromatography mass spectrometry

LNA = Linoleic acid

LRMS = low-resolution mass spectrometry

LRP1 = Low-density lipoprotein 1

MRI = Magnetic resonance imaging

M^{pro} = Main protease

mRNA = Messenger ribonucleic acid

NFT = Neurofibrillary tangle

NMDA = N-methyl-D-aspartate

NMR = Nuclear magnetic resonance

Nucleocapsid protein = N protein

PTA = Phosphotungstic acid

PUFA = polyunsaturated fatty acid

RAGE = Receptor for advanced glycation end products\

RBD = Receptor binding domain

RBM = Receptor binding motif

RFU = Relative fluorescence intensity

RNA = Ribonucleic acid

s-APPα = Soluble amyloid protein precursor α

SAR = Structure-activity relationship

SARS = Severe acute respiratory syndrome

SARS-CoV = Severe acute respiratory syndrome coronavirus

SARS-CoV-2 = Severe acute respiratory syndrome coronavirus 2

S protein = Spike protein

TEM = Transmission electron microscopy

ThT = Thioflavin T

TLC = Thin-layer chromatography

TMPRSS2 = Transmembrane serine protease 2

UPW = Ultra-pure water

UV = Ultra-violet

Chapter 1: Introduction

1.1 Background on Alzheimer's Disease

Dementia is a general term used to describe a group of symptoms related to a decline in cognitive function such as impaired memory, thinking and problem-solving.[1] There are over 50 million cases of dementia worldwide, with this number predicted to increase to 75.6 million by 2030.[2,3] This predicted large increase in cases has been mainly attributed to the growing aging population, as age is the most important risk factor for dementia.[4] After the age of 65, the risk for developing dementia doubles every five years.[5] Alzheimer's disease (AD) is the most common type of dementia, making up about 60% of cases.[2] As of 2020, AD was the ninth leading cause of death in Canada and over 500,000 Canadians were diagnosed with dementia.[6] This number is predicted to increase to 1.7 million by 2050.[7] The rapidly growing number of cases, lack of treatments and the significant impact dementia has had on health, the economy, and families, have made it one of today's largest health care challenges.

The impaired cognitive function associated with dementia can be caused by a variety of factors which are investigated during the diagnosis process. Diagnosing dementia involves evaluating a patient's medical history, cognitive ability, and impairment during daily activities.[8] Clinicians look for changes in language, memory, attention, special orientation and mood over time. Additionally, physical exams, laboratory tests, and imaging can help clinicians determine which type of dementia could be present.[8] For example, magnetic resonance imaging (MRI) scans can be used to generate images of the brain and identify blood vessel abnormalities that lead to the cognitive impairment in vascular dementia.[9] Vascular dementia is the second most common type of dementia and occurs when the blood supply to the brain is damaged, causing brain cells to die.[10] AD is characterized by the presence of amyloid plaques and neurofibrillary tangles (NFTs) in the

brain, and it is generally diagnosed when other possible health conditions such as vascular dementia, frontotemporal dementia, and Lewy body dementia have been ruled out.[11] AD diagnosis can only be confirmed during an autopsy by checking for the presence of amyloid plaques, neurofibrillary tangles, and atrophy of the cerebrum.[11] However, neurological imaging and tests for biomarkers of AD in the blood and cerebrospinal (CSF) fluid can provide a strong indication if AD is present.[12] In recent years, blood tests have become more accurate and can test for AD biomarkers like the toxic form of the protein, amyloid beta (Aβ), that leads to formation of the plaques.[13] These tests are minimally invasive and could help with early diagnosis of AD before symptoms have emerged.[13]

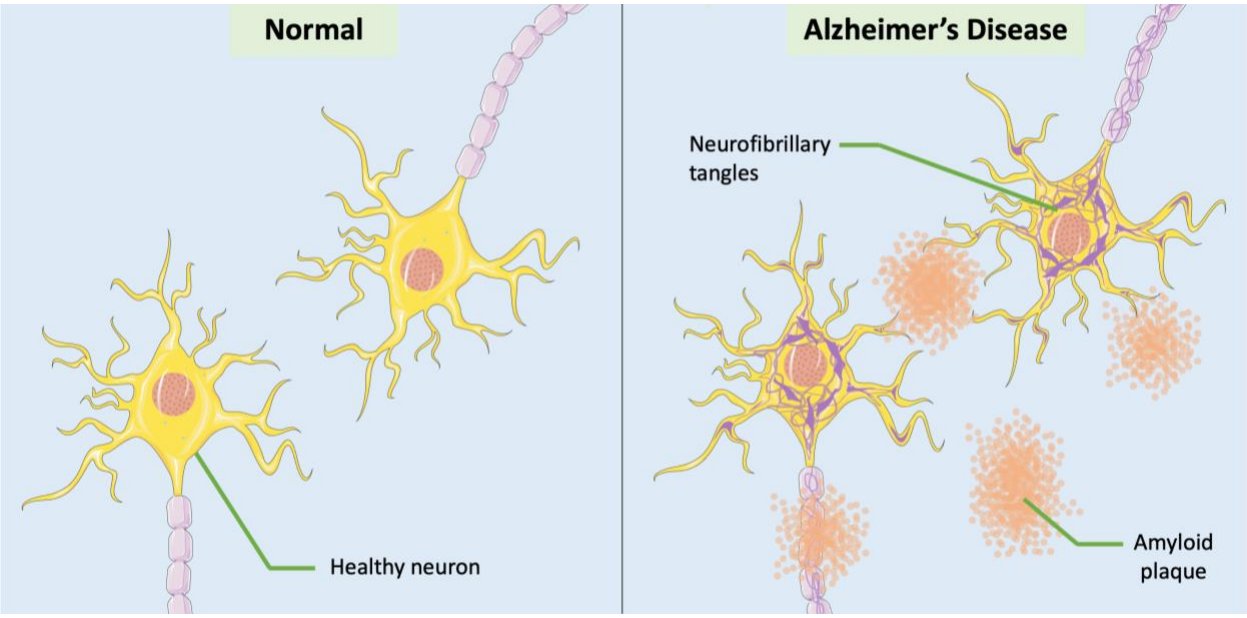

Figure 1.1: Illustration displaying the differences between healthy neurons of the CNS and neurons of AD. Hallmarks of AD include intracellular neurofibrillary tangles and extracellular amyloid plaques.

Hallmarks of AD include extracellular amyloid plaques, intracellular NFTs, and shrinkage of the cerebral cortex (Figure 1.1).[11,14] The extracellular senile plaques seen in patients with AD are

formed by an accumulation of Aβ protein. The neurofibrillary tangles found inside neurons are composed of a form of tau protein that has been hyperphosphorylated abnormally.[14,15] Both Aβ and tau contribute to the deterioration of neurons that leads to the synaptic loss, abnormal levels of neurotransmitters, and inflammatory signalling that are observed in patients with AD and associated with cognitive decline.[14,16] The exact disease process is unknown, however there are several theories giving possible explanations for AD pathogenesis.

The cholinergic hypothesis is one of the oldest and well-studied theories and the basis of most available AD therapies.[17] The cholinergic pathway serves an important role in cognitive functions such as memory and attention, and this pathway has been shown to be impaired or abnormal in patients with AD.[18,19] This theory postulates that the cognitive decline observed in patients with AD is due to damage to this pathway in the central nervous system (CNS).[19,20] Acetylcholine (ACh) is the neurotransmitter in this pathway and lower levels of ACh release and the enzyme that produces it, choline acetyltransferase, are generally observed in the brains of AD patients.[18,19] This hypothesis led to the development of cholinesterase inhibitor medications for treatment of AD.[21] Cholinesterases are enzymes that break down ACh and inhibiting them permits increased ACh levels.[21,22] Three of the four drugs approved in Canada for treatment of AD are cholinesterase inhibitors that can be taken orally (donepezil, galantamine, and rivastigmine).[23] They have been shown to provide some symptomatic relief; however, they do not inhibit the disease process and lose efficacy in later stages of dementia.[17,21]

The fourth and final approved medication in Canada for treatment of AD is memantine, an N-methyl-D-aspartate (NMDA) receptor antagonist.[23] Contrary to ACh, the neurotransmitter glutamate is found at generally higher levels in the brains of patients with AD which can cause impaired cognitive function.[24] Memantine works by preventing activity of the neurotransmitter

glutamate by blocking its binding to the NMDA receptor.[25,26] Like the cholinesterase inhibitors, memantine is taken orally and can provide symptomatic relief and stabilization to AD patients, however it does not stop disease progression.[26]

Aducanumab and lecanemab are monoclonal antibody treatments that recently received accelerated approvals in the United States for mild AD that have the potential to change disease progression.[27] They both target Aβ aggregates to reduce plaques in the brains of AD patients. Lacanemab binds most strongly to a form of Aβ peptide aggregates called protofibrils, and aducanumab targets Aβ plaques and high molecular weight oligomers.[27] Lacanemab has been shown to slow cognitive decline by 27% over 18 months, however aducaneumab has had inconsistent results.[28-31] For both drugs, adverse effects like brain bleeding or swelling are common (>10% each), and further trials are underway to determine whether the drugs have long-term benefits on patient outcomes.[28,30,31]

Discovering a disease-modifying medication that can slow down or halt the progression of AD has been challenging since the disease process is complex and not fully understood. However, with the growing prevalence of AD and the immense impact it has on patients, families, and the health care system, improved treatment options are needed more than ever.[3]

1.2 The Amyloid Cascade Hypothesis

The disease process for AD is complex, and there have been several hypotheses for the etiology of AD presented.[32] However, AD research still lacks a theory that explains the full disease development and all the pathologies observed in patients.[33] The amyloid cascade hypothesis is the primary theory for AD and the basis for development of many novel AD therapeutics, although it does have its limitations.[34-36] This theory was developed in 1998 and suggested that deposition of

Aβ peptide into amyloid plaques is the causative agent for the central nervous system (CNS) damage and cognitive decline observed with AD.[37] Although the amyloid cascade hypothesis has not been able to explain all aspects of the disease process, it is the primary model for AD pathogenesis and hypothesized to be fundamental in AD development.[36,38]

1.2.1 Production and Clearance of Aβ Peptide

The amyloid plaques found surrounding neurons in the brains of patients with AD are mainly composed of Aβ peptide.[39] This 4 kDa Aβ peptide is found throughout the body and derived from cleavage of a protein called amyloid precursor protein (APP). APP is a large integral membrane that is present in tissues all over the body, with a high concentration in the synapses of neurons in the brain.[39] The primary function of APP is unknown; however, it has been shown to be involved in various roles such as synaptic plasticity, brain development, and memory.[16,40,41] APP is cleaved by secretase enzymes to produce soluble Aβ peptide monomers that aggregate and contribute to the pathogenesis of AD.[42] Two pathways for APP cleavage are the amyloidogenic and non-amyloidogenic pathways (Figure 1.2).[43] In the amyloidogenic pathway, APP is initially cleaved by β-secretase, and in the non-amyloidogenic pathway, APP is initially cleaved by α-secretase. The amyloidogenic pathway produces the Aβ peptide that can aggregate to form neurotoxic complexes.[43]

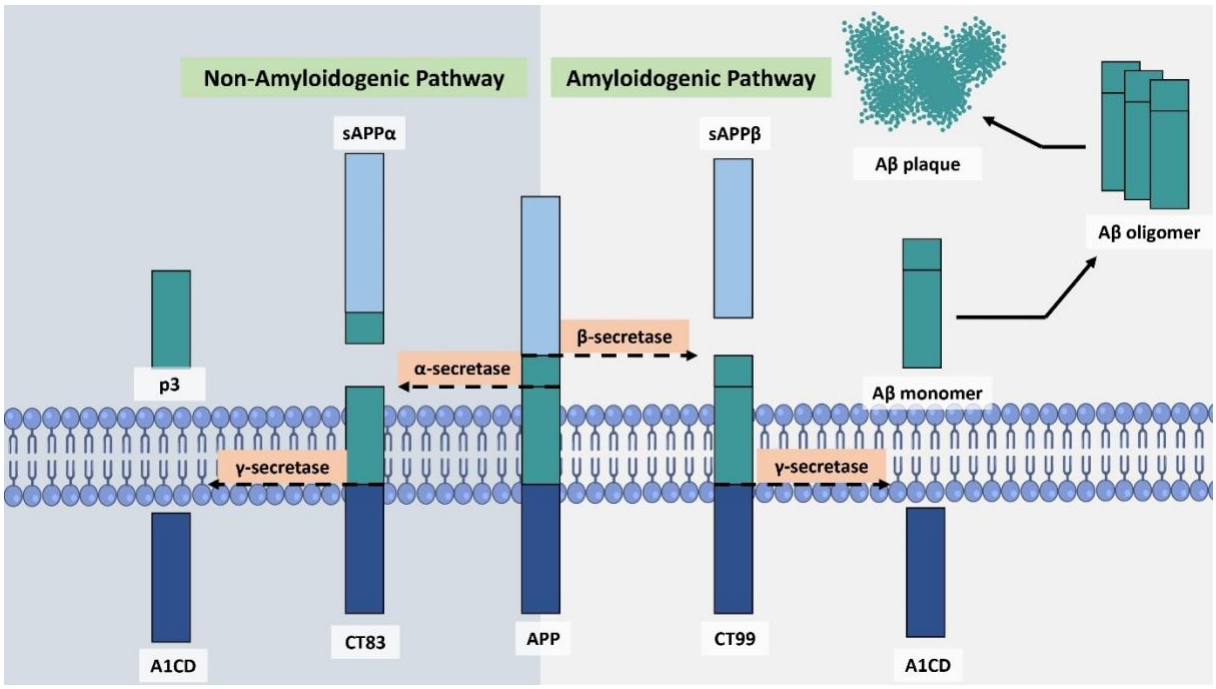

Figure 1.2: Illustration displaying two pathways for APP processing: the non-amyloidogenic and the amyloidogenic pathways. The amyloidogenic pathway produces Aβ peptide which can aggregate to form toxic oligomers which aggregate further to form amyloid plaques.

In the amyloidogenic pathway, APP is cleaved by β-secretase. This produces soluble amyloid protein precursor β (s-APPβ) and a 99-amino acid C-terminal APP fragment (C99).[36,44] Next, C99 is cleaved by γ-secretase to release the Aβ peptide and the APP intracellular domain (AICD) which is theorized to translocate to regulate gene expression in the nucleus.[44] The Aβ peptide monomers can then aggregate together to form higher order structures and form the extracellular plaques observed in the brains of AD patients. On the contrary, the non-amyloidogenic pathway involves the initial cleavage of APP by α-secretase instead of β-secretase to produce soluble amyloid protein precursor α (s-APPα) and an 83-amino acid C-terminal fragment (C83). Then, C83 is cleaved by γ-secretase, to produce the p3 peptide and AICD.[44]

Mutations in APP are associated with early-onset familial AD and have been shown to cause increased levels of Aβ peptide, and an altered ratio of Aβ peptide isoforms.[45] Additionally, a disproportionate number of patients with Down syndrome develop early onset AD, which is hypothesized to be due to the overexpression of the gene coding for APP which is found on chromosome 21[45,46] This information served as strong evidence in support of the amyloidogenic hypothesis when it was initially developed.[37]

Enzymes of the amyloidogenic pathway can be targeted to reduce the production of Aβ peptide, and subsequently reduce formation of aggregates. β-secretase, specifically β-site APP cleaving enzyme 1 (BACE-1), is a promising drug target for AD treatment, as its inhibition could slow down production of Aβ peptide. However, development of BACE-1 inhibitors that can cross the blood-brain barrier (BBB) and are also well tolerated has not been possible thus far.[47]

Additionally, modulating the entry and clearance of Aβ into the brain has been another approach for AD drug development. Levels of Aβ are heavily influenced by the activity of low-density lipoprotein 1 (LRP1) and receptor for advanced glycation end products (RAGE).[48] LRP1 is a lipoprotein that binds to APP and Aβ peptide to transport them out of the brain through the BBB.[49] RAGE is a membrane protein that facilitates transportation of Aβ through the BBB and into the brain.[48] Both LRP1 and RAGE are potential drug targets for treatment of AD, as modulating their activity could lower levels of Aβ peptide in the brain and thus lower the potential for amyloid aggregation.[48,50,51]

1.2.2 Aβ Peptide Structure and Aggregation

Amyloids are protein aggregates that have a distinctive fibrillar morphology and beta sheet structure.[52] Aβ peptide is one of many proteins that can form amyloids. These aggregates can be found in various locations in the body and are associated with many different human diseases such

as Parkinson's disease and Huntington's disease.[53] Monomers are the singular peptides, and when concentrations of the peptide increase, they can self-assemble to form various conformations.[39,52] These conformations include dimers, oligomers, protofibrils and mature fibrils.[39] Oligomers are formed by monomers of an amyloidogenic peptide that undergo a conformational change and form a multi-peptide complex containing β-sheet structures.[52,54] These sheets contain strands of the peptide aligned in a parallel or antiparallel manner with hydrogen bonds forming between adjacent strands and stabilizing them. Once the oligomers have formed, more peptides are added to form protofibrils and finally mature fibrils.[39] Amyloid fibrils are long filaments with high β-sheet content.[52] The oligomers are soluble, however the protofibrils and mature fibrils are not.[39] The amyloid plaques found in the brains of AD patients are mainly composed of the insoluble mature fibrils of Aβ peptide.[55]

Monomers of Aβ peptide in their native state are non-toxic. Suggested physiological roles for the peptide include preventing excessive activation of synapses and protection against infection.[56,57] During the misfolding and aggregation process, the peptide transitions from an α-helical and/or unordered structure to higher order structures rich in β-sheets.[58] Most information about Aβ peptide structure has come from nuclear magnetic resonance (NMR) spectroscopy and molecular dynamics studies, as the peptide cannot be crystallized using common methods.[39] Recently cryogenic electron microscopy (cryo-EM) and solid-state NMR studies have provided the structures of fibrils.[59-61] Aβ peptide contains hydrophobic regions and metal-binding domains that are involved in aggregation into higher-order structures.[62] The Aβ peptide can vary in length and is found mainly in the 40-amino acid Aβ40 form, and less frequently, the 42-amino acid Aβ42 form (Figure 1.3).[63] The Aβ42 form tends to aggregate at a higher rate, giving it a greater

propensity to form amyloids. This is due to the C-terminus of Aβ42 being more structured and less flexible, making it less soluble and more prone to aggregation.[39,63]

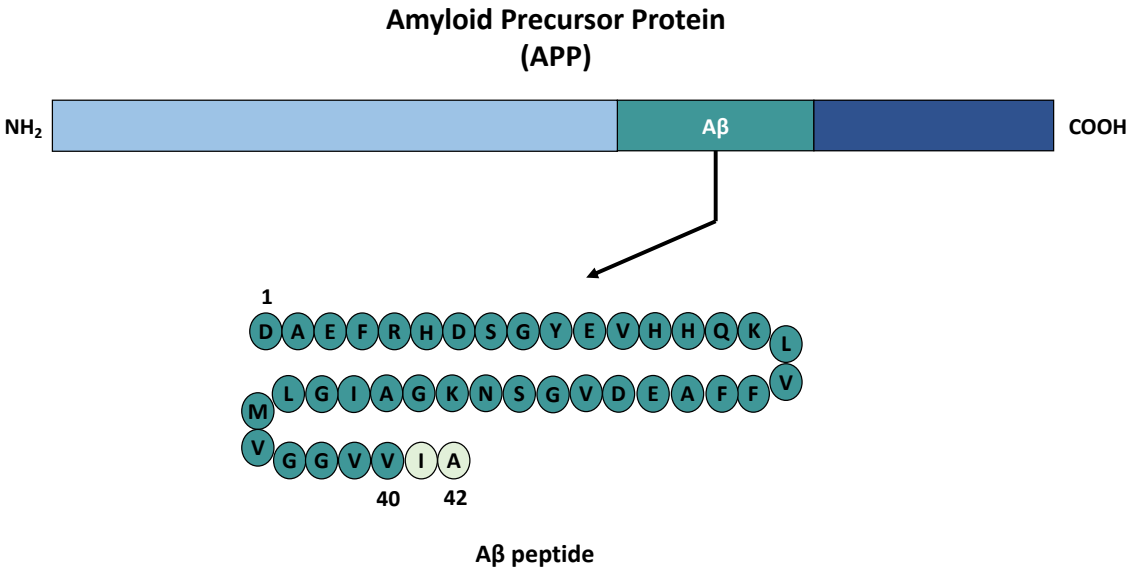

Figure 1.3: APP cleavage by α-secretase followed by γ-secretase produces Aβ peptide. Aβ peptide is most frequently found in its 40-amino acid, Aβ40, and 42-amino acid, Aβ42, forms.

Aggregation of the Aβ peptide occurs through a nucleated polymerization model.[62,64-66] This model involves three phases that follow sigmoid kinetics: the nucleation phase (lag phase), growth phase (exponential phase), and saturation phase (plateau phase) as shown in Figure 1.4.[62,66,67] In the nucleation phase, proteins undergo a conformational change and come together to form an oligomeric nucleus. Formation of the oligomeric nucleus is a thermodynamically unfavourable process and slow.[66] After this, the elongation of the nuclei begins to occur to form protofibrils during the growth phase and this occurs until they are saturated and form mature fibrils. The oligomeric nuclei act as seeds from which the fibrils grow, and their formation is the limiting factor for formation of the fibrils.[67]

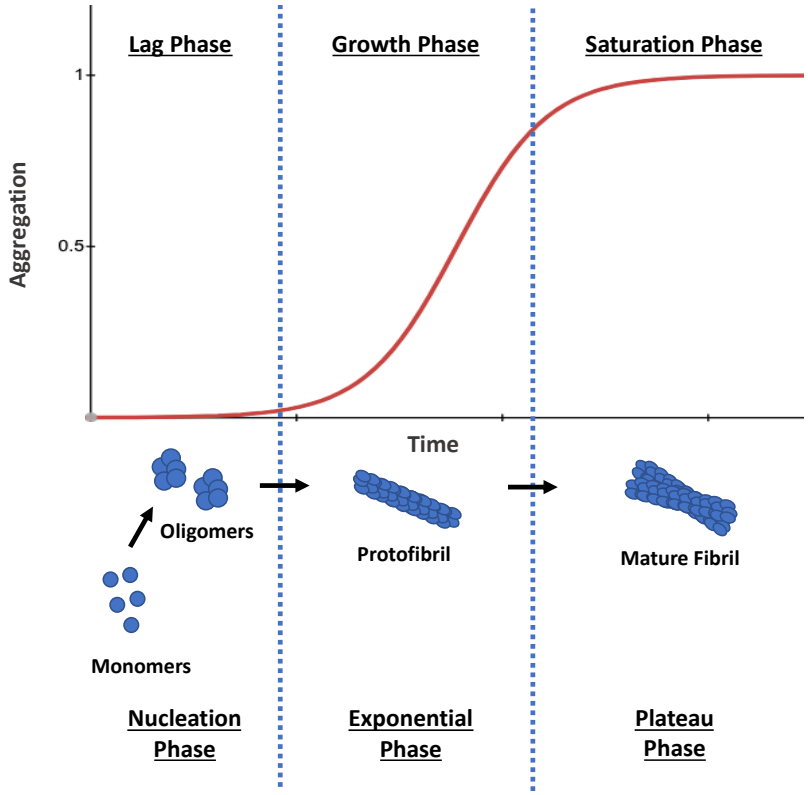

Figure 1.4: The aggregation process of Aβ peptide to form mature fibrils from the monomeric species. This process occurs through a nuclear polymerization model that follows sigmoid kinetics with a lag phase, growth phase, and saturation phase.

1.2.3 Impact of Aβ Aggregation

The oligomeric species of Aβ peptide are believed to be the most neurotoxic conformations of the peptide and the main players in initiating amyloid plaque formation.[67,68] Plaques were originally thought to be the cause of the neuronal cell death and cognitive decline observed with AD; however, this has not been shown to be the case.[34,37] These amyloid plaques are also found in elderly individuals without AD.[34] It is the soluble Aβ aggregates that have been shown to interact with many different receptors in neurons and glial cells to increase inflammation and oxidative stress, disrupt calcium homeostasis, and induce neuronal cell death (Figure 1.5).[69]

Additionally, the amyloid cascade hypothesis postulates that the pathogenic aggregation of Aβ peptide leads to the hyperphosphorylation of tau, a microtubule-associated protein.[70] The microtubule system is part of a cell's cytoskeleton and involved in many functions. When tau is hyperphosphorylated it is no longer able to function properly causing damage to the microtubule system and neuronal structural integrity.[34,70] Furthermore, the abnormally phosphorylated tau forms fibrils within cells which aggregate to form neurofibrillary tangles (NFTs) within neurons. There is evidence that using Aβ peptide immunotherapy can clear hyperphosphorylated tau aggregates and that Aβ40 fibrils can induce formation of NFTs in mice.[71,72] Aβ peptide has been shown to be involved in the hyperphosphorylation of tau by activating kinases involved in the pathway.[73]

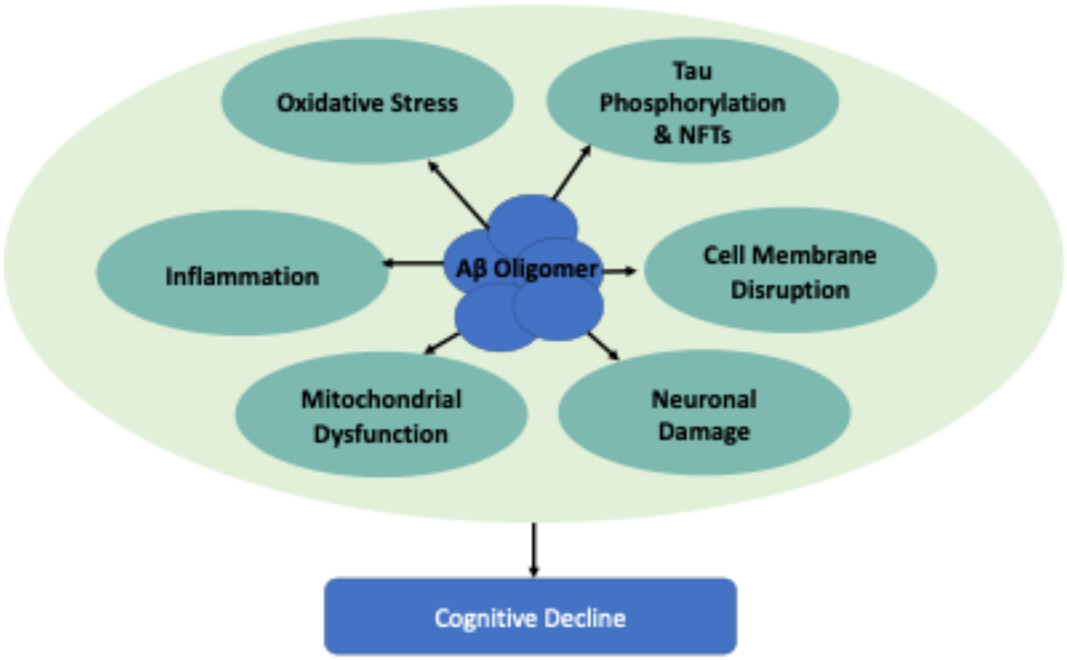

Figure 1.5: Based on the amyloid cascade hypothesis of AD, soluble Aβ oligomers can cause oxidative stress, tau phosphorylation and NFT formation, cell membrane disruption, mitochondrial dysfunction, and inflammation. All these factors contribute to the cognitive decline observed in AD patients.

The damage due to Aβ peptide aggregates causes a decline in the health and function of the neurons, which leads to further disruption in the balance of the amyloidogenic and non-amyloidogenic pathways and increased levels of Aβ peptide. Thus, the aggregation of Aβ peptide is theorized to be a positive-feedback loop, leading to further deterioration of neuronal function as the disease progresses.[36,74]

Inhibition of Aβ peptide aggregation has been a popular approach in AD drug development.[75] Two monoclonal antibody treatments, aducanumab and lecanemab are Aβ aggregation inhibitors recently approved by the United States Food & Drug Administration (FDA) through an accelerated approval program. These drugs have the potential to change disease progression and clinical trials are underway, however, their safety is of concern with a high rate of complications in treatment groups.[27] Additionally, researchers speculate whether treating AD patients who are showing symptoms with Aβ aggregation inhibitors may be ineffective because the disease process starts long before symptoms begin to show. Accumulation of oligomeric Aβ has been found to occur over 20 years before symptoms of AD appear.[76] The results from a clinical trial with lecanemab were promising as the treatment slowed cognitive decline by 27% over 18 months.[29] As the trials are currently being completed, more data on the efficacy and safety of these FDA-approved aggregation inhibitors will be available soon. This will provide valuable information on the viability of Aβ aggregation inhibitors as an approach for AD treatment.

1.3 Background on COVID-19

COVID-19 is an infectious respiratory illness caused by SARS-CoV-2, a coronavirus.[77,78] COVID-19 was first discovered in December 2019 in Wuhan, China, where several cases of pneumonia were reported with an unknown cause.[77] SARS-CoV-2 is the seventh known human-

infecting coronavirus, and a close relative of SARS-CoV, the virus responsible for the 2003 SARS outbreak in China.[78] COVID-19 commonly presents with fever, cough and fatigue. Many patients are asymptomatic; however, some patients develop serious complications such as pneumonia, acute respiratory distress syndrome (ARDS), respiratory failure and organ failure.[79] Increased age and underlying conditions such as diabetes and hypertension cause increased risk for complications with the disease.[80]

COVID-19 has rapidly spread across the world with over 600 million cases and over 6 million deaths reported worldwide at the time of writing.[81] In Canada alone, there have been over 4 million cases and over 40,000 COVID-19-related deaths reported.[82] As a result of the rapidly spreading nature of the disease and its associated complications, many countries instated lockdowns and other measures to manage the spread of COVID-19. The disease and measures to prevent its transmission have led to major social, economic, and health impacts.

1.3.1 Coronaviruses

Coronaviruses are a group of RNA viruses that cause disease in mammals and birds. Their genomes vary between approximately 26,000 and 32,0000 bases, which are the largest genomes of all RNA viruses.[83] Four genera of coronaviruses exist, including alpha- (α-CoV), beta- (β-CoV), gamma- (γ-CoV), and delta- (δ-CoV) coronaviruses. SARS-CoV-2 is classified as a beta coronavirus.[84] Viruses belonging to this genus infect mammals, and the disease reservoir for this group are commonly bats and rodents. SARS-CoV-2 derived its name from SARS-CoV, another beta coronavirus that it is closely related to.[85] OC43 and HKU1 are also beta coronaviruses, however they cause a less severe illness, the common cold.[86]

There are four main structural proteins found in coronaviruses. These include the envelope (E) protein, membrane (M) protein, nucleocapsid (N) protein, and the spike (S) protein.[87] Spike

proteins are found on the surface of the virus. They are generally glycoproteins with a dimeric or trimeric structure that are believed to play a vital role with host cell entry. Their role in host cell entry also makes them important for host range of virions and immune responses in the host organism.[87,88]

1.3.2 SARS-CoV-2 Cell Entry Mechanism

Evidence suggests that SARS-CoV-2 begins its cell entry mechanism via interactions with the human angiotensin converting enzyme 2 (ACE2) receptor through its spike protein (Figure 1.6).[89,90] Coronavirus spike proteins commonly have S1 and S2 subunits located in the ectodomain segment.[91,92] The SARS-CoV-2 spike protein contains a trimeric S2 stalk and three S1 heads. The C-terminal domain of the S1 segment contains the receptor-binding domain (RBD) of the protein.[93] For the virus to enter host cells, the spike protein is cleaved which allows for binding of the S1 subunit to the ACE2 receptor. The enzymes theorized to be involved in the spike protein priming process include furin, cathepsin L, and TMPRSS2.[94,95] After cleavage of the spike protein with host cell enzymes into S1 and S2, S1 can mediate binding to the ACE2 receptor and S2 is cleaved further allowing it to facilitate membrane fusion.[94-96] SARS-CoV-2 can then enter the host cell through an endosome and the viral RNA is released into the cell once the viral and lysosomal membranes fuse. Once the viral genetic material is released in the cell, translation of the RNA genome begins into polypeptide chains pp1a and pp1ab using host cell machinery.[96] After cleavage of the polypeptide chains, active proteins including RNA-dependent RNA polymerase (RdRP) or viral polymerase is released which replicates the genomic RNA.[94,96] The genomic RNA can then be packaged into the nucleocapsid of new virions, and it is also translated into the viral structural proteins. Subsequently, the virions are put together and released by the host cell to infect new hosts (Figure 1.6).[93,94]

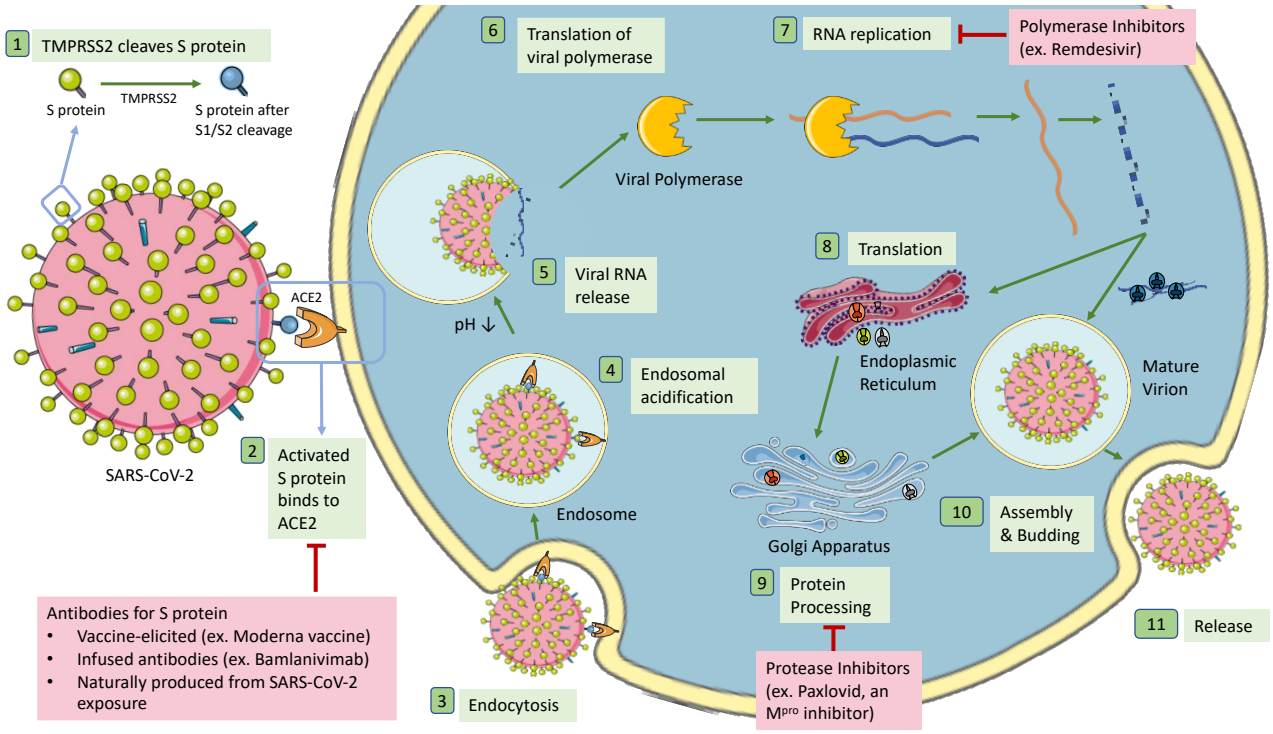

Figure 1.6: The SARS-CoV-2 infection mechanism and the targets of Canadian-approved drugs and vaccines.

1.3.3 COVID-19 Drugs and Vaccines

There are several drugs and vaccines approved in Canada for use against COVID-19. The most common types of COVID-19 vaccines are the mRNA (Pfizer-BioNTech and Moderna) and vector vaccines (AstraZeneca and Johnson & Johnson).[97] Both vaccine types deliver genetic instructions for building SARS-CoV-2 spike protein, and once the protein is built the body creates antibodies against the S protein which can be used to inhibit SARS-CoV-2 entry into cells upon exposure.[98] Vaccination has proven to be an effective strategy at reducing severity of COVID-19 cases, and over 80% of Canadians have received at least one dose.[99-101] However, vaccination still faces challenges as a strategy to combat the disease. There has been shown to be a decrease in vaccine-induced immunity over time and the vaccines are less effective against the growing number of variants of SARS-CoV-2 many of which have been shown to have high-frequency mutations in

the spike protein.[88,101,102] Additionally, with the evolving nature of the SARS-CoV-2 virus, staying protected against new variants of the disease warrants staying up to date with boosters of the vaccine to prevent breakthrough infections.[103,104]

The drugs approved for treatment in Canada include monoclonal antibody treatments and small molecule drugs.[97] The monoclonal antibody treatments are used predominantly for patients who are immunocompromised or have severe cases of COVID-19.[105] All of these monoclonal antibody treatments except one, tocilizumab, target the spike protein of SARS-CoV-2 and face a similar issue with mutation-mediated resistance in variants as a result of mutations in the spike protein.[105,106] Tocilizumab is a human monoclonal antibody against the interleukin-6 receptor and acts as an immunosuppressive drug.[107] The approved small molecule COVID-19 treatments include the intravenous drug remdesivir, and the oral drugs nirmatrelvir and andritonavir (Paxlovid®) which are taken together.[97] Remdesivir is believed to inhibit viral RNA polymerase, which reduces production of viral RNA. Its efficacy has been in debate due to mixed results in studies, and it is currently approved for use in hospitalized adults or high-risk adults who are positive for COVID-19.[108,109] The nirmatrelvir component of Paxlovid® is an inhibitor for M^{pro}, the main protease found in coronaviruses.[110] M^{pro} cleaves the two viral polyproteins and is crucial for the viral replication process.[111] Additionally, M^{pro} is distinct from human proteases, making it a promising drug target. Ritonavir, the second component of Paxlovid®, is a cytochrome P450 3A4 inhibitor and enhances levels of nirmatrelvir in the blood.[110] Paxlovid® has been authorized for treatment of high-risk adults with mild to moderate COVID-19 and it can be taken at home.[112]

The rapidly changing nature of viruses like SARS-CoV-2 means they continue to pose a threat despite the available drugs and vaccines. Additionally, the pathophysiological mechanisms that put patients with diseases such as diabetes, hypertension, and dementia at higher risk of severe

illness and death when infected with COVID-19 is a research area that warrants further exploration.

1.4 Alzheimer's Disease & COVID-19

COVID-19 is primarily regarded as a respiratory illness; however, it can impact multiple organ systems and its severity varies largely.[113] Some patients experience no symptoms, and others develop life-threatening complications such as ARDS and organ failure.[114,115] Advanced age and the presence of other conditions such as dementia, hypertension and diabetes heighten the risk for developing a severe case of COVID-19.[116] People with dementia also tend to be advanced in age, making them likely to experience severe complications for both reasons.[117] The link between COVID-19 and AD is an area currently being explored to get a better understanding of how the diseases interplay and how we can better protect these patients.

COVID-19 patients with dementia are the highest risk group for experiencing hospitalization and death.[118,119] Additionally, neurological symptoms in AD patients tend to get worse while fighting the infection, with one study showing that over 50% of dementia patients diagnosed with COVID-19 experience delirium and decreased functional status as symptoms.[120] This is dissimilar to the typical COVID-19 presentation in patients without dementia, suggesting that COVID-19 could impact dementia patients differently. However, even patients without dementia can experience neurological symptoms from COVID-19 such as headache, brain fog, and loss of smell.[121] The neurological symptoms can be long-lasting and there is evidence that COVID-19 activates pathways that can accelerate the development of AD.[122,123] Additionally, COVID-19 has been shown to be associated with changes in brain structure in a longitudinal imaging study.[124] In this study, brain images of patients before and after infection with COVID-19 were compared, and

there were significant and deleterious changes observed. The effects were mainly seen in the orbitofrontal cortex, parahippocampal gyrus, and regions that connect to the primary olfactory cortex. Furthermore, there was an overall reduction in brain size and cognitive decline observed that was greater in patients with COVID-19 compared to those without.

Inflammation is likely to play a large role in the relationship between COVID-19 and its impact on the CNS. COVID-19 patients describe having neurological symptoms, and studies suggest this could be caused by inflammation of the CNS.[117] Infection with SARS-CoV-2 activates the immune system, and in severe cases of COVID-19, patients develop cytokine storm which is a systemic inflammatory syndrome.[125] The immune system becomes pathologically hyperactivated which can lead to organ failure and death. Dysregulated inflammation of the CNS is also theorized to play a large role in the disease pathogenesis of AD, both in its cause and progression.[126,127] Thus, COVID-19 infection exacerbates the already-dysregulated inflammation in the CNS of AD patients, and this could be the cause of the worsened neurological symptoms observed upon COVID-19 infection (Figure 1.7).[117]

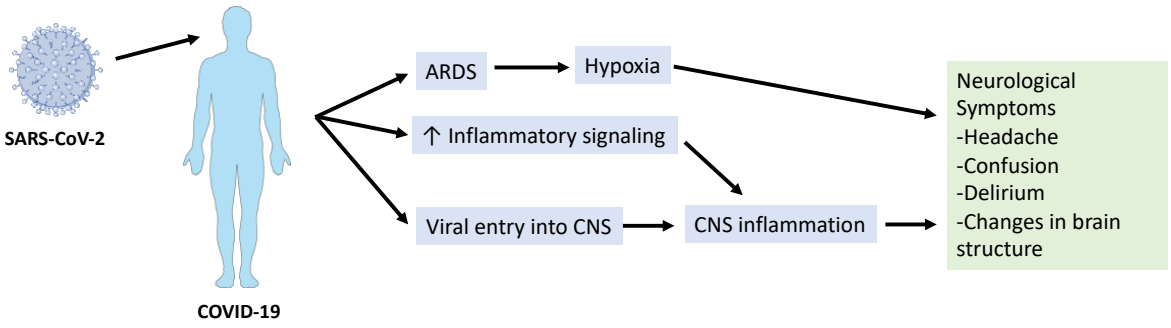

Figure 1.7: SARS-CoV-2 can cause ARDS, increase inflammation and possibly enter the CNS. This can result in CNS inflammation and hypoxia which could cause neurological symptoms and

brain structure changes in COVID-19 patients. In AD patients, CNS inflammation and neurological symptoms are further exacerbated.

In addition to the indirect impact that COVID-19 has on AD through inflammation, there is evidence that SARS-CoV-2 can enter the CNS.[121] SARS-CoV-2 RNA and antigens have been found in the brain samples of COVID-19 patients.[128] Two possible routes for SARS-CoV-2 entry into the CNS include the olfactory nerve and the BBB.[122] This could be facilitated by SARS-CoV-2 binding of ACE2 which initiates cell entry. ACE2 levels were found to be higher in the brains of people with AD, which could impact their viral load and response upon infection with SARS-CoV-2.[129] Additionally, the Aβ42 peptide was found to bind strongly to the SARS-CoV-2 spike protein S1 subunit and increase its attachment to ACE2.[130] This could mean an enhanced ability of SARS-CoV-2 to enter cells which could impact the severity and length of infection. Upon entry, SARS-CoV-2 can cause BBB dysfunction and activate microglial cells.[122] Microglia are the immune cells of the CNS, and their activation can exacerbate inflammation and lead to worsened symptoms in AD patients.[131] BBB dysfunction is also connected with increased inflammation in the CNS.[132] Thus, SARS-CoV-2 may worsen outcomes of AD patients by increasing inflammation indirectly through the production of inflammatory signalling molecules, and directly through interactions with cells of the CNS. Additionally, ARDS caused by COVID-19 can result in hypoxia which could worsen cognitive impairment in AD patients.[122,133]

According to the amyloid cascade hypothesis, increased levels of Aβ peptide and their aggregation are the main players behind development and progression of AD.[36] There is evidence that increased inflammation and oxidative stress as a result of COVID-19 infection could increase the neurotoxicity of Aβ peptide.[36,134] Interestingly, one study found that two peptides from the proteome of SARS-CoV-2 were able to form amyloid aggregates and that the aggregates were

toxic to neuronal cells.[135] Another study found that a peptide fragment from the spike protein of SARS-CoV-2 that may be produced at sites of viral infection is also amyloidogenic.[136] The interactions of human and viral proteins in the context of amyloid formation has been a topic of interest, particularly in the context of neurological diseases.[137,138] Herpes simplex virus type 1 (HSV-1) has been found to promote aggregation of Aβ peptides, and there are several other viruses that have demonstrated interaction with the peptide.[137] Researchers suggest that human protein and viral interactions may have implications in the COVID-19 disease process and why symptoms can be long-lasting for some patients.[137-139]

Whether COVID-19 impacts AD disease progression is inconclusive, as some studies have showed that disease progression during the pandemic has increased, meanwhile others show no difference.[117] It is important to note that the impact of COVID-19 beyond the disease itself could have impacted the outcomes of patients with AD due to the stress and isolation caused by the lockdowns, which have been shown to have a negative effect on neurological symptoms of AD.[117] More studies on the relationship between COVID-19 and AD are urgently needed to gain a better understanding of the connected disease processes and how to best treat patients.

1.5 Fatty Acids

Fatty acids are carboxylic acids with long hydrocarbon tails that serve a variety of physiological roles. They are vital starting materials for production of fat, cell signalling molecules and cell membranes. There is evidence that different types of fatty acids and the ratio consumed from diet play an important role in immune modulation and the prevention of diseases like cardiovascular disease and cancer.[140]

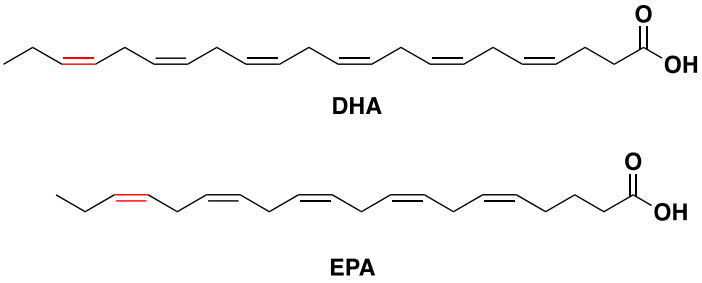

Figure 1.8: The omega-3 polyunsaturated fatty acids DHA and EPA. The omega-3 double bond is highlighted in red.

The omega-3 polyunsaturated fatty acids (PUFAs), particularly docosahexaenoic acid (DHA) and eicosapentaenoic acid (EPA), have been shown to be modulators of immune response and cytokine release.[141] DHA and EPA are associated with decreased markers of inflammation and soluble adhesion molecules.[142] Omega-3 fatty acids are suggested to compete with the same enzymes that use arachidonic acid to produce pro-inflammatory eicosanoid mediators, and thus reduce their production.[141] Additionally, they replace arachidonic acid in the phospholipids of cell membranes, which changes the physical properties of the membrane and signalling pathways.[141] Dysregulated inflammation is believed to play a role in the development of AD and severe cases of COVID-19.[113,127] The impact of omega-3 PUFA supplementation has been investigated for both diseases and has shown the possibility of a positive impact, which will be described in further detail in this section.

DHA is found in high levels in neuronal synapses of the brain and plays an important role in brain development and health.[143] AD patients show decreased levels of DHA, and normal aging leads to lower levels of omega-3 fatty acids as well.[143] Observational studies have shown that high

levels of unsaturated fats in diet and plasma are associated with a reduced risk of development of dementia.[143-146] Furthermore, randomized control trials that supplemented omega-3 fatty acids to patients who have mild cognitive impairment, a precursor to AD, showed a positive effect on cognitive function.[143,144,147] However, the improvement was not observed in patients who already have AD that has progressed, suggesting early intervention is important for improvement to occur.

Omega-3 fatty acids have also been studied for their impact on COVID-19 severity and symptoms. Severe cases of COVID-19 and ARDS are related to hyper-activation of the immune system and the role of omega-3 fatty acids as immune system modulators.[141,148] They have been shown to improve symptoms in patients with COVID-19 and ARDS.[149-151] Adverse outcomes from COVID-19 have been observed for patients who are lower on the omega-3 index or that have omega-3 fatty acid deficiency.[151-153] Additionally, omega-3 fatty acids were able to inhibit binding of SARS-CoV-2 and ACE2 in an in vitro study.[154] EPA, linoleic acid (LNA), and α-linolenic acid (ALA) showed the highest binding affinity to spike protein. LNA and EPA also inhibited binding and entry of a SARS-CoV-2 pseudovirus in A549/hACE2 cells by 15-100%.[154] The mechanism of the interactions of fatty acids with SARS-CoV-2 spike protein are not well understood. Several clinical trials are in progress to determine the preventative and therapeutic potential of omega-3 PUFAs in the context of COVID-19. There is a need to understand the complex interplay between AD and COVID-19 infection to learn how to provide optimal care for patients, and to better understand the risks of comorbidity and mortality. The interactions of fatty acids and COVID-19 in relation to the disease process of AD were investigated in this study.

Chapter 2: Objectives & Hypothesis

Omega-3 PUFAs such as DHA (docosahexaenoic acid) and EPA (eicosapentaenoic acid) are commonly used as dietary supplements. Studies have demonstrated the potential benefit of DHA to reduce the risk of dementia and improve cognitive function.[143,144,147,155] For example, DHA is known to reduce the accumulation of both Aβ and tau aggregates in the 2 x Tg-AD transgenic mouse model.[156] The molecular mechanisms of DHA-mediated benefits in AD are complex and include i) promotion of neurogenesis, ii) improving the antioxidant status, iii) reducing apoptosis and iv) formation of neuroprotective metabolites.[155,157]

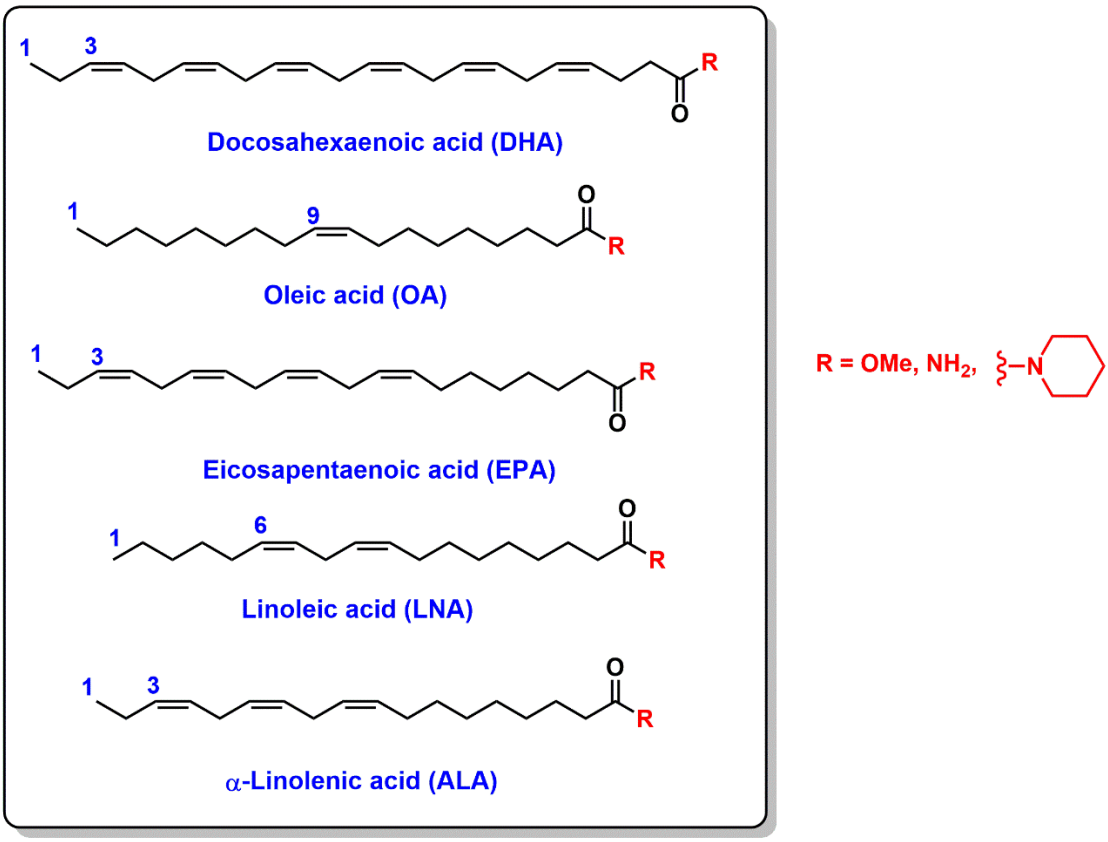

Figure 2.1: The structures of proposed fatty acid derivatives as inhibitors of Aβ42 aggregation.

In a previous study, Nekkar Rao lab demonstrated certain fatty acids can undergo direct interactions with Aβ and reduce their aggregation.[158] Both DHA and were oleic acid (OA) were

identified as inhibitors of Aβ aggregation. This project aims to develop a library of compounds derived from DHA, OA, eicosapentaenoic acid (EPA), linoleic acid (LNA) and α-linolenic acid (ALA) as Aβ42 aggregation inhibitors (Figure 2.1). A computational modeling study of the DHA methyl ester in the oligomer model of Aβ42 shows that the DHA methyl ester was oriented in a perpendicular fashion in the Aβ42 pentamer model and was primarily undergoing several hydrophobic contacts with N- and C-terminal amino acids (Figure 2.2). The S-shaped Aβ42 pentamer model forms a narrow hydrophobic channel at the interface between the N- and C-terminal consisting of amino acids Leu16, Leu17 and Leu34. The molecular docking study shows that the DHA methyl ester was in contact with side chains of these nonpolar amino acids (distance < 5Å), which suggests that the molecule can stabilize the pentamer assembly and reduce its further aggregation. Overall, this computational modeling study suggests that fatty acid derivatives have the potential to interact at the hydrophobic N- and C-terminal interface formed by the Aβ42 pentamer. Therefore, we hypothesize that the DHA, OA, EPA, LNA and ALA-derived compounds will bind in this hydrophobic channel and reduce Aβ42 aggregation. The primary objective of this study is to design, synthesize and evaluate a library of fatty acid derivatives based on DHA, OA, EPA, LNA and ALA as inhibitors of Aβ42 aggregation (Figure 2.1). The terminal carboxylic substituent of the fatty acids will be replaced with other bioisosteres such as the OMe, NH_2 and piperidine substituents to investigate their effect on Aβ42 aggregation and obtain structure-activity relationship (SAR) data. It is anticipated that the lipophilicity and hence brain penetration of proposed ester derivatives of PUFA (R = OMe) would be better than the corresponding carboxylic acids. Increased CNS penetration of carboxylic acid-containing drugs has been demonstrated when they are administered as ester and amide prodrugs.[159,160] It is expected that these fatty acid derivatives will exhibit direct binding to Aβ42 aggregates and reduce their self-assembly into toxic

forms. The proposed experiments include a) synthesis and characterization of fatty acid derivatives by proton nuclear magnetic resonance (^{1}H NMR) and liquid chromatography mass spectrometry (LC-MS) studies, b) in vitro Aβ42 aggregation kinetic studies using the fluorescent dye thioflavin T (ThT) based fluorescence spectroscopy, c) transmission electron microscopy (TEM) studies to determine the morphology of Aβ42 aggregates in the presence of fatty acid derivatives, d) determination of cytotoxicity of synthesized fatty acid derivatives toward HT22 hippocampal neuronal cells using cell counting kit 8 (CCK-8) via UV spectroscopy and e) computational modeling studies using the software Discovery Studio Structure-Based Design to understand the binding interactions of fatty acid derivatives with Aβ42. These investigations will enhance our understanding on the chemical features required to design novel PUFA derivatives as Aβ42 aggregation inhibitors

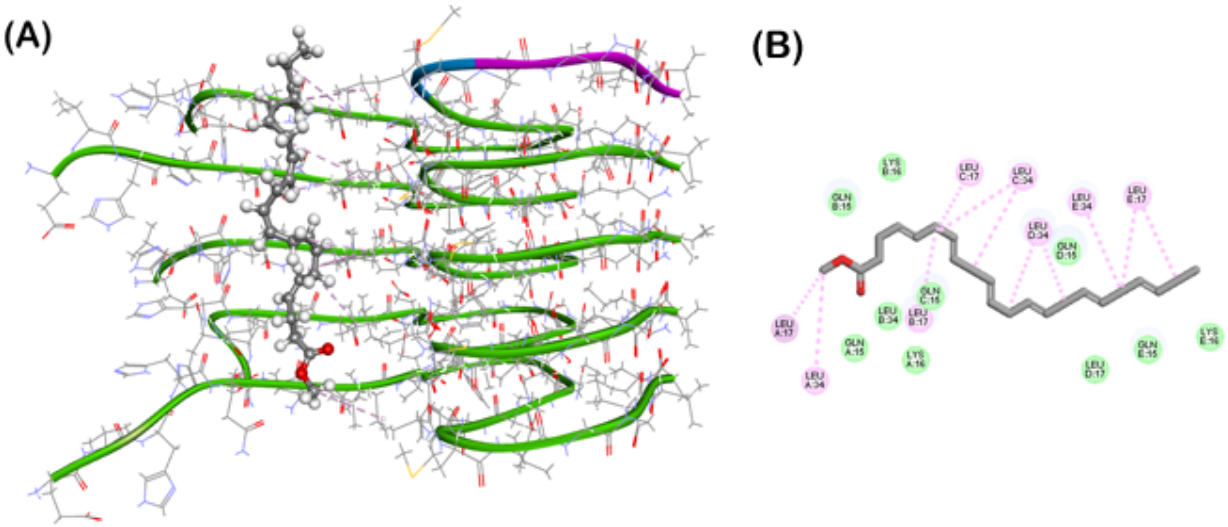

Figure 2.2: (A) The binding interactions of DHA methyl ester in the Aβ42 pentamer model (PDB id: 5KK3); (B) 2D interaction map of DHA methyl ester in the Aβ42 pentamer model.

Furthermore, the secondary objective of this proposal is to investigate the interactions of Aβ42 peptide with the COVID-19/SARS-CoV-2 spike protein fragment. In a recent study, Nystrom and coworkers, were able to discover the aggregation propensity of fragments of SARS-

CoV-2 spike protein.[136] Their study demonstrated that the decapeptide sequence FKNIDGYFKI (segment 194-203, Figure 2.3), derived from the spike protein was prone to undergo self-assembly into amyloidogenic fibrils. Their study also suggests that this segment is involved in COVID-19 associated amyloid formation which has implications in viral infection and inflammatory pathways. Therefore, another objective of this proposal was to understand the interactions of this amyloidogenic fragment of spike protein with Aβ42 peptide to investigate the role of these interactions in promoting cytotoxicity. It is hypothesized that the COVID-19 spike protein fragment will promote Aβ42 fibrillogenesis and will act in a synergistic fashion by direct binding to Aβ42 and increase Aβ42-mediated cytotoxicity. The proposed experiments include a) investigating the effect of FKNIDGYFKI decapeptide on Aβ42 aggregation kinetics which will be monitored by ThT-based fluorescence assay, b) TEM studies to determine the effect of FKNIDGYFKI decapeptide on Aβ42 morphology, and c) determination of cytotoxicity of the full-length spike protein toward HT22 cells using CCK-8 via UV spectroscopy.

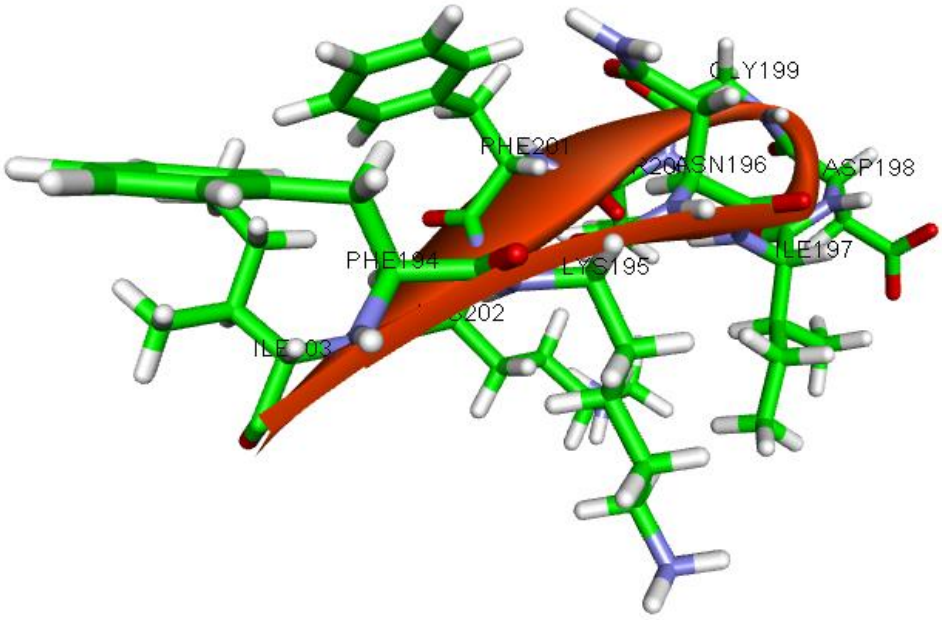

Figure 2.3: The structure of COVID-19 spike protein derived amyloidogenic sequence FKNIDGYFKI. Only the key regions of Aβ42 in contact with the ligand are shown.

Chapter 3: Methodology

All chemicals and reagents were obtained from commercial vendors (Sigma-Aldrich, Thermo Fisher Scientific, Acros Organics, TCI Chemicals, Cayman Chemicals, AA Blocks). Reagents used for chemical synthesis had a minimum purity of 95% and were used without further purification. The spike protein fragment uncapped FKNIDGYFKI peptide was synthesized by Celtek Peptides, TN, USA and was >95% pure. The recombinant SARS-CoV-2 spike protein was obtained from Cusabio, Wuhan, China (product code: CSB-MP3324GMY). ^{1}H NMR (300 MHz) spectra were recorded on a Bruker ® Avance 300 MHz series spectrometer, and all NMR samples were prepared using $CDCl_3$. Coupling constants (J values) were recorded in hertz (Hz) and the abbreviations used for multiplicity of NMR signals are: s = singlet, d = doublet, t = triplet, m = multiplet, and br = broad. The melting points of final products were determined on a Fisher-Johns instrument and are uncorrected. Derivatives were purified using Merck 230-400 mesh silica gel 60, and all products showed a single spot on thin-layer chromatography (TLC) performed on Merck 60 F254 silica gel plates (0.2 mm). TLC was performed using the following solvent systems: 100% EtOAc, n-hexane/EtOAc 1:1, n-hexane/EtOAc 3:1, and n-hexane/EtOAc 3:2. TLCs were stained with a vanillin stain (15g vanillin, 250 mL ethanol, 2.5mL conc. sulfuric acid) for visualization of derivatives. The purity of compounds was measured using an Agilent 6100 series single quad LC-MS connected with an Agilent 1.8 μm Zorbax Eclipse Plus C18 (2.1 x 50 mm). The general method used for LC-MS was 20% of MeOH to 80% of 0.1% formic acid in acetonitrile at a flow rate of 0.5 mL/min and detection at 208 nm by UV.

3.1 Synthetic Chemistry

Synthetic routes used to produce the fatty acid derivatives were adapted from literature and modified to optimize synthesis and yields. After the fatty acid derivatives were purified, their identity was confirmed by ^{1}H NMR and LC-MS. The purity of compounds (>95%) was confirmed using LC-MS before they were used in the in vitro experiments. The general mechanism for forming the fatty acid derivatives was nucleophilic acyl substitution, illustrated in Figure 3.1.

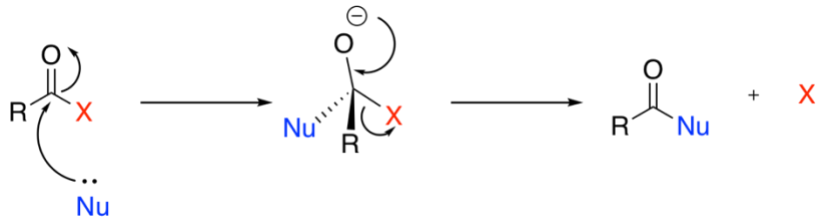

Figure 3.1: Nucleophilic acyl substitution.

3.1.1 General Method to Synthesize Methyl Ester Derivatives (1a, 2a, 3a, 4a, 5a)[161]

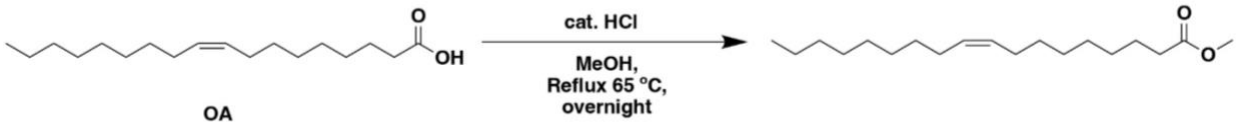

Scheme 3.1: General method to synthesize methyl ester derivatives (**1a, 2a, 3a, 4a, 5a**)

0.283 g of OA (1.0 mmol) or LNA (1.0 mmol) or ALA (0.7 mmol) or EPA (1.0 mmol) or DHA (1.0 mmol) was dissolved in 15 mL of dry MeOH. The mixture was stirred as a few drops of catalytic HCl were added to the flask. The mixture was stirred overnight at reflux (65 °C) and then cooled to room temperature before extracting with DCM (3 x 5 mL). The mixture was washed with water (3 x 10 mL) and brine (1 x 10 mL), and then dried over $MgSO_4$. The product was purified by column chromatography using *n*-hexane/EtOAc (7:1) to yield derivatives **1a, 2a, 3a, 4a,** and **5a.** (47–98% yield)

3.1.2 General Method to Synthesize Amide Derivatives (1b, 2b, 3b)[162]

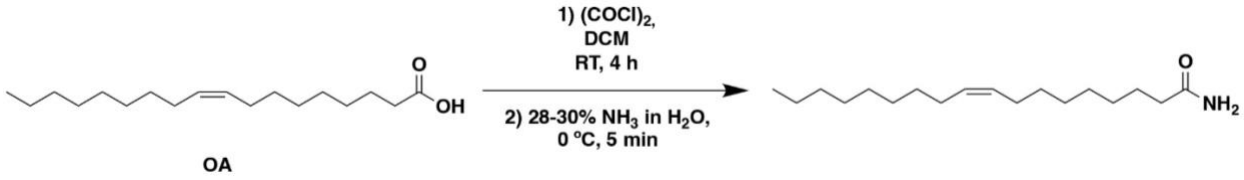

Scheme 3.2: General method to synthesize amide derivatives (**1b, 2b, 3b**)

0.283 g of OA (1.0 mmol) or LNA (1.0 mmol) or ALA (0.7 mmol) was dissolved in 2 mL of DCM. 0.2 mL of oxalyl chloride (2.5 mmol) was added to the solution, and refluxed for 30 minutes at 70°C. The reaction mixture was cooled to room temperature, and solvent was removed under reduced pressure. The mixture was then cooled to 0 °C and 2 mL of 28-30% NH_3 in H_2O (38.6 mmol) was added dropwise with vigorous stirring for 5 mins. The mixture was extracted with EtOAc (3 x 10 mL) and dried over $MgSO_4$. The product was purified by column chromatography using *n*-hexane/EtOAc (1:1) to yield derivatives **1b, 2b,** and **3b.** (21–41% yield)

3.1.3 General Method to Synthesize Piperidinyl Amide Derivatives (1c, 2c)[163]

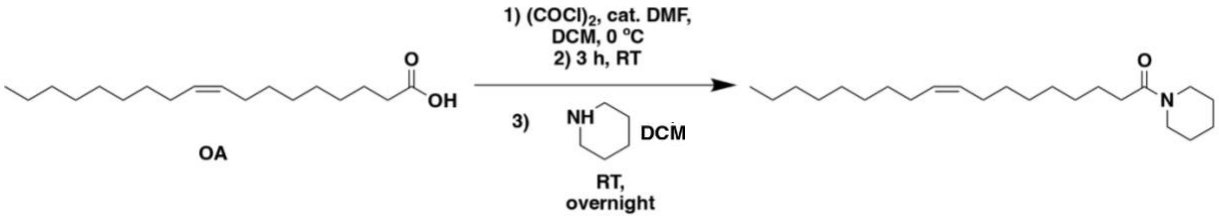

Scheme 3.3: General method to synthesize piperidinyl amide derivatives (**1c, 2c**)

0.283 g of OA (1.0 mmol) or LNA (1.0 mmol) was dissolved in 10 mL of dry DCM. At 0 °C, 0.2 mL of oxalyl chloride (2.5 mmol) was added to the solution, followed by a few drops of catalytic DMF. The mixture was stirred at room temperature for 3 hours, and solvent was removed under reduced pressure. Then, 5 mL of DCM was added to the reaction mixture and followed by

the addition of 0.172 g of piperidine dissolved in 5 mL of DCM. The mixture was stirred overnight, and then an ice-water mixture was added followed by extraction with DCM (3 x 10 mL). The organic layer was then washed with 2N HCl (1 x 5 mL), saturated HCO_3 (1 x 5 mL), water (2 x 5 mL) and brine (1 x 5 mL). The product was dried over $MgSO_4$ and purified by column chromatography using *n*-hexane/EtOAc (1:1) to yield derivatives **1c** and **2c.** (20% yield)

3.2 ThT-Based Aβ Aggregation Kinetics Assay[164,165]

The ThT-based Aβ aggregation kinetics assay was used to investigate the effect of the fatty acid derivatives (**1a-c**, **2a-c**, **3a**, **3b**, **4a** and **5a**) and SARS-CoV-2 spike decapeptide FKNIDGYFKI on aggregation of Aβ42. The aggregation of Aβ can be monitored in this assay by measuring fluorescence in the presence of thioflavin T (ThT). ThT is a benzothiazole dye that gives a strong fluorescence signal at 482 nm upon binding to fibrils of Aβ peptide when excited at 450 nm.[165] The aggregation of amyloidogenic proteins in this assay follows sigmoid kinetics as shown in Figure 3.2.

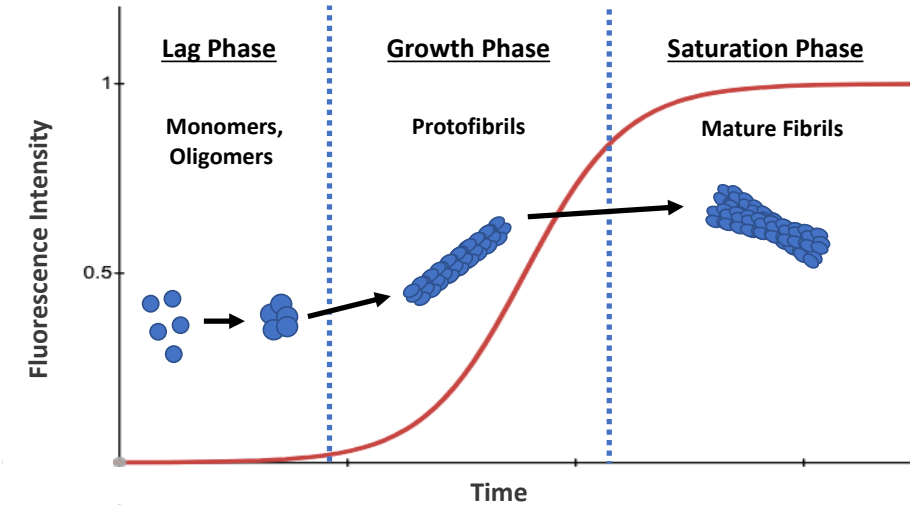

Figure 3.2: The typical aggregation curve of amyloidogenic proteins when monitored in a ThT-based aggregation kinetics assay.

Black Costar 384-well plates with clear bottoms were used for this assay. All buffers and solutions were prepared using ultra-pure water (UPW). 215 mM phosphate buffer was prepared and adjusted to a pH of 7.4. ThT solution (8.25 µM, pH 7.4) was freshly prepared on the day of the assay in 50 mM glycine buffer. Stock solutions of the fatty acid derivatives, spike decapeptide, and reference compounds (resveratrol, methylene blue) were prepared in DMSO or phosphate buffer. Then the stock solutions were diluted to desired concentrations in phosphate buffer, keeping the final concentration of DMSO in wells under 2.5%. ThT solution, buffer, compounds and DMSO were added to wells before preparation and addition of Aβ42. The following plating procedure was used:

Table 3.1: Plating Procedure for ThT-Based Aβ42 Aggregation Kinetics Assay

	ThT	**Buffer**	**DMSO**	**Aβ42**	**Compound**
ThT Background	11 µL	28 µL	1 µL, 2.5%	-	-
Compound Background	11 µL	25 µL	-	-	4 µL
Aβ42 Control	11 µL	12 µL	1 µL, 2.5%	16 µL	-
Compound + Aβ42	11 µL	9 µL	-	16 µL	4 µL

Aβ42 hexafluoro-2-propanol (HFIP) (rPeptide, USA) was dissolved in 1% NH_4OH to achieve a concentration of 1 mg/mL, before diluting with 215 mM phosphate buffer to a concentration of 25 µM. The final concentration of Aβ42 in wells was 10 µM. Plates were sealed with transparent films, and the excitation and emission were measured at 440 nm and 490 nm respectively while incubating the plate at 37 °C with shaking. Readings were taken every 5 minutes by the Biotek Synergy H1 microplate reader over 24-h. ThT background and compound background relative fluorescence intensity (RFU) values were subtracted from wells with Aβ42 to account for any

interference if required. The results were presented as average percent inhibition based on two independent experiments (n = 3). These samples were also used to prepare TEM grids.

3.3 Transmission Electron Microscopy (TEM)

TEM experiments were carried out to examine the effect of fatty acid derivatives (**1a, 2a, 3a, 4a** and **5a)** and SARS-CoV-2 spike decapeptide FKNIDGYFKI on the formation and morphology of Aβ42 fibrils. The TEM studies were conducted on a Philips CM 10 transmission electron microscope at 60kV (Department of Biology, University of Waterloo) with a 14-megapixel AMT camera. 20 μL was drawn from appropriate wells from the ThT-based Aβ aggregation kinetics assay containing Aβ42 co-incubated with compounds, and wells with Aβ42 alone (24-h incubation at 37 °C). The aliquots were placed on copper coated formvar-carbon grids (400 mesh) and samples were air-dried overnight. The samples were then washed with 20 μL of UPW two times, and filter paper was used to quickly remove the water each time. The samples were allowed to air-dry for a few hours before staining them with 20 uL of 2% phosphotungstic acid (PTA) for 10 seconds, and then removing the PTA with filter paper. The samples were washed with 20 μL of UPW two times, quickly removing the water with filter each time. The grids were air-dried for at least 24 hours before scanning them.

3.4 Molecular Docking Studies

3.4.1 Fatty Acid Derivatives with Aβ42 Oligomer Model

The molecular docking experiments were conducted using the computational software Discovery Studio (DS), Structure-Based-Design software program Biovia 2019 (Dassault Systemes, Biovia Corp. 2019, San Diego, USA). The 3D coordinates of Aβ42 peptide was obtained

from the protein data bank (Aβ42 pdb id: 5KK3). The pentamer model of Aβ42 was prepared by extracting the pentamer (Aβ42) assembly and the protein was prepared using CHARMm force field for docking via the Macromolecules module in DS. The binding site of Aβ42 dimer assemblies was defined by a sphere of 20 Å radius each. The fatty acid derivatives **1a**, **2a**, **2b**, **3a** and **5a** were initially prepared in 2D using the software ChemDraw, minimized in ChemBio3D and were opened in DS. CHARMm force field was applied at pH 7.4 and minimized using the Smart Minimizer protocol (RMS gradient of 0.01 kcal/mol) and a distance-dependent dielectric constant to obtain the 3D structures of fatty acid derivatives. The docking of the derivatives was carried out using the LibDock algorithm by employing 100 hotspots, a docking tolerance of 0.25 Å, and an implicit solvent model, with a distance dependent dielectric constant and CHARMm force field. The binding poses obtained were further energy minimized using *Smart minimizer* (1000 steps and an RMS gradient of 0.001 kcal/mol) and ranked using the LibDock scoring function. The ligand binding interactions for the top ranked poses were evaluated by measuring the distance parameters for various intermolecular polar and nonpolar interactions with the ligand and the Aβ42 oligomer.

3.4.2 Spike Protein Fragment FKNIDGYFKI with Aβ42 Oligomer Model

The molecular docking experiments were conducted using the computational software Discovery Studio (DS), Structure-Based-Design software program Biovia 2019 (Dassault Systemes, Biovia Corp. 2019, San Diego, USA). The 3D coordinates of Aβ42 peptide was obtained from the protein data bank (Aβ42 pdb id: 5KK3). The pentamer model of Aβ42 was prepared by extracting the pentamer (Aβ42) assembly and the protein was prepared using CHARMm force field for docking via the Macromolecules module in DS. The binding site of Aβ42 dimer

assemblies was defined by a sphere of 30 Å radius each. The spike protein uncapped decapeptide FKNIDGYFKI was extracted from the cryo-EM structure of SARS-CoV-2 spike protein (pdb id: 6VXX) and was prepared using CHARMm force field at pH 7.4. The docking of uncapped decapeptide FKNIDGYFKI was carried out using the LibDock algorithm by employing 100 hotspots, a docking tolerance of 0.25 Å and an implicit solvent model, with a distance dependent dielectric constant and CHARMm force field. The binding poses obtained were further energy minimized using *Smart minimizer* (1000 steps and an RMS gradient of 0.001 kcal/mol) and ranked using the LibDock scoring function. The ligand binding interactions for the top ranked pose was evaluated by measuring the distance parameters for various intermolecular polar and nonpolar interactions with the ligand and the Aβ42 oligomer.

3.5 Cell Culture & CCK-8 Assay[164]

HT22 mouse hippocampal neuronal cells were grown in 1:1 Dulbecco's modified eagle media (DMEM) and Ham's F12 with the addition of glutamate (2.5 mM), supplemented with 10% (v/v) fetal bovine serum (FBS), and 1% (v/v) 10,000 U/mL penicillin-streptomycin. The cells were incubated at 37°C under 5% CO_2 and passaged at 80% confluence.

To test the cytotoxicity of the fatty acid derivatives and SARS-CoV-2 spike protein, the HT22 cells were seeded into a 96-well plate at a density of 5000 cells/well and incubated for 24 hours. The stock solutions of the fatty acid derivatives, spike protein, and reference compounds (resveratrol, quercetin) were freshly prepared in DMSO or 1:1 DMEM/F12 and then diluted to desired concentrations (25 μM for fatty acid derivatives, 5 and 10 ng/mL for spike decapeptide) in DMEM/F12 1:1. The final concentration of DMSO was kept under 0.5% in wells. Cells were incubated with treatments for 24 hours before analyzing cell viability with the CCK-8 assay. The

CCK-8 assay is a colorimetric assay that can be used to determine measure relative cell viability after treatment. The kit contains a water-soluble tetrazolium salt (WST-8) which produces a water-soluble formazan dye upon reduction with cellular dehydrogenases which is correlated with the amount of living cells (Figure 3.3). After cells had been incubated with treatments for 24 hours, the media was removed and replaced with 100 µL of 1:1 DMEM/F12 and 10 µL of the CCK-8 solution was added to each well. The cells were incubated for 2 hours before absorbance was measured at 450 nm using a BioTek Synergy H1 microplate reader. Percent viability was calculated based on the absorbance values in cells that received treatment relative to untreated cells. The results were expressed as average percent cell viability based on two independent experiments (n = 6).

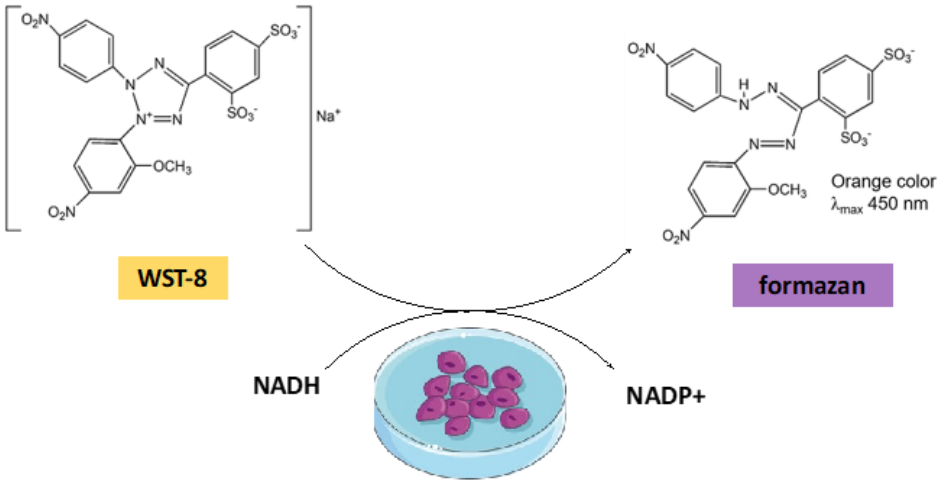

Figure 3.3: Simplified mechanism for production of formazan in CCK-8 assay.

Chapter 4: Results & Discussion

This project investigated the interactions of fatty acid derivatives and the SARS-CoV-2 spike fragment (FKNIDGYFKI decapeptide) on Aβ42 aggregation. A library of 10 fatty acid derivatives were synthesized from DHA, OA, EPA, LNA and ALA. The effect of fatty acid derivatives and spike protein fragment (FKNIDGYFKI decapeptide) on Aβ42 aggregation was assessed by ThT-based aggregation kinetics experiment and TEM imaging studies. The binding interactions of fatty acid derivatives and the spike protein fragment was investigated by molecular docking studies to understand the key regions and binding modes of fatty acid derivatives in the Aβ oligomer model. Additionally, the cytotoxicity profiles of the synthesized fatty acid derivatives and SARS-CoV-2 spike protein were evaluated in mouse hippocampal neuronal cell lines (HT22).

4.1 Synthesis and Characterization of Fatty Acid Derivatives

The methyl esters of the fatty acids were synthesized by Fisher esterification and the amide derivatives were obtained by coupling the acids with corresponding amines. The ester derivatives **1a**, **2a**, **3a, 4a** and **5a** were synthesized by refluxing the corresponding acids OA, LNA, ALA, EPA and DHA with methanol under acidic conditions to afford the target compounds (Scheme 3.1). The amide derivatives **1b**, **1c**, **2b, 2c** and **3b** were prepared by treating the corresponding acids OA, LNA and ALA with oxalyl chloride and then adding ammonium hydroxide or piperidine (Scheme 3.2 and Scheme 3.3). The final compounds were either purified by silica gel column chromatography or were obtained without further purification at >95% purity. They were characterized by ^{1}H NMR and LC-MS analysis (Appendix). **1a**, **2a**, **3a, 4a** and **5a** were not stable under LC-MS conditions, however the ^{1}H NMR data was consistent with their structures. The analytical data of the synthesized compounds is given below:

4.1.1 ^{1}H NMR Data for Fatty Acid Derivatives

Methyl oleate (1a): Yield: 0.25 g, 98%. The product was obtained as a yellow oil. ^{1}H NMR (300 MHz, $CDCl_3$) δ: 5.32 (m, 2H), 3.64 (s, 3H), 2.28 (t, J = 5.7 Hz, 2H), 1.98 (m, 4H), 1.58 (m, 2H), 1.26 (m, 20H), 0.86 (t, J = 6.0 Hz, 3H). $C_{19}H_{36}O_2$. Purity: 95%

Oleamide (1b): Yield: 0.04 g, 21%; MP: 73-75°C. The product was obtained as a white solid and purified using n-hexane/EtOAc (1:1). ^{1}H NMR (300 MHz, $CDCl_3$) δ: 5.34 (m, 2H), 2.24 (t, J = 6.0 Hz, 2H), 1.99 (m, 4H), 1.61 (m, 2H), 1.27 (m, 20H), 0.86 (t, J = 6.0 Hz, 3H). LRMS (ESI) m/z calc for $C_{18}H_{35}NO$ ($[M + H]^+$; 282.3. Purity: 98%

(*Z*)-1-(piperidin-1-yl)octadec-9-en-1-one (1c): Yield: 0.07 g, 20%. The product was obtained as a yellow wax and purified using n-hexane/EtOAc (1:1). ^{1}H NMR (300 MHz, $CDCl_3$) δ: 5.35-5.38 (m, 2H), 3.46 (m, 4H), 2.31 (t, J = 7.5 Hz, 2H), 2.00-2.04 (m, 4H), 1.55-1.66 (m, 8H), 1.29-1.43 (m, 20H), 0.90 (t, J = 3.9 Hz, 3H). LRMS (ESI) m/z calc for $C_{23}H_{43}NO$ ($[M + H]^+$; 350.4. Purity: 98%

Methyl (9*Z*,12*Z*)-octadeca-9,12-dienoate (2a): Yield: 0.29 g, 98%. The product was obtained as a yellow oil. ^{1}H NMR (300 MHz, $CDCl_3$) δ: 5.33 (m, 4H), 3.65 (s, 3H), 2.75 (t, J = 5.7 Hz, 2H), 2.28 (t, J = 7.5 Hz, 2H), 2.02 (m, 4H), 1.60 (m, 2H), 1.33 (m, 14H), 0.87 (t, J = 6.9 Hz, 3H). $C_{19}H_{34}O_2$. Purity: 99%

(9*Z*,12*Z*)-octadeca-9,12-dienamide (2b): Yield: 0.10 g, 37%. The product was obtained as a yellow wax and purified using n-hexane/EtOAc (1:1). ^{1}H NMR (300 MHz, $CDCl_3$) δ: 5.34 (m,

4H), 2.75 (t, J = 6.0 Hz, 2H), 2.20 (t, 2H), 2.02 (m, 4H), 1.62 (m, 2H), 1.30 (m, 14H), 0.87 (t, J = 3.0 Hz, 3H). LRMS (ESI) m/z calc for $C_{18}H_{33}NO$ ($[M + H]^+$; 280.3. Purity: 97%

(9*Z*,12*Z*)-1-(piperidin-1-yl)octadeca-9,12-dien-1-one (2c): Yield: 0.07 g, 20%. The product was obtained as a yellow wax and purified using n-hexane/EtOAc 1:1. ^{1}H NMR (300 MHz, $CDCl_3$) δ: 5.36-5.43 (m, 4H), 3.50 (t, J = 3.3 Hz, 4H), 2.79 (t, J = 5.7 Hz, 2H), 2.34 (t, J = 7.2 Hz, 2H), 2.06-2.10 (m, 4H), 1.57-1.70 (m, 8H), 1.27-1.42 (m, 14H), 0.91 (t, J = 6.6 Hz, 3H). LRMS (ESI) m/z calc for $C_{23}H_{41}NO$ ($[M + H]^+$; 348.3.Purity: 96%

Methyl (9*Z*,12*Z*,15*Z*)-octadeca-9,12,15-trienoate (3a): Yield: 0.15 g, 72%. The product was obtained as a yellow oil. ^{1}H NMR (300 MHz, $CDCl_3$) δ: 5.34 (m, 6H), 3.64 (s, 3H), 2.79 (m, 4H), 2.28 (m, 2H), 2.03 (m, 4H), 1.63-0.97 (m, 10H), 0.96 (t, J = 6.0 Hz, 3H). $C_{19}H_{32}O_2$. Purity: 99%.

(9*Z*,12*Z*,15*Z*)-octadeca-9,12,15-trienamide (3b): Yield**:** 0.08 g, 41%. The product was obtained as a yellow wax and purified using n-hexane/EtOAc (1:1). ^{1}H NMR (300 MHz, $CDCl_3$) δ: 5.32 (m, 6H), 2.79 (m, 4H), 2.20 (m, 2H), 2.04 (m, 4H), 1.62 (m, 2H), 1.30 (m, 8H), 0.96 (t, J = 6.0 Hz, 3H). LRMS (ESI) m/z calc for $C_{18}H_{31}NO$ ($[M + H]^+$; 278.3. Purity: 98%.

Methyl (5*Z*,8*Z*,11*Z*,14*Z*,17*Z*)-icosa-5,8,11,14,17-pentaenoate (4a): Yield**:** 0.25 g, 78%. The product was obtained as a yellow oil and purified using n-hexane/EtOAc (7:1). ^{1}H NMR (300 MHz, $CDCl_3$) δ: 5.35-5.45 (m, 10H), 3.67 (s, 3H), 2.81-2.86 (m, 8H), 2.34 (t, J = 7.5 Hz, 2H), 2.07-2.14 (m, 4H), 1.73 (m, 2H), 1.0 (t, J = 7.5 Hz, 3H). $C_{21}H_{32}O_2$. Purity: 96%

Methyl (4*Z*,7*Z*,10*Z*,13*Z*,16*Z*,19*Z*)-docosa-4,7,10,13,16,19-hexaenoate (5a): Yield**:** 0.16 g, 47%. The product was obtained as a yellow oil and purified using n-hexane/EtOAc (7:1). ^{1}H NMR (300 MHz, $CDCl_3$) δ: 5.33-5.46 (m, 12H), 3.70 (s, 3H), 2.81-2.87 (m, 10H), 2.39 (m, 4H), 2.07-2.12 (m, 2H), 1.0 (t, J = 6.3 Hz, 3H). $C_{23}H_{34}O_2$. Purity: 97%

4.2 ThT-Based Aβ42 Aggregation Kinetics Assay

4.2.1 Effect of Fatty Acid Derivatives on Aβ42 Aggregation

The anti-Aβ42 aggregation activity of fatty acid derivatives (**1a-c; 2a-c; 3a, 3b; 4a** and **5a**) at 25 μM was assessed using ThT-based fluorescence kinetic assays over a period of 24-h (Levine 1993). The parent fatty acids (OA, LNA, ALA, EPA, and DHA) were also tested for comparison. Known Aβ42 aggregation inhibitors methylene blue (MB) and resveratrol were kept as reference compounds. The Aβ42 aggregation inhibition data for the compounds are provided in Table 4.1.

Table 4.1: ThT-based Aβ42 Aggregation Inhibition Data for Fatty Acid Derivatives

Class of Compounds	Compound	% Inhibition (25 μM)[a]
OA Derivatives (1)	**1a** (R = OMe)	44.9 ± 2.5
	1b (R = NH_2)	27.4 ± 8.9
	1c (R = Piperidine)	21.5 ± 34.2
	OA (R = OH)	72.2 ± 3.6
LNA Derivatives (2)	**2a** (R = OMe)	61.4 ± 9.3
	2b (R = NH_2)	40.9 ± 4.6
	2c (R = Piperidine)	34.0 ± 15.2

	LNA (R = OH)	2.9 ± 10.5
ALA Derivatives (3)	**3a** (R = OMe)	51.3 ± 9.6
	3b (R = NH_2)	26.9 ± 17.6
	ALA (R = OH)	20.2 ± 8.5
EPA Derivatives (4)	**4a** (R = OMe)	22.5 ± 3.8
	EPA (R = OH)	68.0 ± 7.6
DHA Derivatives (5)	**5a** (R = OMe)	47.5 ± 11.0
	DHA (R = OH)	43.6 ± 3.4
Controls	Methylene Blue (MB)	98.1 ± 0.3
	Resveratrol	91.7 ± 2.6

[a]The percent inhibition values are based on the inhibition of ThT fluorescence intensity and expressed as the average ± the standard deviation of two independent experiments (n = 3). The values are obtained from ThT-based 24-h aggregation kinetics assay using Aβ42 (10 μM) at pH 7.4 and 37 °C in phosphate buffer.

OA derivatives **1a** (R = OMe), **1b** (R = NH_2) and **1c** (R = piperidine) demonstrated anti-Aβ42 activity and showed 21–45% inhibition at the 24-h time point (Table 4.1). The OA methyl ester (**1a**, R = OMe) exhibited the most potent inhibition (~45%). However, its anti-aggregation activity was ~1.6-fold less as compared to the corresponding acid OA (~72% inhibition). This shows that the modification of the acid functionality was able to retain the anti-aggregation activity, but it led to a decline in its inhibition properties. In contrast, modifying the acid moiety in LNA led to a significant increase in its anti-aggregation activity with the ester derivative **2a** (R

= OMe) exhibiting maximum inhibition (61%) at the 24-h time point whereas the parent LNA (R = OH) itself was inactive (~3% inhibition, Table 4.1). Modifying the LNA to the amide (**2b**, R = NH_2) or piperidine (**2c**) substituent provided 41% and 34% inhibition respectively (Table 4.1). Evaluating the anti-Aβ42 activity of ALA derivatives (**3a**, R = OMe and **3b**, R = NH_2) also shows that the ester derivative exhibited superior activity (51% inhibition, Table 4.1) and was a better inhibitor compared to the parent ALA (20% inhibition, Table 4.1). The piperidine derivatives exhibited weaker inhibition (21% and 34% inhibition for compounds **1c** and **2c**, Table 4.1). These studies suggest that modifying the acid moiety of these fatty acids with an ester substituent could provide better inhibition activity. Accordingly, methyl ester derivatives of EPA and DHA were evaluated. These studies show that replacing the acid moiety with ester (**4a,** R = OMe), led to a significant decline in its anti-Aβ42 activity (22% inhibition), compared to the parent EPA (68% inhibition at 24-h, Table 4.1). Replacing the acid moiety with a methyl ester in DHA, provided similar inhibition (**5a**, R = OMe, ~47% inhibition at 24-h, Table 4.1) as the parent DHA (43% inhibition). None of the fatty acids were able to exhibit similar activity as the reference agents MB and resveratrol at 25 μM, 24-h (98% and 92% inhibition respectively, Table 4.1). The anti-Aβ42 activity profile was of the order **2a** (R = OMe) > **3a** (R = OMe) > **5a** (R = OMe) ~ **1a** (R = OMe) > **4a** (R = OMe). These studies show that ester derivatives of the fatty acids were able to reduce Aβ42 aggregation. Among the tested compounds, methyl ester derivatives of LNA and ALA (**2a** and **3a**) were able to exhibit superior inhibition compared to their acid counterparts. The percent inhibition of Aβ42 aggregation by the fatty acids and derivatives in the ThT-based 24-h aggregation kinetic assays are displayed in Figure 4.1.

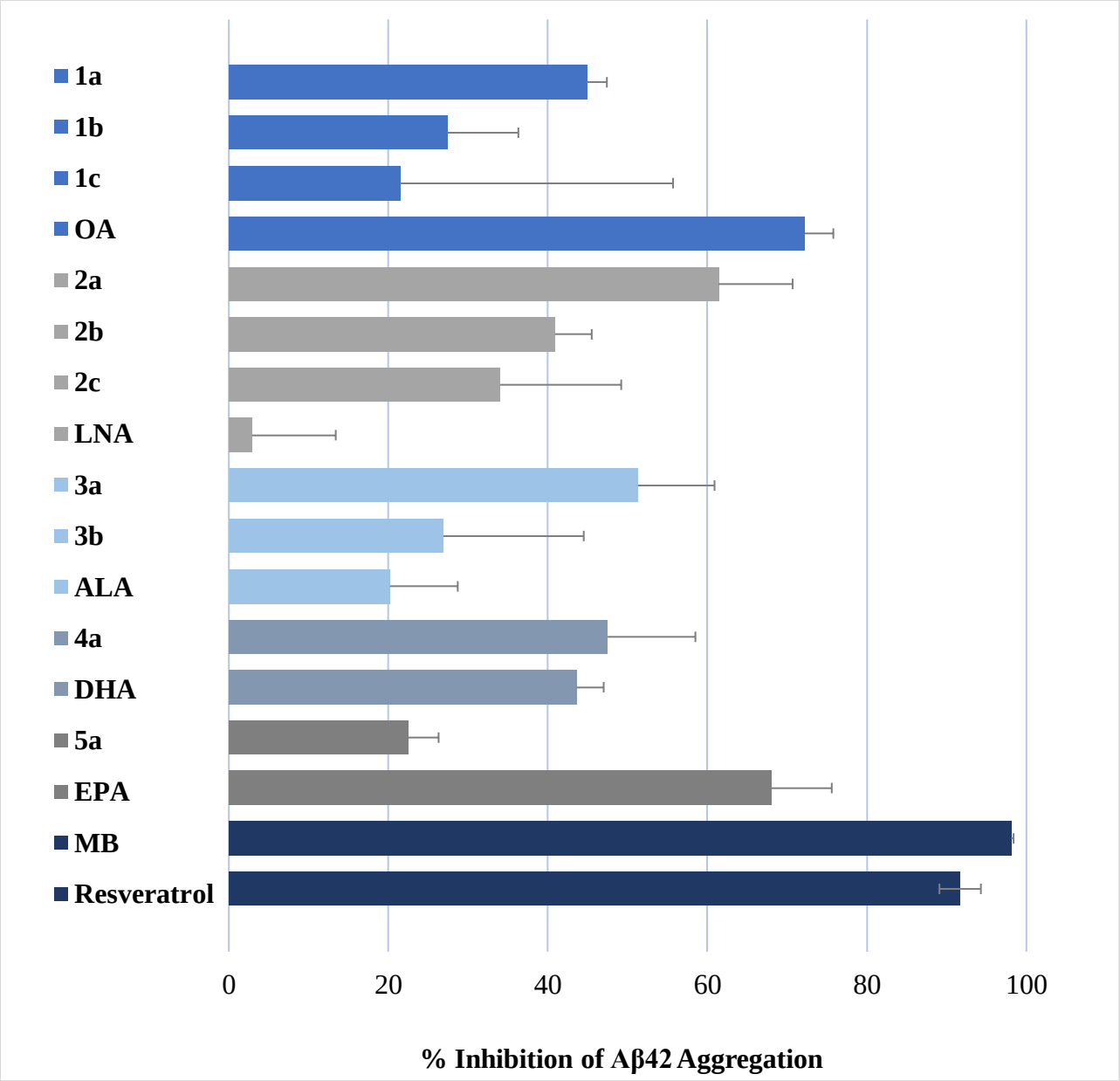

Figure 4.1: The percent inhibition of Aβ42 (10 μM) aggregation in the presence of 25 μM of the fatty acid derivatives (**1a-c, 2a-c, 3a, 3b, 4a, 5a**), fatty acids (OA, LNA, ALA, DHA, EPA), MB, and resveratrol after 24 hours. This data is based on inhibition of fluorescence intensity in a ThT-based Aβ42 aggregation kinetics assays with pH 7.4, 37 °C and phosphate buffer.

The effect of fatty acid derivatives and resveratrol on Aβ42 aggregation kinetics over a 24-h time period are shown in Figures 4.2–4.7. In the absence of either fatty acid derivative or

resveratrol, Aβ42 exhibits a typical sigmoid curve with a short lag phase of less than 2 hours before aggregation accelerates during the growth phase (Figure 4.2). This phase of rapid acceleration occurs until about 8 hours when aggregation begins to slow down at the saturation phase. Resveratrol showed 92% inhibition at 25 μM (Figure 4.2). It is clear from the kinetic aggregation curve that resveratrol is a potent inhibitor of Aβ42 aggregation and can interact and reduce the self-assembly of Aβ42 monomers, dimers and other lower order aggregates formed early during the self-assembly process.

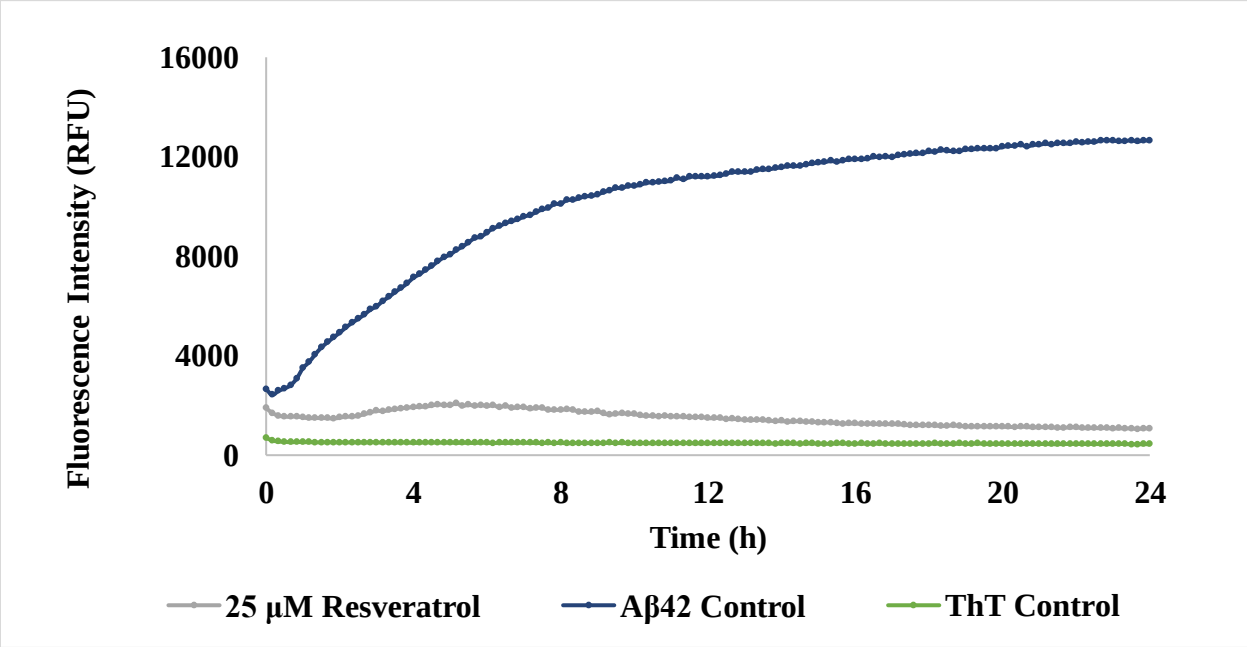

Figure 4.2: ThT-based aggregation kinetics curve of Aβ42 (10 μM) curve with 25 μM of resveratrol over 24 hours at pH 7.4, 37 °C and phosphate buffer.

The effect of OA and its ester derivative **1a** on Aβ42 aggregation kinetics over a 24-h time period is shown in Figure 4.4. The shape of the aggregation curves of OA and **1a** are different. **1a** shows a sigmoidal shape similar to the Aβ42 control curve (Figure 4.4 Panel A), whereas OA shows a much flatter curve which indicates its better inhibition and better interaction with lower

order aggregates of Aβ42 assemblies that are formed early during their self-assembly (Figure 4.3 Panel B). These observations suggest that the polar and ionic COOH group of OA plays and important role in its binding interactions and inhibition of Aβ42 aggregation.

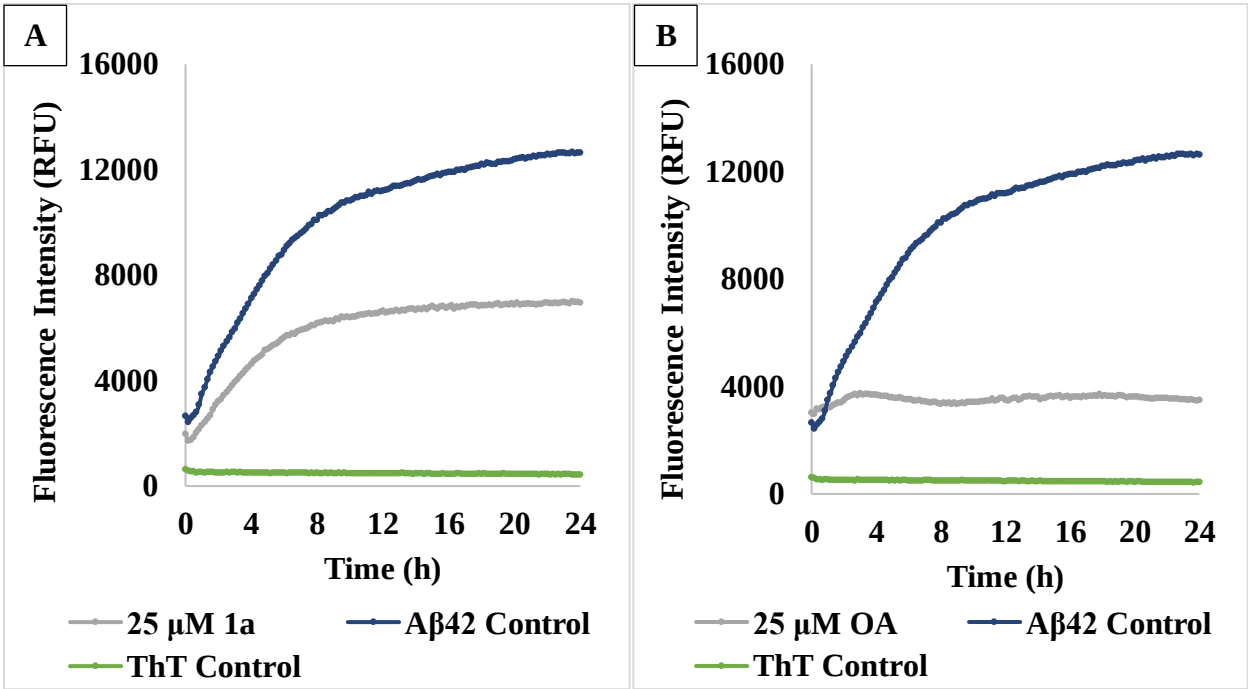

Figure 4.3: ThT-based aggregation kinetics curves of Aβ42 (10 µM) with 25 µM of **1a** (Panel A) and OA (Panel B) over 24 hours at pH 7.4, 37 °C and in phosphate buffer.

LNA is an omega-6 polyunsaturated fatty acid with two double bonds along its hydrophobic tail. The synthesized LNA derivatives **(2a-c)** showed inhibition of ThT-monitored Aβ42 aggregation from 31–64%. The inhibition by **2a-c** was higher than the inhibition shown by LNA which was only 3% or inactive. However, this is contrary to a previous study by the Nekkar Rao lab where LNA showed much stronger inhibition of Aβ420.[158] This contrasting finding is suspected to be caused by potential solubility issues during dilution steps with phosphate buffer and also during the storage process which can lead to compound precipitation. In this study, methyl ester **2a** showed the greatest inhibition activity at 64%, which was the highest among all the

screened synthetic fatty acid derivatives. The Aβ42 aggregation kinetic curves of **2a** and LNA at 25 μM are displayed in Figure 4.4. **2a** largely suppressed the growth phase of the Aβ42 aggregation curve, whereas LNA shows a very similar curve to the Aβ42 control and appears to have no anti-Aβ42 activity. The aggregation kinetic curve for **2a** shows that it was able to reduce both Aβ42 fibril load and fibrillogenesis during the 24-h time period.

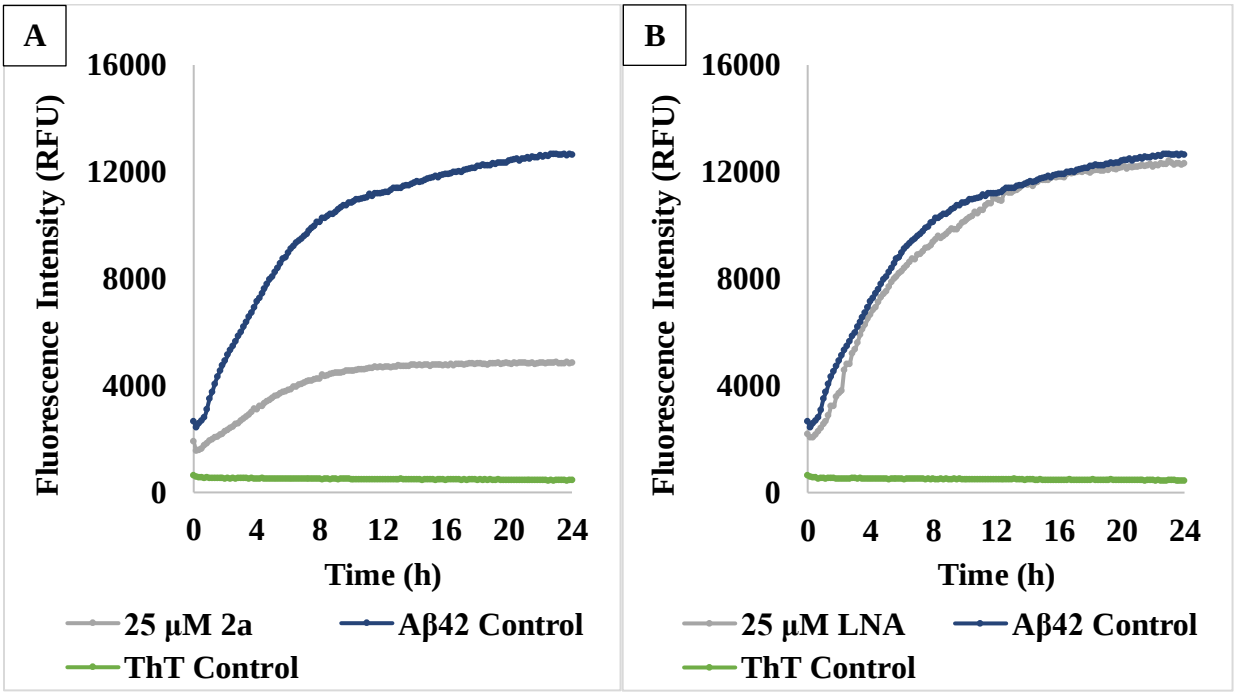

Figure 4.4: ThT-based aggregation kinetics curves of Aβ42 (10 μM) with 25 μM of **2a** (Panel A) and LNA (Panel B) over 24 hours at pH 7.4, 37 °C and in phosphate buffer.

ALA is an omega-3 polyunsaturated fatty acid, and it was found to inhibit Aβ42 aggregation by 20%. ALA was also shown to be an inhibitor of Aβ42 aggregation in the previous study by the Nekkar Rao lab.[158] **3b** showed similar aggregation inhibition (21%) to ALA. **3a,** the methyl ester derivative of ALA, showed increased inhibition activity (57%) compared to ALA. **3a** appears to lengthen the lag phase and suppress the growth phase in the Aβ42 aggregation curve

(Figure 4.5 Panel A). Clearly, **3a** was able to reduce Aβ42 aggregation. The ThT-based Aβ42 aggregation kinetic curve of ALA is shown in Figure 4.5 Panel B for comparison.

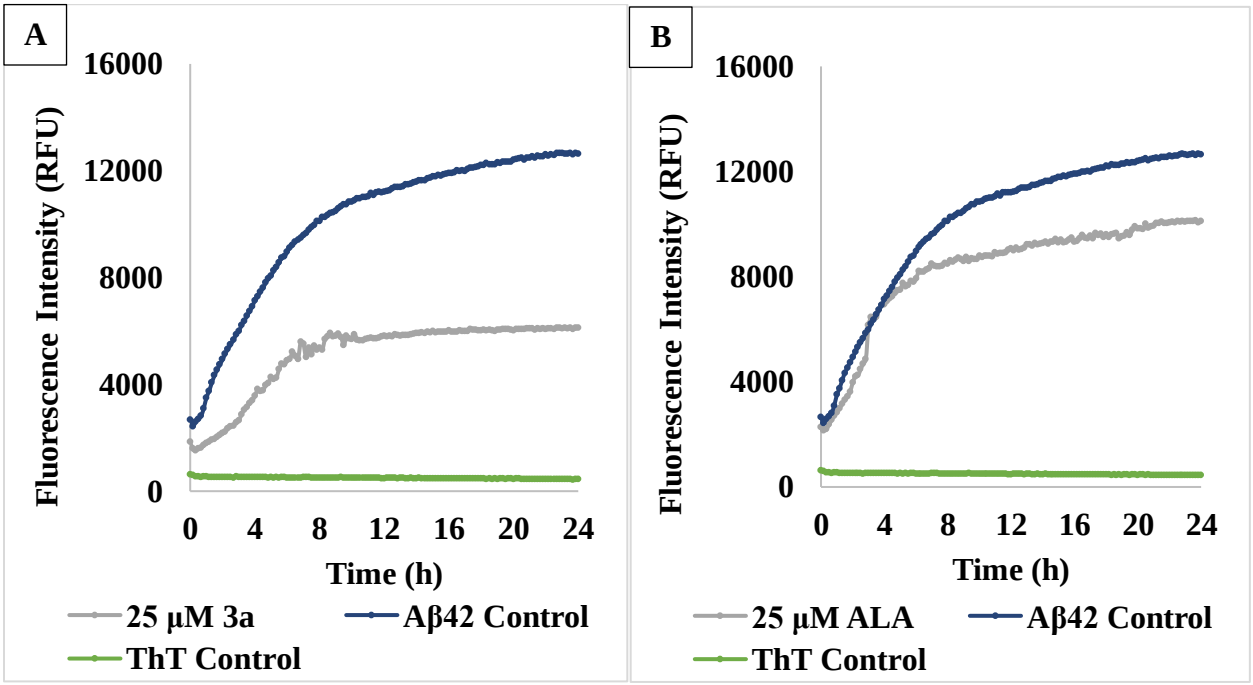

Figure 4.5: ThT-based aggregation kinetics curves of Aβ42 (10 µM) with 25 µM of **3a** (Panel A) and ALA (Panel B) over 24 hours at pH 7.4, 37 °C and in phosphate buffer.

EPA, an omega-3 polyunsaturated fatty acid, was previously shown to be an inhibitor of Aβ42 aggregation.[158] EPA strongly inhibited Aβ42 aggregation in this study (68%), and its methyl ester derivative **4a**, also showed inhibition activity (23%), however it was weaker than the original acid. However, the aggregation kinetics curve for **4a** shows that it did not affect the lag phase, growth phase or saturation phase to a significant extent whereas the parent fatty acid EPA shows a strong suppression of the growth phase compared to the Aβ42 control curve. A comparison of the Aβ42 aggregation kinetics curves of **4a** (Panel A) and EPA (Panel B) are shown in Figure 4.6.

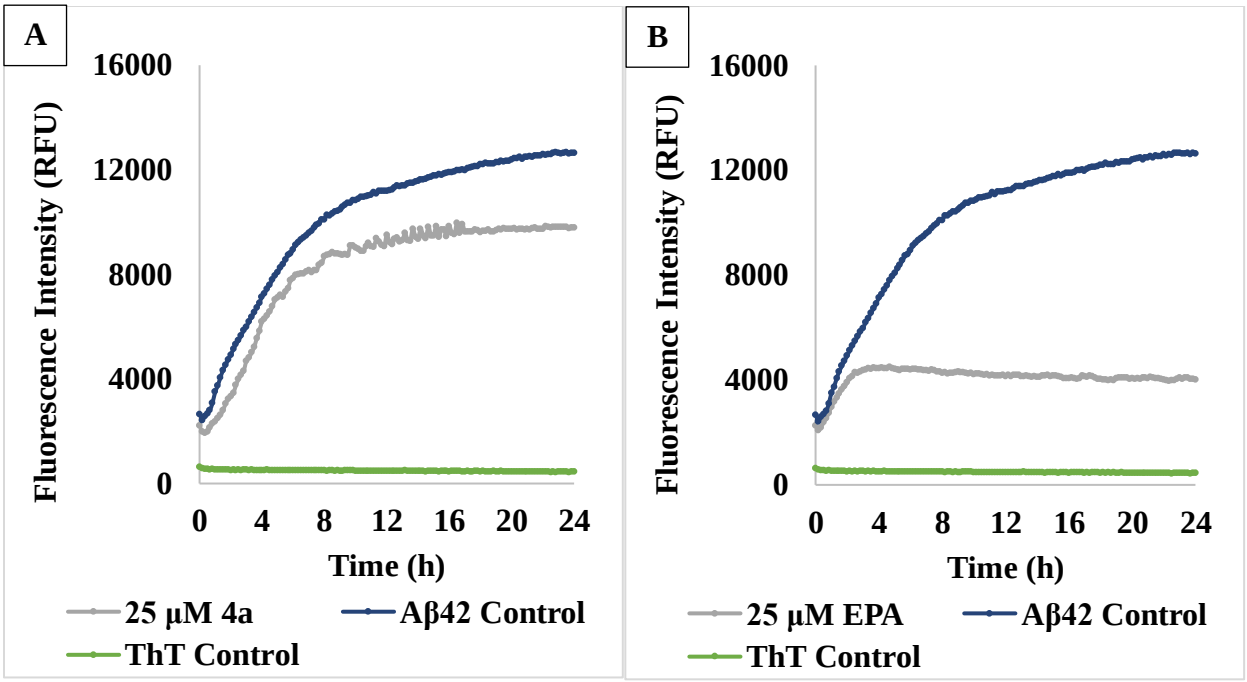

Figure 4.6: ThT-based aggregation kinetics curves of Aβ42 (10 µM) with 25 µM of **4a** (Panel A) and EPA (Panel B) over 24 hours at pH 7.4, 37 °C and in phosphate buffer.

DHA is an omega-3 polyunsaturated fatty acid, and it has the longest hydrophobic tail and number of unsaturated bonds out of all the fatty acids evaluated in this project. DHA and its methyl ester derivative, **5a**, show similar inhibition of Aβ42 aggregation at 44% and 48% respectively. This suggests that replacement of the carboxyl group did not affect its anti-Aβ42 activity, and possibly that there are similar interactions happening with Aβ42 to suppress aggregation despite the change in functional group. Both compounds show a reduction in the growth phase of the Aβ42 aggregation curve in comparison to the Aβ42 control (Figure 4.7).

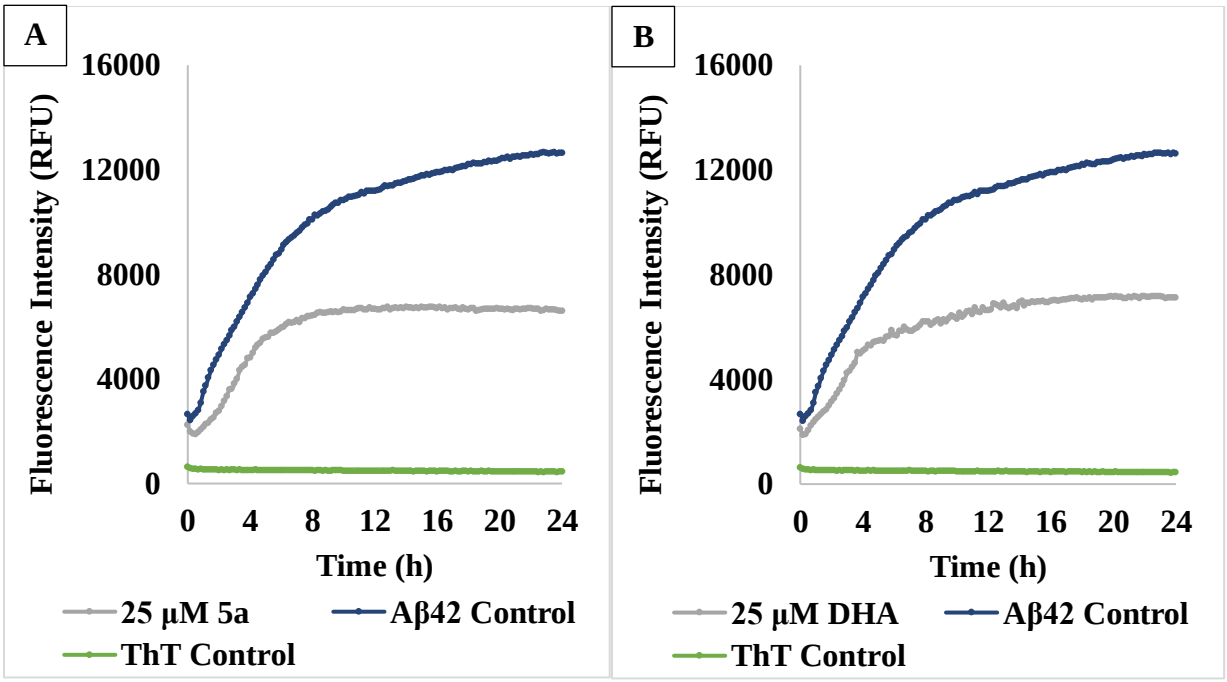

Figure 4.7: ThT-based aggregation kinetics curves of Aβ42 (10 µM) with 25 µM of **5a** (Panel A) and DHA (Panel B) over 24 hours at pH 7.4, 37 °C and in phosphate buffer.

Overall, all the fatty acid derivatives show Aβ42 aggregation inhibition activity, with the methyl ester functional group displaying the most inhibition across compound classes. **1a, 2a,** and **3a** all displayed the highest Aβ42 aggregation inhibition activity when compared to the amide derivatives of the same class (45–61%). **2a** was the most potent inhibitor of Aβ42 aggregation from the derivatives tested, showing a 61% decrease in Aβ42 aggregation. When comparing the Aβ42 aggregation inhibition activity of the parent fatty acids to that of their methyl ester derivatives, inhibition was enhanced for LNA (3% to 61%) and ALA (20% to 51%), a decline is activity for both OA (72% to 45%) and EPA (68% and 22%), and there was little change for DHA (44% to 48%). The difference in number of double bonds, length of the hydrophobic tails and the terminal functional group could affect their binding interactions with Aβ42 and consequently their inhibition profiles.

Interestingly, it should be noted that esters of fatty acids can serve as prodrugs. Masking the polar COOH group with a more lipophilic ester is a common strategy to increase the oral absorption, bioavailability, metabolic stability and in vivo half-life of polar drugs, as well as increase CNS penetration.[159,160] In this regard, the parent fatty acids exhibit CLogP values ranging from 6.8–7.5 which suggests that the fatty acids can get across the CNS as these values are much higher than the Lipinski's rule (CLogP values of 5 or less) for potential drug candidates.[166] The ester derivatives of the fatty acids are expected to be much more lipophilic compared to the parent fatty acids. The results from this study demonstrate that the esterification of fatty acids not only offers a potential prodrug concept, but also shows that even the ester derivatives also possess anti-Aβ activity thereby providing additional SAR optimization strategies to develop novel molecules.

4.2.2 Effect of SARS-CoV-2 Spike Fragment on Aβ42 Aggregation

ThT-based fluorescence kinetic assays were used to determine the effect of the SARS-CoV-2 spike decapeptide, FKNIDGYFKI on Aβ42 aggregation over a 24-h time period. This is the first report where the effect of the amyloidogenic fragment of spike protein was evaluated in the Aβ42 aggregation kinetics assay. The spike protein fragment was tested at 1, 5, 10, 25, and 50 μM concentrations. Resveratrol, a known inhibitor of Aβ42 aggregation, was also tested at the same concentrations for comparison. The Aβ42 aggregation inhibition data at 24-h for the spike protein fragment and resveratrol are shown in Table 4.2.

Table 4.2: ThT-based Aβ42 Aggregation Inhibition Data for Spike Protein Fragment

Compound	% Inhibition (1μM)[a]	% Inhibition (5 μM)[a]	% Inhibition (10 μM)[a]	% Inhibition (25 μM)[a]	% Inhibition (50 μM)[a]
Spike Protein Fragment	52.3 ± 4.5	49.3 ± 10.2	45.4 ± 11.6	37.4 ± 4.3	40.3 ± 0.3
Resveratrol	77.0 ± 4.5	80.6 ± 4.7	88.5 ± 4.7	91.1 ± 3.4	93.4 ± 1.6

[a]The percent inhibition values are based on the inhibition of ThT fluorescence intensity and expressed as the average ± the standard deviation of two independent experiments (n = 3). The values are obtained from ThT-based 24-h aggregation kinetics assay using Aβ42 (10 μM) at pH 7.4 and 37 °C in phosphate buffer.

Interestingly, SARS-CoV-2 spike protein fragment showed inhibition of Aβ42 aggregation at all concentrations (37–52%). This did not appear to be a concentration dependent effect, as at 1 μM, the peptide showed the highest inhibition of Aβ42 aggregation (52%, Table 4.2). The Aβ42 aggregation kinetic curves in the presence of 1, 5, 10, 25, and 50 μM spike decapeptide (Panel A), and the same concentrations of the reference compound resveratrol (Panel B) are displayed in Figure 4.8.

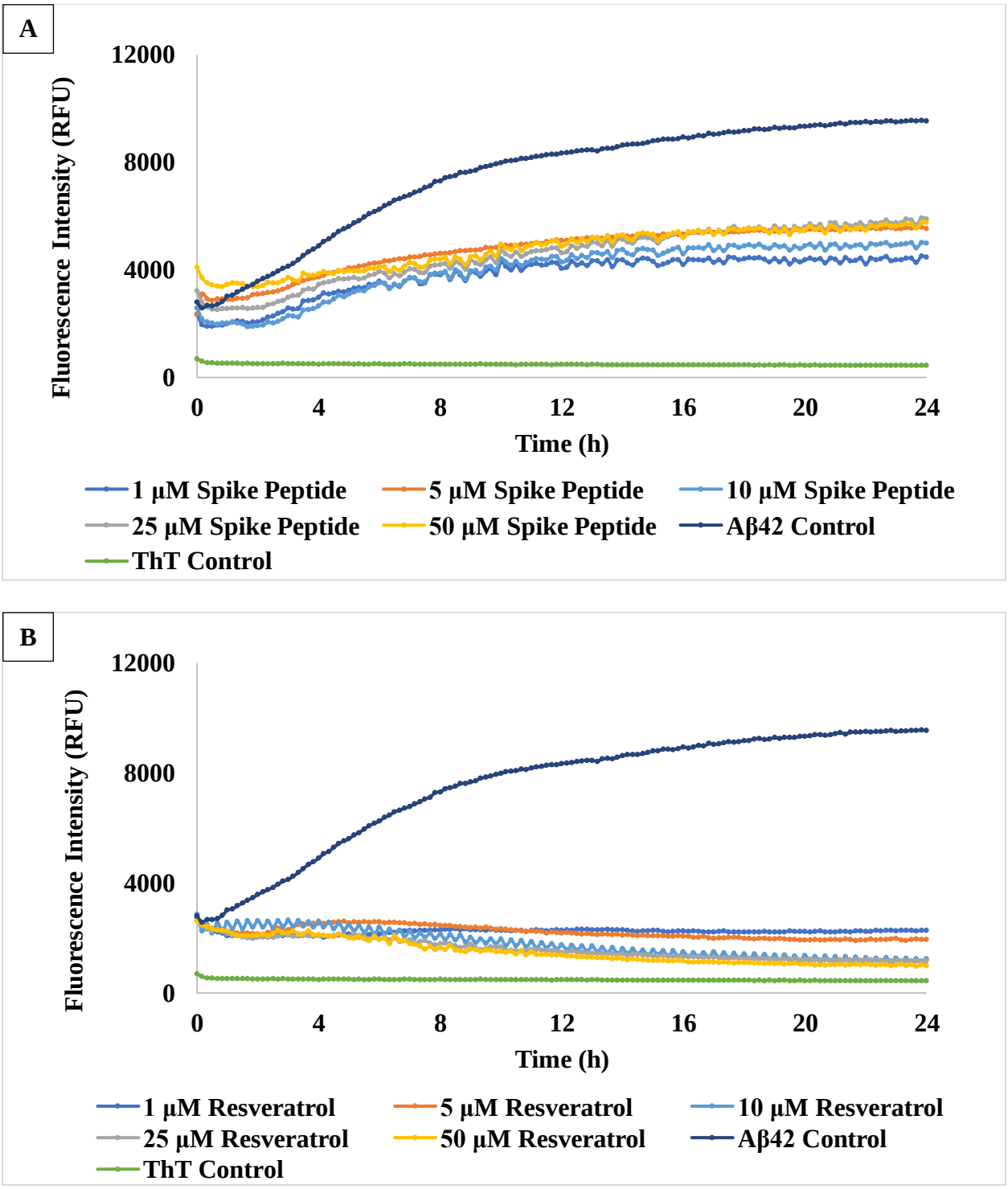

Figure 4.8: ThT-based aggregation kinetics curves of Aβ42 (10 µM) with 1, 5, 10, 25, and 50 µM spike decapeptide (Panel A) and resveratrol (Panel B) over 24 hours at pH 7.4, 37 °C and in phosphate buffer.

In the presence of the spike protein fragment, the lag phase of Aβ42 aggregation was increased at all the tested concentrations (Figure 4.8 Panel A). There was ~2 h extension of the lag phase. Furthermore, the spike protein fragment was able to suppress the growth phase as well at all the tested concentrations. These results show that the spike protein fragment was able to reduce Aβ42 fibrillogenesis at all the tested concentrations. These results were in contrast with our proposed hypothesis, as we expected that the amyloidogenic nature of this decapeptide would work in a synergistic fashion and promote the aggregation of Aβ42. The opposite was observed with up to a 52% decrease in Aβ42 fibrillogenesis upon incubation with the decapeptide. However, this is not surprising, as the KLVFF peptide which is another amyloid-forming peptide derived from Aβ, has also been shown to inhibit the formation of Aβ42 fibrils.[167] The similarity in the structures of these amyloid-forming peptides could allow them to bind to one another and inhibit the formation of higher-order structures like fibrils. Furthermore, the lack of concentration-dependent effect of the spike protein fragment on Aβ42 aggregation suggests the possibility of the interaction of the shorter spike peptide aggregates with the longer Aβ42. These results demonstrate the ability of the spike peptide fragment to inhibit Aβ42 aggregation, and the need for further exploration of the interactions of these peptides to gain insight on their role in SARS-CoV-2 and AD comorbidity. Additionally, structural features of the spike peptide can be exploited when designing novel Aβ42 aggregation inhibitors.

4.3 Transmission Electron Microscopy (TEM) Studies

TEM studies were used to examine the effect of the lead fatty acid derivatives that exhibited anti-Aβ activity in the ThT based fluorescence assay. The effect of 25 μM of derivatives **1a, 2a, 3a, 4a, 5a** on Aβ42 aggregation morphology was determined after 24-h incubation. A similar study

was also carried out with the SARS-CoV-2 spike decapeptide (50 μM) to determine its effect on the aggregation morphology of Aβ42 after 24-h. These studies further support the anti-Aβ42 activity observed in the ThT-based Aβ42 aggregation kinetic assays.

4.3.1 TEM Studies of Fatty Acid Derivatives with Aβ42

Incubation of Aβ42 (10 μM) alone over a 24-h period led to the formation fibril-rich, dense aggregates (Figure 4.10, Panel A). In contrast, when Aβ42 (10 μM) was incubated with 25 μM of the fatty acid derivatives (**1a, 2a, 3a, 4a** and **5a),** there was a significant decline in the fibril formation compared to Aβ42 control image (Figure 4.10 Panels A–F).

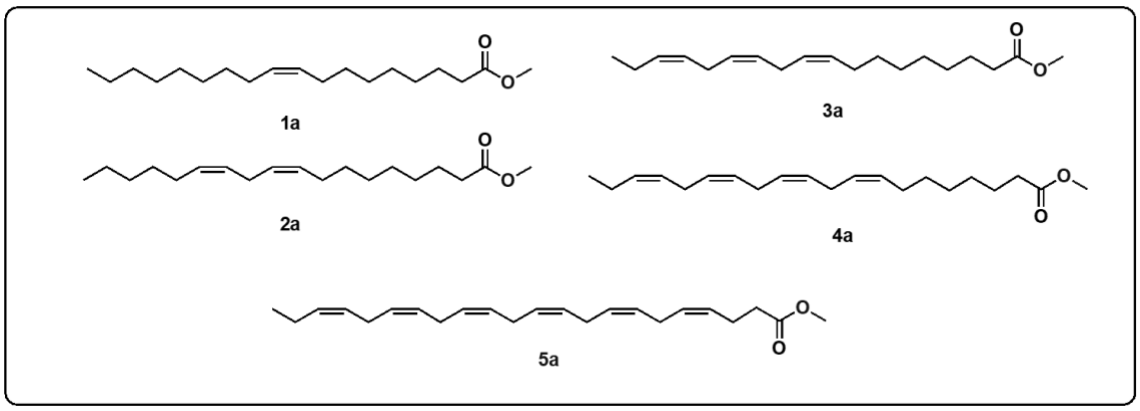

Figure 4.9: The chemical structures of the fatty acid derivatives used in the TEM experiments (**1a, 2a, 3a, 4a** and **5a**).

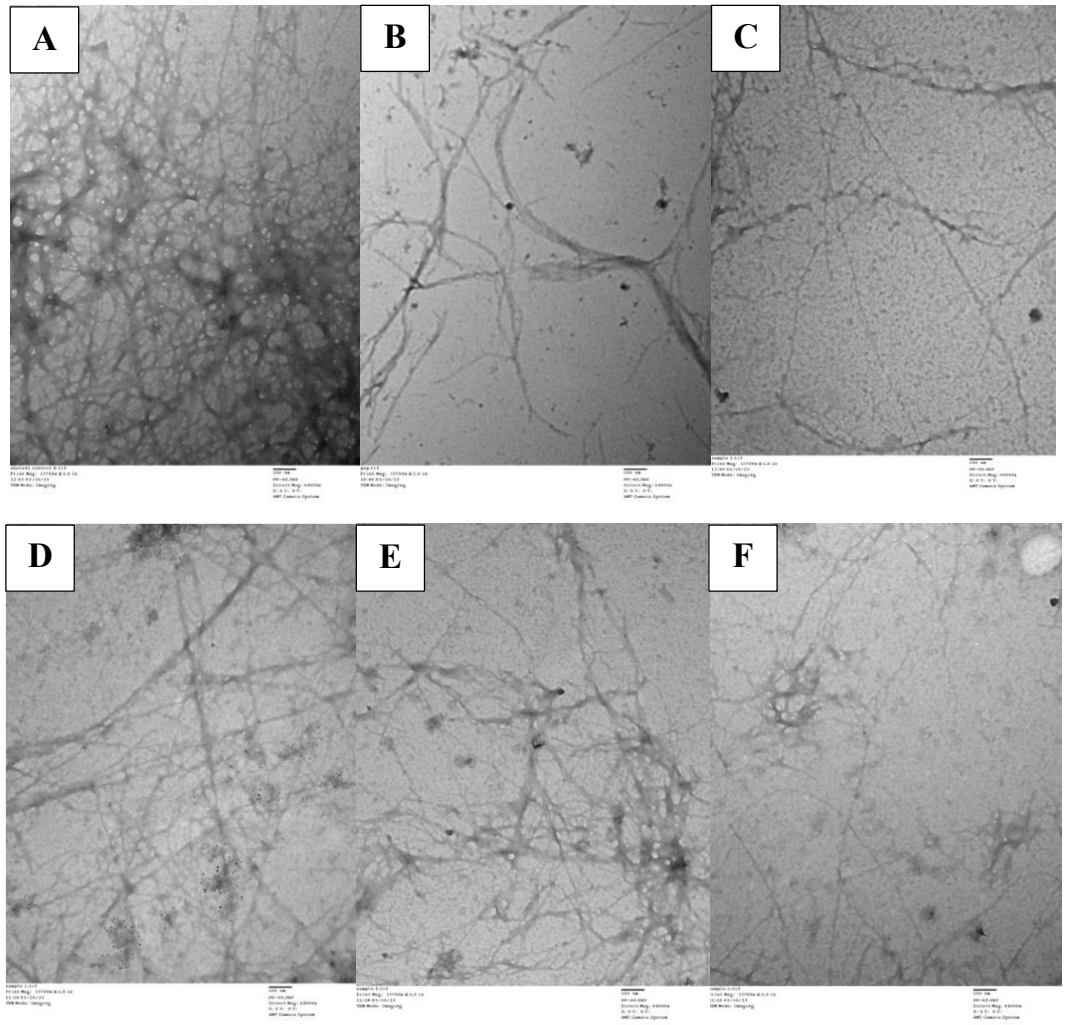

Figure 4.10: TEM images of Aβ42 (10 μM) incubated for 24 hours alone (Panel A), with 25 μM of **1a** (Panel B), **2a** (Panel C), **3a** (Panel D), **4a** (Panel E), and **5a** (Panel F). 100 nm scale.

TEM images obtained show that all lead compounds (**1a, 2a, 3a, 4a** and **5a)** showed a reduction in the formation of fibrils compared to the Aβ42 control (Panel A) as displayed in Figure 4.10. Particularly, the images with **1a** (Panel B) and **2a** (Panel C) show a large reduction in the Aβ42 fibril formation. These results support findings from the ThT-based Aβ42 aggregation kinetics assays and confirm the ability of these lead compounds to inhibit aggregation of Aβ42 into higher order structures.

4.3.2 TEM Studies of Spike Protein Fragment with Aβ42

TEM assessment was also conducted with the SARS-CoV-2 spike decapeptide FKNIDGYFKI at 50 μM in the presence of Aβ42 (10 μM). for 24-h. When comparing the images of the Aβ42 control (Panel A, Figure 4.11) to that with Aβ42 and 50 μM decapeptide (Panel B, Figure 4.11), there was a significant reduction in fibril formation as shown in in Figure 4.11. These images support the findings from the ThT-based Aβ42 aggregation kinetics assays and provides further evidence that the spike protein fragment can inhibit Aβ42 aggregation.

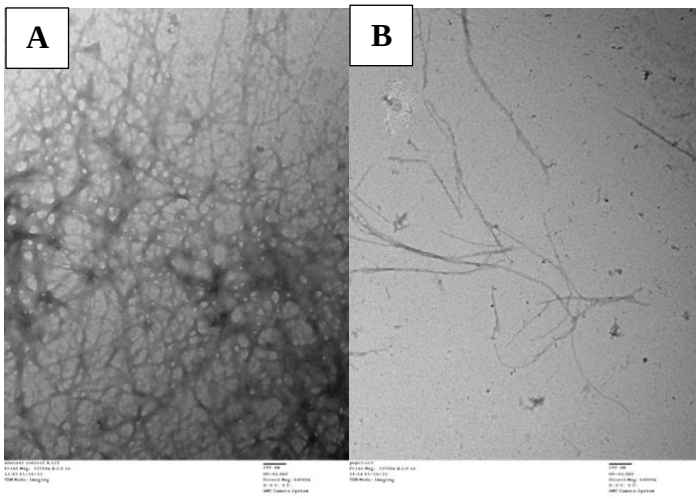

Figure 4.11: TEM images of Aβ42 (10 μM) incubated for 24 hours alone (Panel A), and with 50 μM of SARS-CoV-2 spike decapeptide FKNIDGYFKI (Panel B). 100 nm scale.

4.4 Molecular Docking Studies

The interactions of fatty acid derivatives that exhibited over 40% inhibition of Aβ42 aggregation (**1a**, **2a**, **2b**, **3a** and **5a**) were investigated with molecular docking studies. The top docked ligand pose obtained was analyzed by studying binding modes, conformation, and polar and non-polar contacts in the Aβ42 oligomer model. The solid-state NMR structure of an Aβ42 amyloid fibril was used to obtain the Aβ42 oligomer model.[168] A similar study was carried out to

determine the binding interactions of the uncapped spike protein fragment FKNIDGYFKI. These computational investigations provide further insights on the ability of these ligands to reduce Aβ42 fibrillogenesis.

4.4.1 Molecular Docking Studies of Fatty Acids in the Aβ42 Oligomer Model

The solved structures of Aβ42 fibrils show that it exhibits a horseshoe or S-shape.[61,168] In solution, Aβ42 can exist either as a pentamer or hexamer and we used the Aβ42 pentamer model to carry out molecular docking studies of fatty acid derivatives that exhibited greater than 40% inhibition of Aβ42 aggregation based on the ThT-based aggregation kinetics experimental data.[169,170]

The docked pose of **1a** (OA derivative, 45% inhibition) shows that it was able to orient at the narrow interface between the N- and C-termini (Figure 4.12). The alkyl tail was interacting with non-polar regions consisting of amino acids Gln15, Leu17 and Leu34. The methyl, methylene and the alkene groups of **1a**, underwent a number of van der Waals and hydrophobic interactions with side chains of Leu34 (distance < 5 Å). The ester substituent was oriented closer to the polar amino acid His14 at the N-terminus. The backbone N*H* of His14 underwent hydrogen bonding interaction with the oxygen atom of *O*Me (distance = 2.0 Å), Figure 4.12).

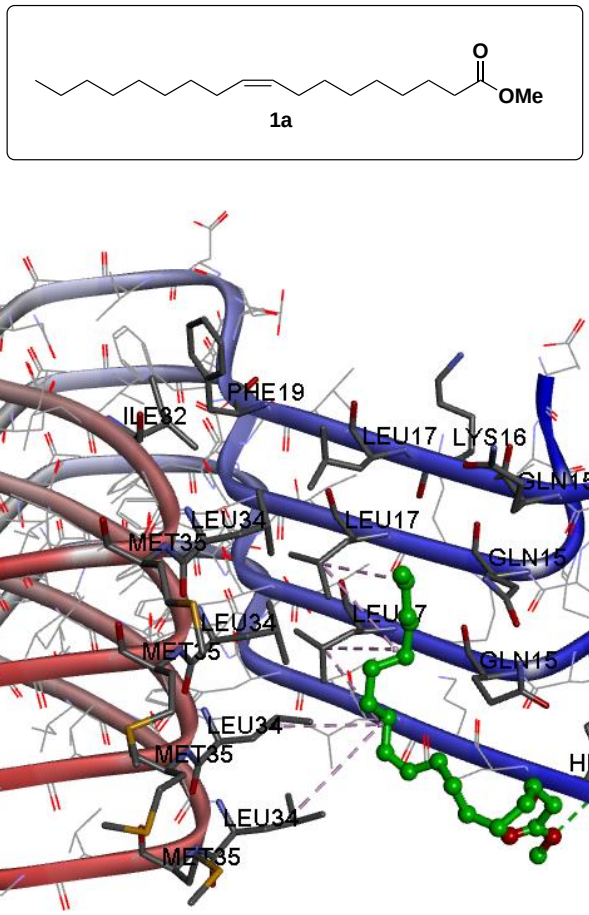

Figure 4.12: The binding interactions of **1a** (ball and stick) in the Aβ42 pentamer model (pdb id: 5KK3). The pentamer is shown as a ribbon diagram with the N- and C-termini color coded as blue and red respectively. The hydrogen atoms were removed to enhance clarity (LibDock Score = 115.60). Only the key regions of Aβ42 in contact with the ligand are shown.

The docking of the LNA ester derivative (**2a**, 61% inhibition) in the Aβ42 pentamer model shows that it was also able to bind in the narrow channel formed by the N- and C-termini (Figure 4.13). **2a** exhibited a linear extended conformation and underwent a number of van der Waals and hydrophobic contacts with side chains of Leu17 and Leu34 (distance < 5 Å). The ester moiety was oriented in a different region compared to **1a** and was surrounded by Lys16, Leu17 and Val18 (distance < 5 Å). The O*Me* of ester was in contact with Val18 side chain via hydrophobic

interactions and the C=*O* of ester was forming a hydrogen bond with the backbone N*H* of Val18 (distance = 1.9 Å, Figure 4.13).

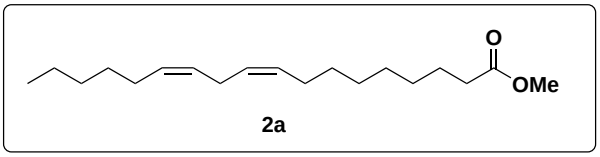

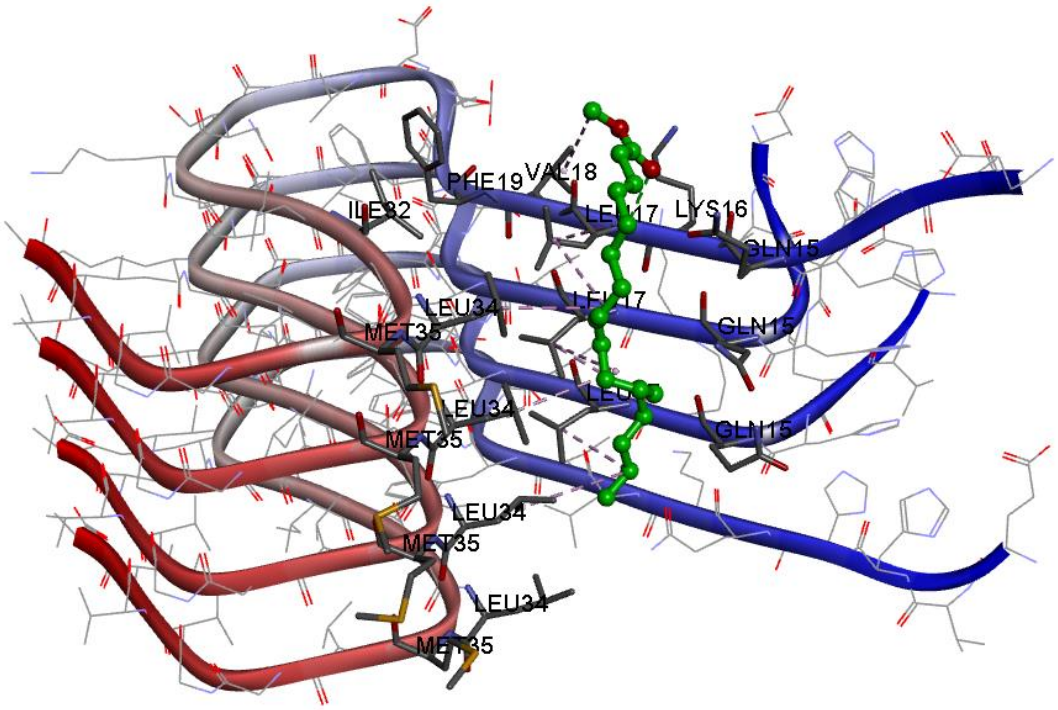

Figure 4.13: The binding interactions of **2a** (ball and stick) in the Aβ42 pentamer model (pdb id: 5KK3). The pentamer is shown as a ribbon diagram with the N- and C-termini color coded as blue and red respectively. The hydrogen atoms were removed to enhance clarity (LibDock Score = 103.51). Only the key regions of Aβ42 in contact with the ligand are shown.

The interactions of the corresponding amide derivative **2b** (LNA derivative, 41% inhibition) shows that the amide substituent was oriented closer to a polar region in the Aβ42 pentamer model, whereas the alkyl tail was oriented in the narrow N- and C-termini interface (Figure 4.14). One of the amide hydrogens underwent hydrogen bonding interaction with

backbone C=*O* of Gln15 (distance = 2.1 Å), whereas the amide C=*O* was in contact with the backbone N*H* of His14 (distance = 2.5 Å, Figure 4.14). The alkyl tail underwent a number of van der Waal's and hydrophobic interactions with Leu17 and Leu34 side chains (distance < 5 Å).

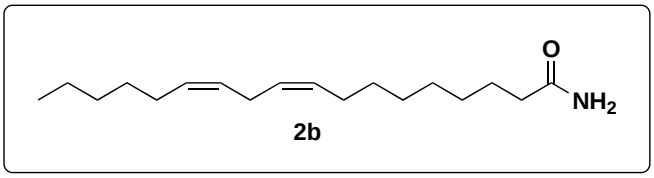

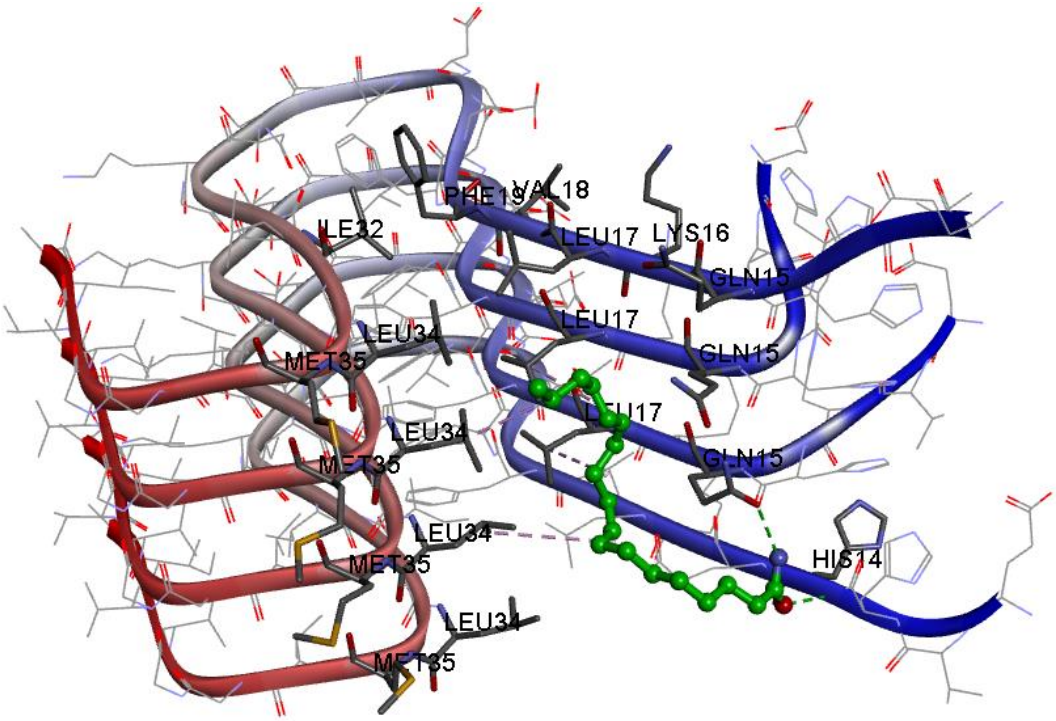

Figure 4.14: The binding interactions of **2b** (ball and stick) in the Aβ42 pentamer model (pdb id: 5KK3). The pentamer is shown as a ribbon diagram with the N- and C-termini color coded as blue and red respectively. The hydrogen atoms were removed to enhance clarity (LibDock Score = 107.78). Only the key regions of Aβ42 in contact with the ligand are shown.

The binding interactions of the ALA derivative **3a** (51% inhibition) was investigated using the Aβ42 pentamer model (Figure 4.15). This study shows that similar to **1a** and **2b**, the methyl ester group was oriented toward a polar region consisting of His13 and His14 (Figure 4.15),

whereas the alkyl tail was interacting with nonpolar amino acids Leu17 and Leu34 (Figure 4.15). The O*Me* of the ester group was in van der Waal's contact with the aromatic ring of His13 (π-alkyl, distance < 5 Å). The ester C=*O* was in contact with backbone NH of His14 (distance = 2.6 Å). The methyl, methylene and alkene groups were in hydrophobic contact with Leu17 and Leu34 side chains (distance < 5 Å).

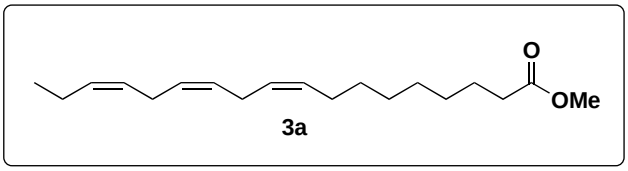

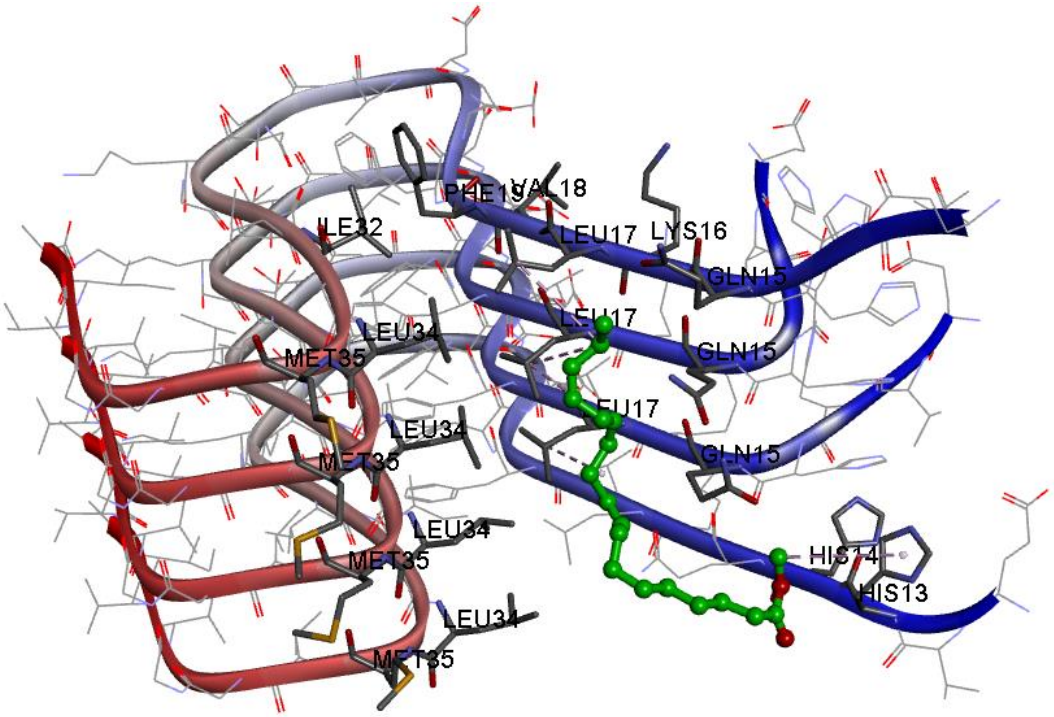

Figure 4.15: The binding interactions of **3a** (ball and stick) in the Aβ42 pentamer model (pdb id: 5KK3). The pentamer is shown as a ribbon diagram with the N- and C-termini color coded as blue and red respectively. The hydrogen atoms were removed to enhance clarity (LibDock Score = 105.85). Only the key regions of Aβ42 in contact with the ligand are shown.

Figure 4.16 shows the docked pose of **5a** (DHA derivative, 47.5% inhibition) in the Aβ42 pentamer model. **5a** contains a long lipophilic tail made up of 22-carbons and this was oriented in narrow groove lined by nonpolar amino acids Leu17, Leu34 and Met35 where it underwent van der Waal's and hydrophobic interactions (distance < 5 Å). The ester O*Me* was in contact with side chains of Leu17 and Leu34 (distance < 5 Å).

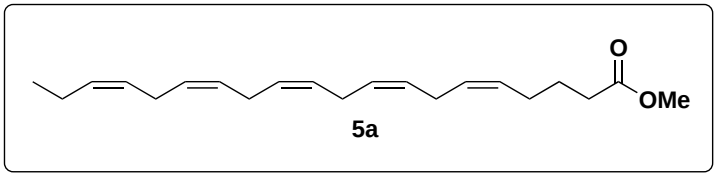

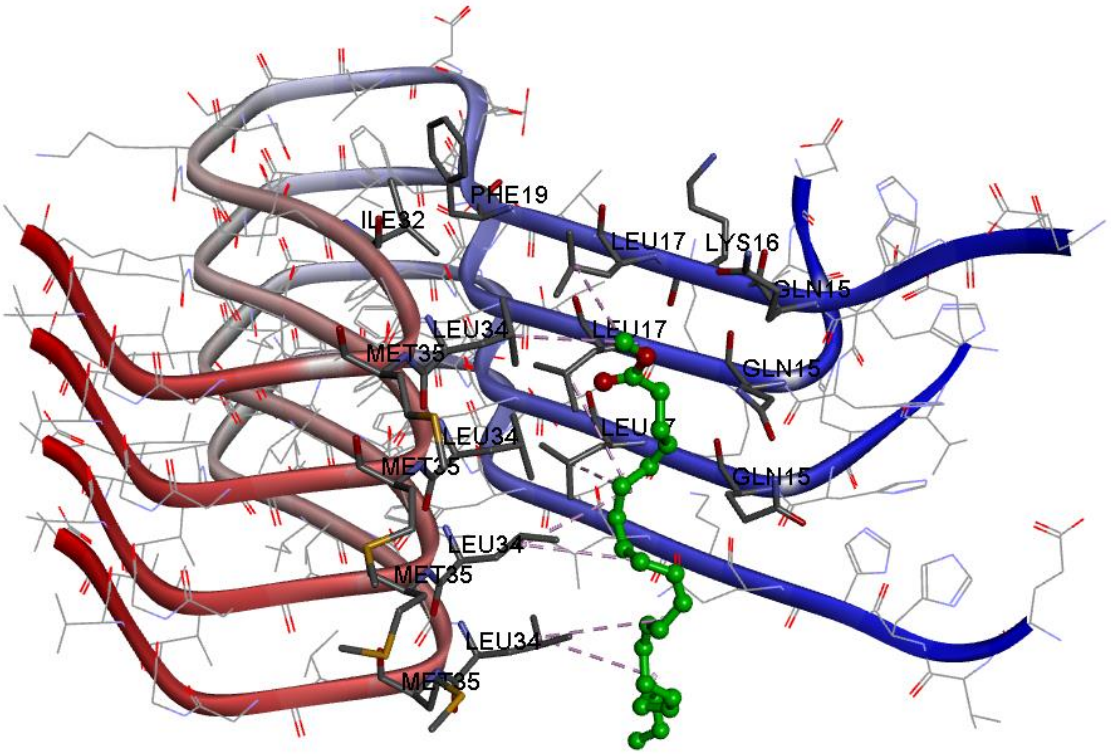

Figure 4.16: The binding interactions of **5a** (ball and stick) in the Aβ42 pentamer model (pdb id: 5KK3). The pentamer is shown as a ribbon diagram with the N- and C-termini color coded as blue and red respectively. The hydrogen atoms were removed to enhance clarity (LibDock Score = 115.60). Only the key regions of Aβ42 in contact with the ligand are shown.

The molecular docking studies of fatty acid derivatives show that they all bind in a common region at the interface between the N- and C-termini in the Aβ42 pentamer model. This region is fairly hydrophobic due to the presence of Leu16, Leu17, Leu34 and Met35 at the C-terminus. All the derivatives possessing long alkyl chains primarily interact with side chains of Leu17 and Leu34, and also with Gln15 side chains, closer to the N-terminus. The ester groups of the derivatives can orient in polar region such as His13 and His14, or near Lys16 or Val18 where they undergo polar interactions. The binding of the fatty acid derivatives to the Aβ42 pentamer can stabilize it and reduce its oligomerization into more toxic species. The 19-carbon LNA ester derivative **2a** exhibited maximum inhibition of Aβ42 aggregation (61%) in the ThT-based Aβ42 aggregation kinetics studies and its binding to Aβ42 pentamer shows that it was able interact in the entire region of the narrow interface and that its carbon chain was not exposed to solvent. This shows that **2a** can exhibit efficient binding which supports its better inhibition activity among the evaluated fatty acid derivatives. This information is useful, as the SAR data for the fatty acid derivatives can be used for designing novel Aβ42 aggregation inhibitors, as well as better understanding the interactions of Aβ42 and fatty acids.

4.4.2 Molecular Docking Studies of Spike Protein Fragment in the Aβ42 Oligomer Model

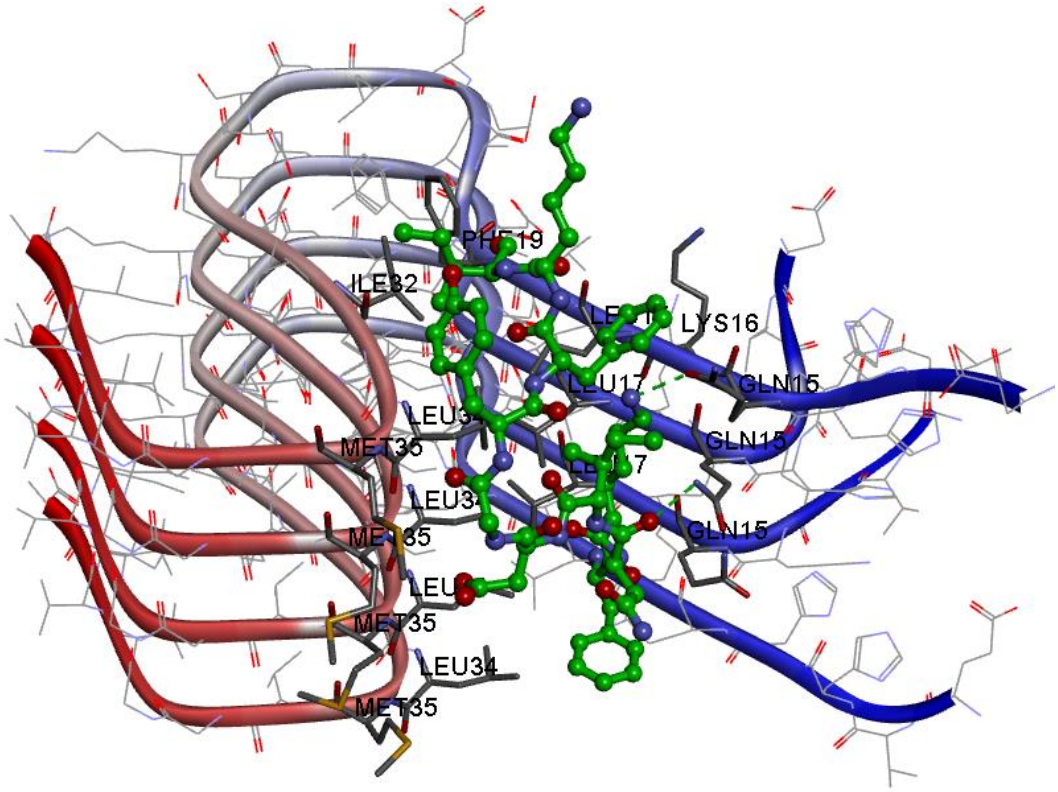

Figure 4.17: The binding interactions of the spike protein fragment FKNIDGFYKI (ball and stick) in the Aβ42 pentamer model (pdb id: 5KK3). The pentamer is shown as a ribbon diagram with the N- and C-termini color coded as blue and red respectively. The hydrogen atoms were removed to enhance clarity (LibDock Score = 180.63). Only the key regions of Aβ42 in contact with the ligand are shown.

The binding interactions of spike protein fragment FKNIDGFYKI was investigated in the Aβ42 pentamer model (Figure 4.17). The decapeptide was interacting in the entire narrow channel formed between the N- and C-terminal in the pentamer assembly and exhibited a perpendicular orientation along the fiber axis. The spike peptide underwent several polar and nonpolar contacts with the Aβ42 pentamer. The Lys194 side chain (F*K*NIDGFYKI) was forming a hydrogen bonding

interaction with Gln15 amide side chain (C*O*NH_2, distance = 1.6 Å, Figure 4.17) closer to the N-terminal. Amino acids Gly199, Phe200 and Tyr201 (FKNID*GFY*KI) were in contact with Leu34 and Met35 side chains via π-alkyl and hydrophobic interactions (distance < 5Å) near the C-terminal. Furthermore, additional hydrophobic contacts were seen with Ile203 (FKNIDGFYK*I*) and side chains of Phe19 and Ile32 at the C-terminal (distance < 5Å), and the Gln15 side chain of Aβ42 was in contact with Phe193 (distance = 2.7 Å). These interactions stabilize the pentamer assembly and reduce the conversion of Aβ42 into more toxic species. This study also shows that aromatic amino acids (eg: phenylalanine and tyrosine) along with polar amino acids (eg: lysine and glutamine) present in the spike protein decapeptide fragment, play a key role in their binding and inhibition of Aβ42 aggregation. These structural features can be exploited to design novel peptide and small molecule-based inhibitors of Aβ42 aggregation.

4.5 Cell Viability Assays

Cell counting kit-8 (CCK-8) was used to examine the effect of the library of fatty acid derivatives on mouse hippocampal HT22 neuronal cell viability over a 24-h time period. A similar experiment was carried out using the full-length SARS-CoV-2 spike protein to determine its effect on HT22 cell viability. The cells were incubated with treatments for 24-h, after which CCK-8 was used to assess the cell viability for each treatment group compared to untreated cells by measuring absorbance at 450 nm using the microplate reader.

4.5.1 Effect of Fatty Acid Derivatives on Cell Viability

HT22 cells were incubated with 25 μM of the synthesized fatty acid derivatives (**1a-c, 2a-c, 3a, 3b, 4a** and **5a)** for 24-h. Resveratrol was used as a reference compound. The results of the HT22 cell viability assay are listed in Table 4.3.

Table 4.3: HT22 Cell Cytotoxicity Assay Data for Fatty Acid Derivatives

Compound (25 uM)	% Cell Viability[a]
1a (R = OMe)	94.4 ± 10.5
1b (R = NH_2)	104.1 ± 9.4
1c (R = Piperidinyl)	98.1 ± 0.3
2a (R = OMe)	100.8 ± 0.1
2b (R = NH_2)	103.2 ± 5.5
2c (R = Piperidinyl)	104.3 ± 3.7
3a (R = OMe)	103.8 ± 7.6
3b (R = NH_2)	120.4 ± 14.7
4a (R = OMe)	92.8 ± 7.7
5a (R = OMe)	96.4 ± 1.4
Resveratrol	94.5 ± 8.1

[a]The percent cell viability values are based on the inhibition of absorbance values relative to untreated cells and expressed as the average ± the standard deviation of two independent experiments (n = 6). The values are obtained from CCK-8 assays on HT22 cells.

Cell viability studies show that the fatty acid derivatives were not toxic to HT22 mouse hippocampal neuronal cells and exhibited viability in the range of 93–120% at 25 μM (Table 4.3). Resveratrol was also not toxic to HT22 cells. A summary of cell viability data for the fatty acid derivatives and resveratrol at 25 μM is displayed in Figure 4.18. These cell viability studies demonstrate that the changing the acidic moiety to esters did not affect their cytotoxicity to HT22 hippocampal neuronal cells.

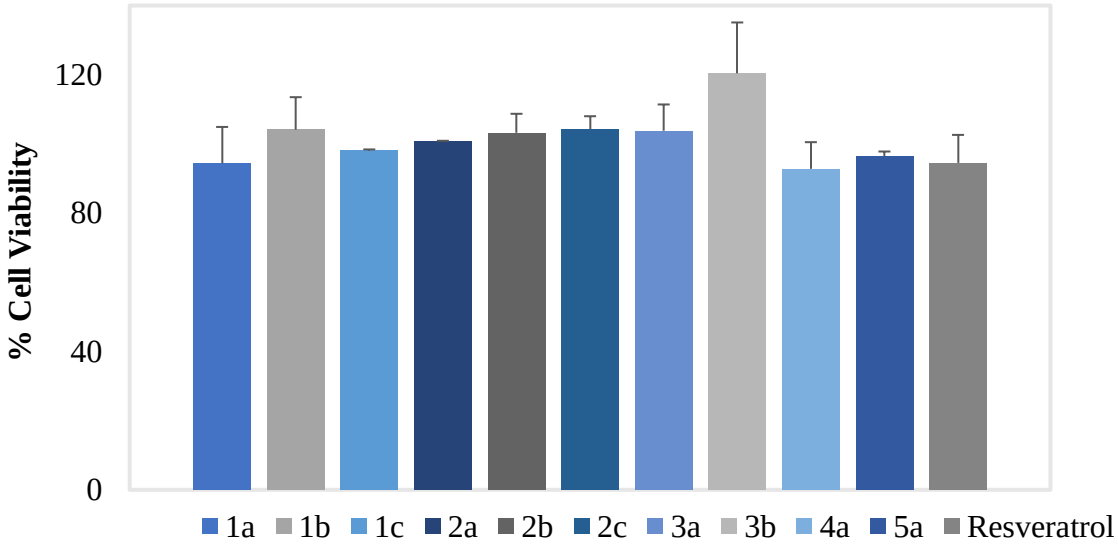

Figure 4.18: HT22 cell cytotoxicity assay data after 24-hour incubation with 25 μM of 1a-c, 2a-c, 3a, 3b, 4a, 5a, and resveratrol.

4.5.2 Effect of of Full-Length SARS-CoV-2 Spike Protein on Cell Viability

HT22 cells were incubated with 5 ng/mL and 10 ng/mL of full-length SARS-CoV-2 spike protein for 24 hours. Quercetin at 10 μM was used as a reference compound. The results of the HT22 cell viability assay are shown in Table 4.4.

Table 4.4: HT22 Cell Cytotoxicity Assay Data for Spike Protein

Treatment	% Cell Viability
Spike Protein 5 ng/mL	101.4 ± 13.9
Spike Protein 10 ng/mL	112.4 ± 11.5
Quercetin 10 μM	102.3 ± 24.1

[a]The percent cell viability values are based on the inhibition of absorbance values relative to untreated cells and expressed as the average ± the standard deviation of two independent experiments (n = 5). The values are obtained from CCK-8 assays on HT22 cells.

Based on these results and contrary to our hypothesis, full-length spike protein did not show toxicity to HT22 cells at the 5 ng/mL and 10 ng/mL concentrations. Relative to untreated cells, viability for the treated cells was greater than 100%. Thus, at the 5 ng/mL and 10 ng/mL concentrations and 24-h incubation time, the spike protein did not show a decrease in cell counts relative to untreated cells. The control compound quercetin was also non-toxic to HT22 cells. The cell viability assay data is displayed in Figure 4.19. It should also be noted that the spike protein might cause a concentration-dependent effect on cell viability. In addition, spike protein is known to increase the cell permeability and promote the formation of proinflammatory mediators which can lead to time-dependent cytotoxicity to cells. Therefore, further investigation is required to study the cytotoxicity of spike protein to brain cells.[171]

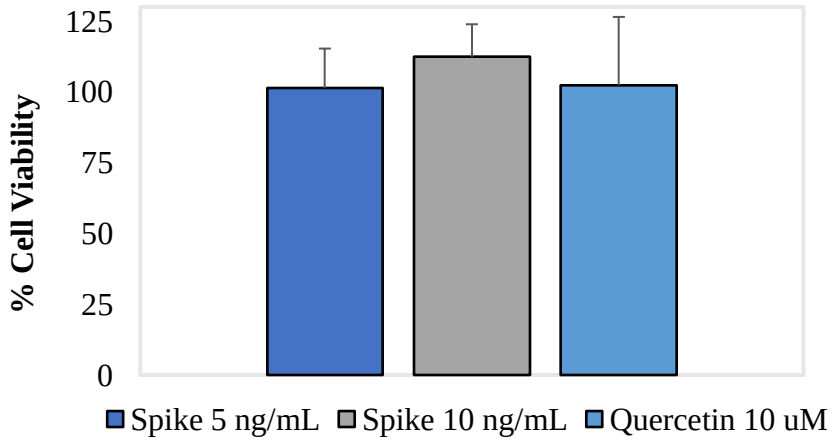

Figure 4.19: HT22 cell cytotoxicity assay data after 24h incubation with 5 ng/mL and 10 ng/mL full length SARS-CoV-2 spike protein**,** and quercetin.

Chapter 5: Conclusion & Future Directions

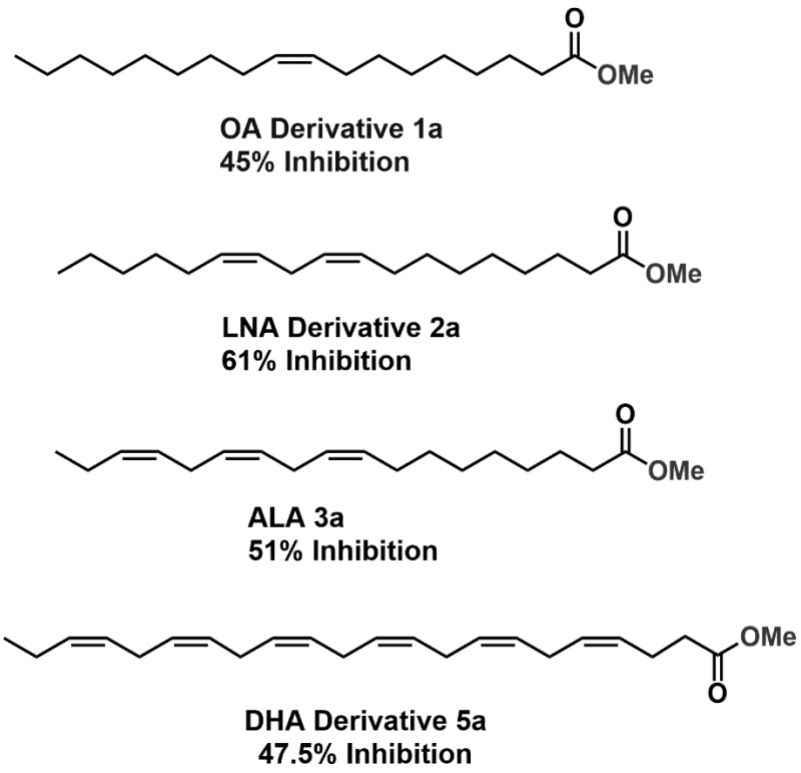

Figure 5.1: Chemical structures of lead fatty acid derivatives with anti-Aβ42 activity (**1a, 2a., 3a, 5a**).

The primary objective of this thesis was to synthesize and evaluate novel fatty acid derivatives that can exhibit Aβ42 aggregation inhibition. A library of 10 fatty acid derivatives were synthesized and the carboxylic acid group was replaced with methyl esters, amides, or cyclic piperidine substituents. These fatty acid derivatives were characterized by ^{1}H NMR and LC-MS. Their anti-Aβ42 activity was evaluated in vitro using ThT-based aggregation kinetic studies which led to the identification of derivatives **1a**, **2a**, **3a** and **5a** (Figure 5.1) that exhibited moderate to good inhibition activity of Aβ42 aggregation (45–61% inhibition at 25 μM). **2a**, the methyl ester of LNA showed the greatest inhibition of Aβ42 aggregation at 61%. Investigating the Aβ42 morphology by TEM studies also confirmed the anti-Aβ42 activity of the leading compounds.

Therefore, changing the fatty acids to their corresponding methyl esters led to retention of anti-Aβ42 activity. Furthermore, cell culture studies demonstrated that the derivatives were not toxic to HT22 mouse hippocampal cells (cell viability ~94–104% at 25 μM). Additionally, methyl esters could serve as potential prodrugs for their corresponding acids. Computational modeling studies suggest that the ester derivatives of the fatty acids are more lipophilic and can interact with a hydrophobic surface in the Aβ42 pentamer assembly which helps in preventing further conversion of the pentamer into more toxic oligomers.

The secondary objective of this proposal was to determine the interactions of the amyloidogenic peptide fragment derived from the SARS-CoV-2 spike protein, decapeptide FKNIDGYFKI. The ThT-based aggregation kinetic studies showed that this peptide was acting as an inhibitor of Aβ42 aggregation at all the tested concentrations, which did not align with our original hypothesis. This is a novel and interesting discovery which suggests that the spike protein decapeptide sequence offers a unique opportunity to discover both peptide- and small molecule-based novel Aβ42 aggregation inhibitors. Additionally, full-length SARS-CoV-2 spike protein did not show toxicity to HT22 cells. Our results further emphasize that the risk of increased mortality in AD patients with COVID-19 is a complex topic and that several factors are at play including triggering of inflammatory mediators by the SARS-CoV-2 spike protein as well as the existing neuroinflammatory events in AD patients, and further research is needed to understand their relationship.

The results of this study provide evidence that both the synthesized fatty acid derivatives, and unexpectedly, a SARS-CoV-2 peptide fragment, are inhibitors of Aβ42 aggregation. This information is valuable for studying Aβ42 aggregation and designing both small molecule-based and peptide-based novel inhibitors of Aβ42 aggregation. Additionally, this research sheds light on

the interactions between Aβ42 and SARS-CoV-2 spike protein and emphasizes the need to expand research in this field to gain a better understanding of the mechanisms behind AD and COVID-19 as well as how they interact in order to provide the best treatment options to patients.

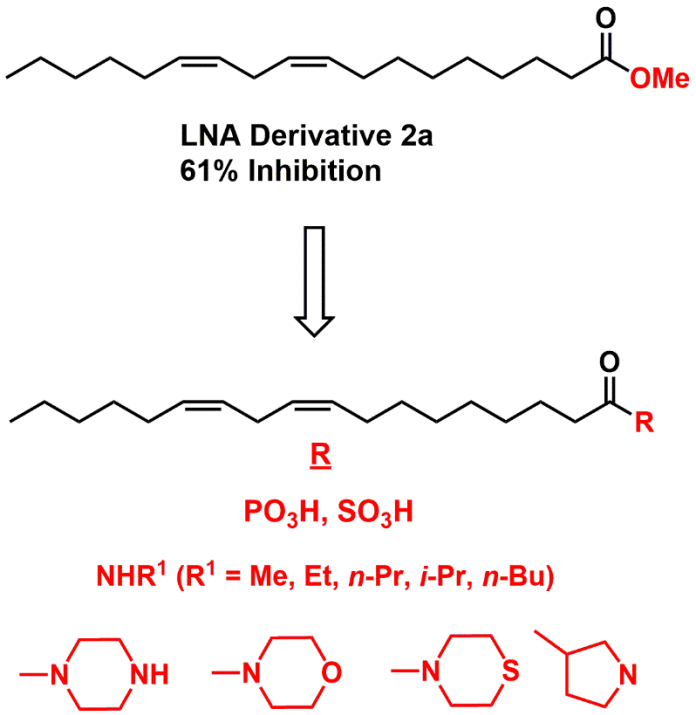

Figure 5.2: Proposed modification of fatty acids as novel inhibitors of Aβ42 aggregation.

To expand on this research, other acidic bioiosteres such as PO_3H or SO_3H groups can be explored to investigate their impact on Aβ42 aggregation and whether they can maintain the inhibitory activity of their parent fatty acids. In addition, other cyclic and acylic amines with various electronic and steric properties can be incorporated to study their effect on Aβ42 aggregation (Figure 5.2). More proposed studies include the evaluation of promising fatty acid derivatives to protect HT22 hippocampal cells from Aβ42-induced neurotoxicity, and to carry out similar experiments with the spike protein decapeptide fragment. Other peptides from SARS-CoV-

2 can also be investigated for their impact on Aβ42 aggregation to shed more light on the complex relationship between AD and COVID-19.

The results from this study and future studies will provide insight on the Aβ aggregation mechanism and the disease process of AD. Additionally, this study has provided novel data on the interactions of Aβ42 with spike protein fragment and fatty acids, which are biologically relevant molecules. Furthermore, the SAR data obtained from these studies will be useful for identifying promising structural features when designing both peptide and small-molecule-based novel Aβ aggregation inhibitors.

References

1. Chang, F.; Patel, T.; Schulz, M. E. The "rising tide" of dementia in Canada: what does it mean for pharmacists and the people they care for? *Can. Pharm. J. (Ott)* **2015**, *148*, 193-199.

2. World Health Organization dementia. *https://www.who.int/news-room/fact-sheets/detail/dementia#:~:text=Currently%20more%20than%2055%20million,injuries%20that%20affect%20the%20brain.* (accessed February 02, 2023).

3. Alzheimer's Disease International world Alzheimer report 2013. *https://www.alzint.org/u/WorldAlzheimerReport2013.pdf*.

4. Guerreiro, R.; Bras, J. The age factor in Alzheimer's disease. *Genome Med.* **2015**, *7*, 106-5.

5. Jorm, A. F.; Jolley, D. The incidence of dementia: a meta-analysis. *Neurology* **1998**, *51*, 728-733.

6. Statistics Canada leading causes of death, total population, by age group. *https://www150.statcan.gc.ca/t1/tbl1/en/tv.action?pid=1310039401* (accessed February 01, 2023).

7. Alzheimer Society of Canada navigating the path forward for dementia in Canada: the landmark study report #1. *https://alzheimer.ca/en/research/reports-dementia/landmark-study-report-1-path-forward* (accessed February 01, 2023).

8. Arvanitakis, Z.; Shah, R. C.; Bennett, D. A. Diagnosis and management of dementia: review. *JAMA* **2019**, *322*, 1589-1599.

9. van Straaten, E. C. W.; Scheltens, P.; Barkhof, F. MRI and CT in the diagnosis of vascular dementia. *J. Neurol. Sci.* **2004**, *226*, 9-12.

10. Korczyn, A. D.; Vakhapova, V.; Grinberg, L. T. Vascular dementia. *J. Neurol. Sci.* **2012**, *322*, 2-10.

11. Sabbagh, M. N.; Lue, L.; Fayard, D.; Shi, J. Increasing precision of clinical diagnosis of Alzheimer's disease using a combined algorithm incorporating clinical and novel biomarker data. *Neurol. Ther.* **2017**, *6*, 83-95.

12. d'Abramo, C.; D'Adamio, L.; Giliberto, L. Significance of blood and cerebrospinal fluid biomarkers for Alzheimer's Disease: sensitivity, specificity and potential for clinical use. *J. Pers. Med.* **2020**, *10*, 116. doi: 10.3390/jpm10030116.

13. Shea, D.; Colasurdo, E.; Smith, A.; Paschall, C.; Jayadev, S.; Keene, C. D.; Galasko, D.; Ko, A.; Li, G.; Peskind, E.; Daggett, V. SOBA: Development and testing of a soluble oligomer binding assay for detection of amyloidogenic toxic oligomers. *Proc. Natl. Acad. Sci. U. S. A.* **2022**, *119*, e2213157119.

14. Breijyeh, Z.; Karaman, R. Comprehensive review on Alzheimer's disease: causes and treatment. *Molecules* **2020**, *25*, 5789. doi: 10.3390/molecules25245789.

15. Lee, V. M.; Goedert, M.; Trojanowski, J. Q. Neurodegenerative tauopathies. *Annu. Rev. Neurosci.* **2001**, *24*, 1121-1159.

16. Ma, C.; Hong, F.; Yang, S. Amyloidosis in Alzheimer's disease: pathogeny, etiology, and related therapeutic directions. *Molecules* **2022**, *27*, 1210. doi: 10.3390/molecules27041210.

17. Chen, Z.; Huang, J.; Yang, S.; Hong, F. Role of cholinergic signaling in Alzheimer's disease. *Molecules* **2022**, *27*, 1816. doi: 10.3390/molecules27061816.

18. Ladner, C. J.; Lee, J. M. Pharmacological drug treatment of Alzheimer disease: the cholinergic hypothesis revisited. *J. Neuropathol. Exp. Neurol.* **1998**, *57*, 719-731.

19. Bartus, R. T. On neurodegenerative diseases, models, and treatment strategies: lessons learned and lessons forgotten a generation following the cholinergic hypothesis. *Exp. Neurol.* **2000**, *163*, 495-529.

20. Bartus, R. T.; Dean, R. L. 3.; Beer, B.; Lippa, A. S. The cholinergic hypothesis of geriatric memory dysfunction. *Science* **1982**, *217*, 408-414.

21. Anand, P.; Singh, B. A review on cholinesterase inhibitors for Alzheimer's disease. *Arch. Pharm. Res.* **2013**, *36*, 375-399.

22. Mesulam, M.; Guillozet, A.; Shaw, P.; Levey, A.; Duysen, E. G.; Lockridge, O. Acetylcholinesterase knockouts establish central cholinergic pathways and can use butyrylcholinesterase to hydrolyze acetylcholine. *Neuroscience* **2002**, *110*, 627-639.

23. Government of Canada dementia: symptoms and treatment. *https://www.canada.ca/en/public-health/services/diseases/dementia/symptoms-treatment.html* (accessed February 03, 2023).

24. Danysz, W.; Parsons, C. G. The NMDA receptor antagonist memantine as a symptomatological and neuroprotective treatment for Alzheimer's disease: preclinical evidence. *Int. J. Geriatr. Psychiatry* **2003**, *18*, 23.

25. Matsunaga, S.; Kishi, T.; Iwata, N. Memantine monotherapy for Alzheimer's disease: a systematic review and meta-analysis. *PLoS One* **2015**, *10*, e0123289.

26. Yiannopoulou, K. G.; Papageorgiou, S. G. Current and future treatments in Alzheimer disease: An Update. *J. Cent. Nerv. Syst. Dis.* **2020**, *12*, 1179573520907397.

27. Shi, M.; Chu, F.; Zhu, F.; Zhu, J. Impact of anti-amyloid-β monoclonal antibodies on the pathology and clinical profile of Alzheimer's disease: a focus on aducanumab and lecanemab. *Front. Aging Neurosci.* **2022**, *14*, 870517.

28. Swanson, C. J.; Zhang, Y.; Dhadda, S.; Wang, J.; Kaplow, J.; Lai, R. Y. K.; Lannfelt, L.; Bradley, H.; Rabe, M.; Koyama, A.; Reyderman, L.; Berry, D. A.; Berry, S.; Gordon, R.; Kramer, L. D.; Cummings, J. L. A randomized, double-blind, phase 2b proof-of-concept clinical trial in early Alzheimer's disease with lecanemab, an anti-Aβ protofibril antibody. *Alzheimers Res. Ther.* **2021**, *13*, 80-8.

29. van Dyck, C. H.; Swanson, C. J.; Aisen, P.; Bateman, R. J.; Chen, C.; Gee, M.; Kanekiyo, M.; Li, D.; Reyderman, L.; Cohen, S.; Froelich, L.; Katayama, S.; Sabbagh, M.; Vellas, B.; Watson, D.; Dhadda, S.; Irizarry, M.; Kramer, L. D.; Iwatsubo, T. Lecanemab in early Alzheimer's disease. *N. Engl. J. Med.* **2023**, *388*, 9-21.

30. Vaz, M.; Silva, V.; Monteiro, C.; Silvestre, S. Role of aducanumab in the treatment of Alzheimer's disease: challenges and opportunities. *Clin. Interv. Aging* **2022**, *17*, 797-810.

31. Kuller, L. H.; Lopez, O. L. Engage and emerge: truth and consequences? *Alzheimers Dement.* **2021**, *17*, 692-695.

32. Liu, P.; Xie, Y.; Meng, X.; Kang, J. History and progress of hypotheses and clinical trials for Alzheimer's disease. *Signal. Transduct Target Ther.* **2019**, *4*, 29-8. eCollection 2019.

33. Du, X.; Wang, X.; Geng, M. Alzheimer's disease hypothesis and related therapies. *Transl. Neurodegener* **2018**, *7*, 2-y. eCollection 2018.

34. Kametani, F.; Hasegawa, M. Reconsideration of amyloid hypothesis and tau hypothesis in Alzheimer's disease. *Front. Neurosci.* **2018**, *12*, 25.

35. Morris, G. P.; Clark, I. A.; Vissel, B. Inconsistencies and controversies surrounding the amyloid hypothesis of Alzheimer's disease. *Acta Neuropathol. Commun.* **2014**, *2*, 135-5.

36. Hampel, H.; Hardy, J.; Blennow, K.; Chen, C.; Perry, G.; Kim, S. H.; Villemagne, V. L.; Aisen, P.; Vendruscolo, M.; Iwatsubo, T.; Masters, C. L.; Cho, M.; Lannfelt, L.; Cummings, J. L.; Vergallo, A. The amyloid-β pathway in Alzheimer's disease. *Mol. Psychiatry* **2021**, *26*, 5481-5503.

37. Hardy, J. A.; Higgins, G. A. Alzheimer's disease: the amyloid cascade hypothesis. *Science* **1992**, *256*, 184-185.

38. Selkoe, D. J.; Hardy, J. The amyloid hypothesis of Alzheimer's disease at 25 years. *EMBO Mol. Med.* **2016**, *8*, 595-608.

39. Chen, G.; Xu, T.; Yan, Y.; Zhou, Y.; Jiang, Y.; Melcher, K.; Xu, H. E. Amyloid beta: structure, biology and structure-based therapeutic development. *Acta Pharmacol. Sin.* **2017**, *38*, 1205-1235.

40. Nalivaeva, N. N.; Turner, A. J. The amyloid precursor protein: a biochemical enigma in brain development, function and disease. *FEBS Lett.* **2013**, *587*, 2046-2054.

41. Priller, C.; Bauer, T.; Mitteregger, G.; Krebs, B.; Kretzschmar, H. A.; Herms, J. Synapse formation and function is modulated by the amyloid precursor protein. *J. Neurosci.* **2006**, *26*, 7212-7221.

42. Nunan, J.; Small, D. H. Regulation of APP cleavage by alpha-, beta- and gamma-secretases. *FEBS Lett.* **2000**, *483*, 6-10.

43. de Paula, V. d. J. R.; Guimarães, F. M.; Diniz, B. S.; Forlenza, O. V. Neurobiological pathways to Alzheimer's disease: amyloid-beta, tau protein or both? *Dement. Neuropsychol.* **2009**, *3*, 188-194.

44. Chow, V. W.; Mattson, M. P.; Wong, P. C.; Gleichmann, M. An overview of APP processing enzymes and products. *Neuromolecular Med.* **2010**, *12*, 1-12.

45. Tcw, J.; Goate, A. M. Genetics of β-amyloid precursor protein in Alzheimer's disease. *Cold Spring Harb Perspect. Med.* **2017**, *7*, a024539. doi: 10.1101/cshperspect.a024539.

46. Rumble, B.; Retallack, R.; Hilbich, C.; Simms, G.; Multhaup, G.; Martins, R.; Hockey, A.; Montgomery, P.; Beyreuther, K.; Masters, C. L. Amyloid A4 protein and its precursor in Down's syndrome and Alzheimer's disease. *N. Engl. J. Med.* **1989**, *320*, 1446-1452.

47. Moussa-Pacha, N. M.; Abdin, S. M.; Omar, H. A.; Alniss, H.; Al-Tel, T. H. BACE1 inhibitors: current status and future directions in treating Alzheimer's disease. *Med. Res. Rev.* **2020**, *40*, 339-384.

48. Cai, Z.; Liu, N.; Wang, C.; Qin, B.; Zhou, Y.; Xiao, M.; Chang, L.; Yan, L.; Zhao, B. Role of RAGE in Alzheimer's disease. *Cell. Mol. Neurobiol.* **2016**, *36*, 483-495.

49. Kanekiyo, T.; Bu, G. The low-density lipoprotein receptor-related protein 1 and amyloid-β clearance in Alzheimer's disease. *Front. Aging Neurosci.* **2014**, *6*, 93.

50. Yan, S. D.; Bierhaus, A.; Nawroth, P. P.; Stern, D. M. RAGE and Alzheimer's disease: a progression factor for amyloid-beta-induced cellular perturbation? *J. Alzheimers Dis.* **2009**, *16*, 833-843.

51. Storck, S. E.; Pietrzik, C. U. Endothelial LRP1 - a potential target for the treatment of Alzheimer's disease. *Pharm. Res.* **2017**, *34*, 2637-2651.

52. Greenwald, J.; Riek, R. Biology of amyloid: structure, function, and regulation. *Structure* **2010**, *18*, 1244-1260.

53. Chiti, F.; Dobson, C. M. Protein misfolding, functional amyloid, and human disease. *Annu. Rev. Biochem.* **2006**, *75*, 333-366.

54. Yoshiike, Y.; Minai, R.; Matsuo, Y.; Chen, Y.; Kimura, T.; Takashima, A. Amyloid oligomer conformation in a group of natively folded proteins. *PLoS One* **2008**, *3*, e3235.

55. Wang, R.; Sweeney, D.; Gandy, S. E.; Sisodia, S. S. The profile of soluble amyloid beta protein in cultured cell media. Detection and quantification of amyloid beta protein and variants by immunoprecipitation-mass spectrometry. *J. Biol. Chem.* **1996**, *271*, 31894-31902.

56. Sadigh-Eteghad, S.; Sabermarouf, B.; Majdi, A.; Talebi, M.; Farhoudi, M.; Mahmoudi, J. Amyloid-beta: a crucial factor in Alzheimer's disease. *Med. Princ Pract.* **2015**, *24*, 1-10.

57. Yu, H.; Wu, J. Amyloid-β: A double agent in Alzheimer's disease? *Biomed. Pharmacother.* **2021**, *139*, 111575.

58. Kumar, S.; Walter, J. Phosphorylation of amyloid beta (Aβ) peptides - a trigger for formation of toxic aggregates in Alzheimer's disease. *Aging.* **2011**, *3*, 803-812.

59. Daskalov, A.; El Mammeri, N.; Lends, A.; Shenoy, J.; Lamon, G.; Fichou, Y.; Saad, A.; Martinez, D.; Morvan, E.; Berbon, M.; Grélard, A.; Kauffmann, B.; Ferber, M.; Bardiaux, B.; Habenstein, B.; Saupe, S. J.; Loquet, A. Structures of pathological and functional amyloids and prions, a solid-state NMR perspective. *Front. Mol. Neurosci.* **2021**, *14*, 670513.

60. Gremer, L.; Schölzel, D.; Schenk, C.; Reinartz, E.; Labahn, J.; Ravelli, R. B. G.; Tusche, M.; Lopez-Iglesias, C.; Hoyer, W.; Heise, H.; Willbold, D.; Schröder, G. F. Fibril structure of amyloid-β(1-42) by cryo-electron microscopy. *Science* **2017**, *358*, 116-119.

61. Yang, Y.; Arseni, D.; Zhang, W.; Huang, M.; Lövestam, S.; Schweighauser, M.; Kotecha, A.; Murzin, A. G.; Peak-Chew, S. Y.; Macdonald, J.; Lavenir, I.; Garringer, H. J.; Gelpi, E.; Newell, K. L.; Kovacs, G. G.; Vidal, R.; Ghetti, B.; Ryskeldi-Falcon, B.; Scheres, S. H. W.; Goedert, M. Cryo-EM structures of amyloid-β 42 filaments from human brains. *Science* **2022**, *375*, 167-172.

62. Kulikova, A. A.; Makarov, A. A.; Kozin, S. A. The role of zinc ions and structural polymorphism of β-amyloid in the Alzheimer's disease initiation. *Mol. Biol. (Mosk)* **2015**, *49*, 249-263.

63. Jan, A.; Gokce, O.; Luthi-Carter, R.; Lashuel, H. A. The ratio of monomeric to aggregated forms of Abeta40 and Abeta42 is an important determinant of amyloid-beta aggregation, fibrillogenesis, and toxicity. *J. Biol. Chem.* **2008**, *283*, 28176-28189.

64. Harper, J. D.; Lansbury, P. T. J. Models of amyloid seeding in Alzheimer's disease and scrapie: mechanistic truths and physiological consequences of the time-dependent solubility of amyloid proteins. *Annu. Rev. Biochem.* **1997**, *66*, 385-407.

65. Ni, C.; Shi, H.; Yu, H.; Chang, Y.; Chen, Y. Folding stability of amyloid-beta 40 monomer is an important determinant of the nucleation kinetics in fibrillization. *FASEB J.* **2011**, *25*, 1390-1401.

66. Jarrett, J. T.; Lansbury, P. T. J. Seeding "one-dimensional crystallization" of amyloid: a pathogenic mechanism in Alzheimer's disease and scrapie? *Cell* **1993**, *73*, 1055-1058.

67. Huang, Y.; Liu, R. The toxicity and polymorphism of β-amyloid oligomers. *Int. J. Mol. Sci.* **2020**, *21*, 4477. doi: 10.3390/ijms21124477.

68. Prusiner, S. B. Cell biology. A unifying role for prions in neurodegenerative diseases. *Science* **2012**, *336*, 1511-1513.

69. Walsh, D. M.; Selkoe, D. J. Deciphering the molecular basis of memory failure in Alzheimer's disease. *Neuron* **2004**, *44*, 181-193.

70. Medeiros, R.; Baglietto-Vargas, D.; LaFerla, F. M. The role of tau in Alzheimer's disease and related disorders. *CNS Neurosci. Ther.* **2011**, *17*, 514-524.

71. Oddo, S.; Billings, L.; Kesslak, J. P.; Cribbs, D. H.; LaFerla, F. M. Abeta immunotherapy leads to clearance of early, but not late, hyperphosphorylated tau aggregates via the proteasome. *Neuron* **2004**, *43*, 321-332.

72. Götz, J.; Chen, F.; van Dorpe, J.; Nitsch, R. M. Formation of neurofibrillary tangles in P301l tau transgenic mice induced by Abeta 42 fibrils. *Science* **2001**, *293*, 1491-1495.

73. Bloom, G. S. Amyloid-β and tau: the trigger and bullet in Alzheimer disease pathogenesis. *JAMA Neurol.* **2014**, *71*, 505-508.

74. Doig, A. J. Positive feedback loops in Alzheimer's disease: the Alzheimer's feedback hypothesis. *J. Alzheimers Dis.* **2018**, *66*, 25-36.

75. Wang, Q.; Yu, X.; Li, L.; Zheng, J. Inhibition of amyloid-β aggregation in Alzheimer's disease. *Curr. Pharm. Des.* **2014**, *20*, 1223-1243.

76. Cline, E. N.; Bicca, M. A.; Viola, K. L.; Klein, W. L. The amyloid-β oligomer hypothesis: beginning of the third decade. *J. Alzheimers Dis.* **2018**, *64*, S567-S610.

77. Zhu, N.; Zhang, D.; Wang, W.; Li, X.; Yang, B.; Song, J.; Zhao, X.; Huang, B.; Shi, W.; Lu, R.; Niu, P.; Zhan, F.; Ma, X.; Wang, D.; Xu, W.; Wu, G.; Gao, G. F.; Tan, W. A novel coronavirus from patients with pneumonia in China, 2019. *N. Engl. J. Med.* **2020**, *382*, 727-733.

78. Tizaoui, K.; Zidi, I.; Lee, K. H.; Ghayda, R. A.; Hong, S. H.; Li, H.; Smith, L.; Koyanagi, A.; Jacob, L.; Kronbichler, A.; Shin, J. I. Update of the current knowledge on genetics, evolution, immunopathogenesis, and transmission for coronavirus disease 19 (COVID-19). *Int. J. Biol. Sci.* **2020**, *16*, 2906-2923.

79. Mehta, O. P.; Bhandari, P.; Raut, A.; Kacimi, S. E. O.; Huy, N. T. Coronavirus disease (COVID-19): comprehensive review of clinical presentation. *Front. Public. Health.* **2021**, *8*, 582932.

80. Ng, W. H.; Tipih, T.; Makoah, N. A.; Vermeulen, J.; Goedhals, D.; Sempa, J. B.; Burt, F. J.; Taylor, A.; Mahalingam, S. Comorbidities in SARS-CoV-2 patients: a systematic review and meta-analysis. *mBio* **2021**, *12*, e03647-20.

81. World Health Organization coronavirus (COVID-19) dashboard. *https://covid19.who.int/* (accessed January 03, 2023).

82. Government of Canada coronavirus disease (COVID-19). *https://www.canada.ca/en/public-health/services/diseases/coronavirus-disease-covid-19.html* (accessed January 03, 2023).

83. Woo, P. C. Y.; Huang, Y.; Lau, S. K. P.; Yuen, K. Coronavirus genomics and bioinformatics analysis. *Viruses* **2010**, *2*, 1804-1820.

84. Hassan, S. A.; Sheikh, F. N.; Jamal, S.; Ezeh, J. K.; Akhtar, A. Coronavirus (COVID-19): a review of clinical features, diagnosis, and treatment. *Cureus* **2020**, *12*, e7355.

85. Coronaviridae Study Group of the International Committee on Taxonomy of Viruses. The species severe acute respiratory syndrome-related coronavirus: classifying 2019-nCoV and naming it SARS-CoV-2. *Nat. Microbiol.* **2020**, *5*, 536-544.

86. Liu, D. X.; Liang, J. Q.; Fung, T. S. Human coronavirus-229E, -OC43, -NL63, and -HKU1 (Coronaviridae). *Encyclopedia of Virology* **2021**, 428-440.

87. Fehr, A. R.; Perlman, S. Coronaviruses: an overview of their replication and pathogenesis. *Methods Mol. Biol.* **2015**, *1282*, 1-23.

88. Wang, Q.; Ye, S.; Zhou, Z.; Li, J.; Lv, J.; Hu, B.; Yuan, S.; Qiu, Y.; Ge, X. Key mutations on spike protein altering ACE2 receptor utilization and potentially expanding host range of emerging SARS-CoV-2 variants. *J. Med. Virol.* **2023**, *95*, e28116.

89. Shang, J.; Wan, Y.; Luo, C.; Ye, G.; Geng, Q.; Auerbach, A.; Li, F. Cell entry mechanisms of SARS-CoV-2. *Proc. Natl. Acad. Sci. U. S. A.* **2020**, *117*, 11727-11734.

90. Ni, W.; Yang, X.; Yang, D.; Bao, J.; Li, R.; Xiao, Y.; Hou, C.; Wang, H.; Liu, J.; Yang, D.; Xu, Y.; Cao, Z.; Gao, Z. Role of angiotensin-converting enzyme 2 (ACE2) in COVID-19. *Crit. Care* **2020**, *24*, 422-0.

91. Li, F. Structure, function, and evolution of coronavirus spike proteins. *Annu. Rev. Virol.* **2016**, *3*, 237-261.

92. Huang, Y.; Yang, C.; Xu, X.; Xu, W.; Liu, S. Structural and functional properties of SARS-CoV-2 spike protein: potential antivirus drug development for COVID-19. *Acta Pharmacol. Sin.* **2020**, *41*, 1141-1149.

93. V'kovski, P.; Kratzel, A.; Steiner, S.; Stalder, H.; Thiel, V. Coronavirus biology and replication: implications for SARS-CoV-2. *Nat. Rev. Microbiol.* **2021**, *19*, 155-170.

94. Harrison, A. G.; Lin, T.; Wang, P. Mechanisms of SARS-CoV-2 transmission and pathogenesis. *Trends Immunol.* **2020**, *41*, 1100-1115.

95. Hoffmann, M.; Kleine-Weber, H.; Schroeder, S.; Krüger, N.; Herrler, T.; Erichsen, S.; Schiergens, T. S.; Herrler, G.; Wu, N.; Nitsche, A.; Müller, M. A.; Drosten, C.; Pöhlmann, S. SARS-CoV-2 cell entry depends on ACE2 and TMPRSS2 and is blocked by a clinically proven protease inhibitor. *Cell* **2020**, *181*, 271-280.e8.

96. Perlman, S.; Netland, J. Coronaviruses post-SARS: update on replication and pathogenesis. *Nat. Rev. Microbiol.* **2009**, *7*, 439-450.

97. Health Canada Drug and vaccine authorizations for COVID-19: List of authorized drugs, vaccines and expanded indications. *https://www.canada.ca/en/health-canada/services/drugs-health-products/covid19-industry/drugs-vaccines-treatments/authorization/list-drugs.html* (accessed March 01, 2023).

98. Mascellino, M. T.; Di Timoteo, F.; De Angelis, M.; Oliva, A. Overview of the main anti-SARS-CoV-2 vaccines: mechanism of action, efficacy and safety. *Infect. Drug Resist* **2021**, *14*, 3459-3476.

99. Government of Canada. COVID-19 vaccination in Canada. *https://health-infobase.canada.ca/covid-19/vaccination-coverage/* (accessed March 08, 2023).

100. Graña, C.; Ghosn, L.; Evrenoglou, T.; Jarde, A.; Minozzi, S.; Bergman, H.; Buckley, B. S.; Probyn, K.; Villanueva, G.; Henschke, N.; Bonnet, H.; Assi, R.; Menon, S.; Marti, M.; Devane, D.; Mallon, P.; Lelievre, J.; Askie, L. M.; Kredo, T.; Ferrand, G.; Davidson, M.; Riveros, C.; Tovey, D.; Meerpohl, J. J.; Grasselli, G.; Rada, G.; Hróbjartsson, A.; Ravaud, P.; Chaimani, A.; Boutron, I. Efficacy and safety of COVID-19 vaccines. *Cochrane Database Syst. Rev.* **2022**, *12*, CD015477.

101. Ssentongo, P.; Ssentongo, A. E.; Voleti, N.; Groff, D.; Sun, A.; Ba, D. M.; Nunez, J.; Parent, L. J.; Chinchilli, V. M.; Paules, C. I. SARS-CoV-2 vaccine effectiveness against infection, symptomatic and severe COVID-19: a systematic review and meta-analysis. *BMC Infect. Dis.* **2022**, *22*, 439-y.

102. Mengist, H. M.; Kombe Kombe, A. J.; Mekonnen, D.; Abebaw, A.; Getachew, M.; Jin, T. Mutations of SARS-CoV-2 spike protein: implications on immune evasion and vaccine-induced immunity. *Semin. Immunol.* **2021**, *55*, 101533.

103. Hacisuleyman, E.; Hale, C.; Saito, Y.; Blachere, N. E.; Bergh, M.; Conlon, E. G.; Schaefer-Babajew, D. J.; DaSilva, J.; Muecksch, F.; Gaebler, C.; Lifton, R.; Nussenzweig, M. C.;

Hatziioannou, T.; Bieniasz, P. D.; Darnell, R. B. Vaccine breakthrough infections with SARS-CoV-2 variants. *N. Engl. J. Med.* **2021**, *384*, 2212-2218.

104. Elena, S. F.; Sanjuán, R. Adaptive value of high mutation rates of RNA viruses: separating causes from consequences. *J. Virol.* **2005**, *79*, 11555-11558.

105. Focosi, D.; McConnell, S.; Casadevall, A.; Cappello, E.; Valdiserra, G.; Tuccori, M. Monoclonal antibody therapies against SARS-CoV-2. *Lancet Infect. Dis.* **2022**, *22*, e311-e326.

106. Cox, M.; Peacock, T. P.; Harvey, W. T.; Hughes, J.; Wright, D. W.; COVID-19 Genomics UK (COG-UK) Consortium; Willett, B. J.; Thomson, E.; Gupta, R. K.; Peacock, S. J.; Robertson, D. L.; Carabelli, A. M. SARS-CoV-2 variant evasion of monoclonal antibodies based on in vitro studies. *Nat. Rev. Microbiol.* **2023**, *21*, 112-124.

107. Rosas, I. O.; Bräu, N.; Waters, M.; Go, R. C.; Hunter, B. D.; Bhagani, S.; Skiest, D.; Aziz, M. S.; Cooper, N.; Douglas, I. S.; Savic, S.; Youngstein, T.; Del Sorbo, L.; Cubillo Gracian, A.; De La Zerda, D. J.; Ustianowski, A.; Bao, M.; Dimonaco, S.; Graham, E.; Matharu, B.; Spotswood, H.; Tsai, L.; Malhotra, A. Tocilizumab in hospitalized patients with severe COVID-19 pneumonia. *N. Engl. J. Med.* **2021**, *384*, 1503-1516.

108. Grundeis, F.; Ansems, K.; Dahms, K.; Thieme, V.; Metzendorf, M.; Skoetz, N.; Benstoem, C.; Mikolajewska, A.; Griesel, M.; Fichtner, F.; Stegemann, M. Remdesivir for the treatment of COVID-19. *Cochrane Database Syst. Rev.* **2023**, *1*, CD014962.

109. Government of Canada. Veklury - COVID-19. *https://covid-vaccine.canada.ca/info/veklury-en.html* (accessed March 07, 2023).

110. Hung, Y.; Lee, J.; Chiu, C.; Lee, C.; Tsai, P.; Hsu, I.; Ko, W. Oral nirmatrelvir/ritonavir therapy for COVID-19: the dawn in the dark? *Antibiotics (Basel)* **2022**, *11*, 220. doi: 10.3390/antibiotics11020220.

111. Hu, Q.; Xiong, Y.; Zhu, G.; Zhang, Y.; Zhang, Y.; Huang, P.; Ge, G. The SARS-CoV-2 main protease (M(pro)): structure, function, and emerging therapies for COVID-19. *MedComm (2020)* **2022**, *3*, e151.

112. Government of Canada. Paxlovid. *https://covid-vaccine.canada.ca/paxlovid/product-details* (accessed March 08, 2023).

113. Tay, M. Z.; Poh, C. M.; Rénia, L.; MacAry, P. A.; Ng, L. F. P. The trinity of COVID-19: immunity, inflammation and intervention. *Nat. Rev. Immunol.* **2020**, *20*, 363-374.

114. Hu, B.; Huang, S.; Yin, L. The cytokine storm and COVID-19. *J. Med. Virol.* **2021**, *93*, 250-256.

115. Huang, C.; Wang, Y.; Li, X.; Ren, L.; Zhao, J.; Hu, Y.; Zhang, L.; Fan, G.; Xu, J.; Gu, X.; Cheng, Z.; Yu, T.; Xia, J.; Wei, Y.; Wu, W.; Xie, X.; Yin, W.; Li, H.; Liu, M.; Xiao, Y.; Gao, H.; Guo, L.; Xie, J.; Wang, G.; Jiang, R.; Gao, Z.; Jin, Q.; Wang, J.; Cao, B. Clinical features of patients infected with 2019 novel coronavirus in Wuhan, China. *Lancet* **2020**, *395*, 497-506.

116. Gilyazova, I.; Timasheva, Y.; Karunas, A.; Kazantseva, A.; Sufianov, A.; Mashkin, A.; Korytina, G.; Wang, Y.; Gareev, I.; Khusnutdinova, E. COVID-19: Mechanisms, risk factors, genetics, non-coding RNAs and neurologic impairments. *Noncoding RNA Res.* **2023**, *8*, 240-254.

117. Huang, P.; Zhang, L.; Tan, Y.; Chen, S. Links between COVID-19 and Parkinson's disease/Alzheimer's disease: reciprocal impacts, medical care strategies and underlying mechanisms. *Transl. Neurodegener* **2023**, *12*, 5-1.

118. Atkins, J. L.; Masoli, J. A. H.; Delgado, J.; Pilling, L. C.; Kuo, C.; Kuchel, G. A.; Melzer, D. Preexisting comorbidities predicting COVID-19 and mortality in the UK biobank community cohort. *J. Gerontol. A Biol. Sci. Med. Sci.* **2020**, *75*, 2224-2230.

119. Yu, Y.; Travaglio, M.; Popovic, R.; Leal, N. S.; Martins, L. M. Alzheimer's and Parkinson's diseases predict different COVID-19 outcomes: a UK biobank study. *Geriatrics (Basel)* **2021**, *6*, 10. doi: 10.3390/geriatrics6010010.

120. Bianchetti, A.; Rozzini, R.; Guerini, F.; Boffelli, S.; Ranieri, P.; Minelli, G.; Bianchetti, L.; Trabucchi, M. Clinical presentation of COVID19 in dementia patients. *J. Nutr. Health Aging* **2020**, *24*, 560-562.

121. Haidar, M. A.; Shakkour, Z.; Reslan, M. A.; Al-Haj, N.; Chamoun, P.; Habashy, K.; Kaafarani, H.; Shahjouei, S.; Farran, S. H.; Shaito, A.; Saba, E. S.; Badran, B.; Sabra, M.; Kobeissy, F.; Bizri, M. SARS-CoV-2 involvement in central nervous system tissue damage. *Neural Regen. Res.* **2022**, *17*, 1228-1239.

122. Golzari-Sorkheh, M.; Weaver, D. F.; Reed, M. A. COVID-19 as a risk factor for Alzheimer's disease. *J. Alzheimers Dis.* **2023**, *91*, 1-23.

123. Wang, L.; Davis, P. B.; Volkow, N. D.; Berger, N. A.; Kaelber, D. C.; Xu, R. Association of COVID-19 with new-onset Alzheimer's disease. *J. Alzheimers Dis.* **2022**, *89*, 411-414.

124. Douaud, G.; Lee, S.; Alfaro-Almagro, F.; Arthofer, C.; Wang, C.; McCarthy, P.; Lange, F.; Andersson, J. L. R.; Griffanti, L.; Duff, E.; Jbabdi, S.; Taschler, B.; Keating, P.; Winkler, A. M.; Collins, R.; Matthews, P. M.; Allen, N.; Miller, K. L.; Nichols, T. E.; Smith, S. M. SARS-CoV-2 is associated with changes in brain structure in UK Biobank. *Nature* **2022**, *604*, 697-707.

125. Ren, X.; Wen, W.; Fan, X.; Hou, W.; Su, B.; Cai, P.; Li, J.; Liu, Y.; Tang, F.; Zhang, F.; Yang, Y.; He, J.; Ma, W.; He, J.; Wang, P.; Cao, Q.; Chen, F.; Chen, Y.; Cheng, X.; Deng, G.; Deng, X.; Ding, W.; Feng, Y.; Gan, R.; Guo, C.; Guo, W.; He, S.; Jiang, C.; Liang, J.; Li, Y.; Lin, J.; Ling, Y.; Liu, H.; Liu, J.; Liu, N.; Liu, S.; Luo, M.; Ma, Q.; Song, Q.; Sun, W.; Wang, G.; Wang, F.; Wang, Y.; Wen, X.; Wu, Q.; Xu, G.; Xie, X.; Xiong, X.; Xing, X.; Xu, H.; Yin, C.; Yu, D.; Yu, K.; Yuan, J.; Zhang, B.; Zhang, P.; Zhang, T.; Zhao, J.; Zhao, P.; Zhou, J.; Zhou, W.; Zhong, S.; Zhong, X.; Zhang, S.; Zhu, L.; Zhu, P.; Zou, B.; Zou, J.; Zuo, Z.; Bai, F.; Huang, X.; Zhou, P.; Jiang, Q.; Huang, Z.; Bei, J.; Wei, L.; Bian, X.; Liu, X.; Cheng, T.; Li, X.; Zhao, P.; Wang, F.; Wang, H.; Su, B.; Zhang, Z.; Qu, K.; Wang, X.; Chen, J.; Jin, R.; Zhang, Z. COVID-19 immune features revealed by a large-scale single-cell transcriptome atlas. *Cell* **2021**, *184*, 1895-1913.e19.

126. Decourt, B.; D'Souza, G. X.; Shi, J.; Ritter, A.; Suazo, J.; Sabbagh, M. N. The cause of Alzheimer's disease: the theory of multipathology convergence to chronic neuronal stress. *Aging Dis.* **2022**, *13*, 37-60.

127. Kinney, J. W.; Bemiller, S. M.; Murtishaw, A. S.; Leisgang, A. M.; Salazar, A. M.; Lamb, B. T. Inflammation as a central mechanism in Alzheimer's disease. *Alzheimers Dement. (N. Y)* **2018**, *4*, 575-590.

128. Mukerji, S. S.; Solomon, I. H. What can we learn from brain autopsies in COVID-19? *Neurosci. Lett.* **2021**, *742*, 135528.

129. Ding, Q.; Shults, N. V.; Gychka, S. G.; Harris, B. T.; Suzuki, Y. J. Protein expression of angiotensin-converting enzyme 2 (ACE2) is upregulated in brains with Alzheimer's disease. *Int. J. Mol. Sci.* **2021**, *22*, 1687. doi: 10.3390/ijms22041687.

130. Hsu, J. T.; Tien, C.; Yu, G.; Shen, S.; Lee, Y.; Hsu, P.; Wang, Y.; Chao, P.; Tsay, H.; Shie, F. The effects of Aβ(1-42) finding to the SARS-CoV-2 spike protein S1 subunit and angiotensin-converting enzyme 2. *Int. J. Mol. Sci.* **2021**, *22*, 8226. doi: 10.3390/ijms22158226.

131. Awogbindin, I. O.; Ben-Azu, B.; Olusola, B. A.; Akinluyi, E. T.; Adeniyi, P. A.; Di Paolo, T.; Tremblay, M. Microglial implications in SARS-CoV-2 infection and COVID-19: Lessons from viral RNA neurotropism and possible relevance to Parkinson's disease. *Front. Cell. Neurosci.* **2021**, *15*, 670298.

132. Kim, S. Y.; Buckwalter, M.; Soreq, H.; Vezzani, A.; Kaufer, D. Blood-brain barrier dysfunction-induced inflammatory signaling in brain pathology and epileptogenesis. *Epilepsia* **2012**, *53 Suppl 6*, 37-44.

133. Matias-Guiu, J. A.; Delgado-Alonso, C.; Yus, M.; Polidura, C.; Gómez-Ruiz, N.; Valles-Salgado, M.; Ortega-Madueño, I.; Cabrera-Martín, M. N.; Matias-Guiu, J. "Brain fog" by COVID-19 or Alzheimer's disease? A case report. *Front. Psychol.* **2021**, *12*, 724022.

134. Chiricosta, L.; Gugliandolo, A.; Mazzon, E. SARS-CoV-2 exacerbates beta-amyloid neurotoxicity, inflammation and oxidative stress in Alzheimer's disease patients. *Int. J. Mol. Sci.* **2021**, *22*, 13603. doi: 10.3390/ijms222413603.

135. Charnley, M.; Islam, S.; Bindra, G. K.; Engwirda, J.; Ratcliffe, J.; Zhou, J.; Mezzenga, R.; Hulett, M. D.; Han, K.; Berryman, J. T.; Reynolds, N. P. Neurotoxic amyloidogenic peptides in the proteome of SARS-COV2: potential implications for neurological symptoms in COVID-19. *Nat. Commun.* **2022**, *13*, 3387-1.

136. Nyström, S.; Hammarström, P. Amyloidogenesis of SARS-CoV-2 spike protein. *J. Am. Chem. Soc.* **2022**, *144*, 8945-8950.

137. Michiels, E.; Rousseau, F.; Schymkowitz, J. Mechanisms and therapeutic potential of interactions between human amyloids and viruses. *Cell Mol. Life Sci.* **2021**, *78*, 2485-2501.

138. Tavassoly, O.; Safavi, F.; Tavassoly, I. Seeding brain protein aggregation by SARS-CoV-2 as a possible long-term complication of COVID-19 infection. *ACS Chem. Neurosci.* **2020**, *11*, 3704-3706.

139. Idrees, D.; Kumar, V. SARS-CoV-2 spike protein interactions with amyloidogenic proteins: potential clues to neurodegeneration. *Biochem. Biophys. Res. Commun.* **2021**, *554*, 94-98.

140. Simopoulos, A. P. The importance of the ratio of omega-6/omega-3 essential fatty acids. *Biomed. Pharmacother.* **2002**, *56*, 365-379.

141. Calder, P. C. Omega-3 fatty acids and inflammatory processes. *Nutrients* **2010**, *2*, 355-374.

142. Chapkin, R. S.; Kim, W.; Lupton, J. R.; McMurray, D. N. Dietary docosahexaenoic and eicosapentaenoic acid: emerging mediators of inflammation. *Prostaglandins Leukot. Essent. Fatty Acids* **2009**, *81*, 187-191.

143. Thomas, J.; Thomas, C. J.; Radcliffe, J.; Itsiopoulos, C. Omega-3 fatty acids in early prevention of inflammatory neurodegenerative disease: a focus on Alzheimer's disease. *Biomed. Res. Int.* **2015**, *2015*, 172801.

144. Canhada, S.; Castro, K.; Perry, I. S.; Luft, V. C. Omega-3 fatty acids' supplementation in Alzheimer's disease: a systematic review. *Nutr. Neurosci.* **2018**, *21*, 529-538.

145. Lopez, L. B.; Kritz-Silverstein, D.; Barrett Connor, E. High dietary and plasma levels of the omega-3 fatty acid docosahexaenoic acid are associated with decreased dementia risk: the Rancho Bernardo study. *J. Nutr. Health Aging* **2011**, *15*, 25-31.

146. Laitinen, M. H.; Ngandu, T.; Rovio, S.; Helkala, E.; Uusitalo, U.; Viitanen, M.; Nissinen, A.; Tuomilehto, J.; Soininen, H.; Kivipelto, M. Fat intake at midlife and risk of dementia and Alzheimer's disease: a population-based study. *Dement. Geriatr. Cogn. Disord.* **2006**, *22*, 99-107.

147. Passeri, E.; Elkhoury, K.; Morsink, M.; Broersen, K.; Linder, M.; Tamayol, A.; Malaplate, C.; Yen, F. T.; Arab-Tehrany, E. Alzheimer's disease: treatment strategies and their limitations. *Int. J. Mol. Sci.* **2022**, *23*, 13954. doi: 10.3390/ijms232213954.

148. Lucas, C.; Wong, P.; Klein, J.; Castro, T. B. R.; Silva, J.; Sundaram, M.; Ellingson, M. K.; Mao, T.; Oh, J. E.; Israelow, B.; Takahashi, T.; Tokuyama, M.; Lu, P.; Venkataraman, A.; Park, A.; Mohanty, S.; Wang, H.; Wyllie, A. L.; Vogels, C. B. F.; Earnest, R.; Lapidus, S.; Ott, I. M.; Moore, A. J.; Muenker, M. C.; Fournier, J. B.; Campbell, M.; Odio, C. D.; Casanovas-Massana, A.; Yale IMPACT Team; Herbst, R.; Shaw, A. C.; Medzhitov, R.; Schulz, W. L.; Grubaugh, N. D.; Dela Cruz, C.; Farhadian, S.; Ko, A. I.; Omer, S. B.; Iwasaki, A. Longitudinal analyses reveal immunological misfiring in severe COVID-19. *Nature* **2020**, *584*, 463-469.

149. Langlois, P. L.; D'Aragon, F.; Hardy, G.; Manzanares, W. Omega-3 polyunsaturated fatty acids in critically ill patients with acute respiratory distress syndrome: A systematic review and meta-analysis. *Nutrition* **2019**, *61*, 84-92.

150. Sedighiyan, M.; Abdollahi, H.; Karimi, E.; Badeli, M.; Erfanian, R.; Raeesi, S.; Hashemi, R.; Vahabi, Z.; Asanjarani, B.; Mansouri, F.; Abdolahi, M. Omega-3 polyunsaturated fatty acids supplementation improve clinical symptoms in patients with Covid-19: a randomised clinical trial. *Int. J. Clin. Pract.* **2021**, *75*, e14854.

151. Zsichla, L.; Müller, V. Risk Factors of Severe COVID-19: A review of host, viral and environmental factors. *Viruses* **2023**, *15*, 175. doi: 10.3390/v15010175.

152. Zapata B, R.; Müller, J. M.; Vásquez, J. E.; Ravera, F.; Lago, G.; Cañón, E.; Castañeda, D.; Pradenas, M.; Ramírez-Santana, M. Omega-3 index and clinical outcomes of severe COVID-19: preliminary results of a cross-sectional study. *Int. J. Environ. Res. Public. Health.* **2021**, *18*, 7722. doi: 10.3390/ijerph18157722.

153. Mazidimoradi, A.; Alemzadeh, E.; Alemzadeh, E.; Salehiniya, H. The effect of polyunsaturated fatty acids on the severity and mortality of COVID patients: a systematic review. *Life Sci.* **2022**, *299*, 120489.

154. Goc, A.; Niedzwiecki, A.; Rath, M. Polyunsaturated ω-3 fatty acids inhibit ACE2-controlled SARS-CoV-2 binding and cellular entry. *Sci. Rep.* **2021**, *11*, 5207-1.

155. Cole, G. M.; Frautschy, S. A. DHA may prevent age-related dementia. *J. Nutr.* **2010**, *140*, 869-874.

156. Xiao, M.; Xiang, W.; Chen, Y.; Peng, N.; Du, X.; Lu, S.; Zuo, Y.; Li, B.; Hu, Y.; Li, X. DHA ameliorates cognitive ability, reduces amyloid deposition, and nerve fiber production in Alzheimer's disease. *Front. Nutr.* **2022**, *9*, 852433.

157. Heath, R. J.; Wood, T. R. Why have the benefits of DHA not been borne out in the treatment and prevention of Alzheimer's disease? A narrative review focused on DHA metabolism and adipose tissue. *Int. J. Mol. Sci.* **2021**, *22*, 11826. doi: 10.3390/ijms222111826.

158. El Shatshat, A.; Pham, A. T.; Rao, P. P. N. Interactions of polyunsaturated fatty acids with amyloid peptides Aβ40 and Aβ42. *Arch. Biochem. Biophys.* **2019**, *663*, 34-43.

159. Pavan, B.; Dalpiaz, A.; Ciliberti, N.; Biondi, C.; Manfredini, S.; Vertuani, S. Progress in drug delivery to the central nervous system by the prodrug approach. *Molecules* **2008**, *13*, 1035-1065.

160. Ballatore, C.; Huryn, D. M.; Smith, A. B. 3. Carboxylic acid (bio)isosteres in drug design. *ChemMedChem* **2013**, *8*, 385-395.

161. Májer, F.; Sharma, R.; Mullins, C.; Keogh, L.; Phipps, S.; Duggan, S.; Kelleher, D.; Keely, S.; Long, A.; Radics, G.; Wang, J.; Gilmer, J. F. New highly toxic bile acids derived from deoxycholic acid, chenodeoxycholic acid and lithocholic acid. *Bioorg. Med. Chem.* **2014**, *22*, 256-268.

162. Xu, M.; Lee, W. S.; Kim, M. J.; Park, D.; Yu, H.; Tian, G.; Jeong, T.; Park, H. Acyl-CoA: cholesterol acyltransferase inhibitory activities of fatty acid amides isolated from Mylabris phalerate Pallas. *Bioorg. Med. Chem. Lett.* **2004**, *14*, 4277-4280.

163. Schöffmann, A.; Wimmer, L.; Goldmann, D.; Khom, S.; Hintersteiner, J.; Baburin, I.; Schwarz, T.; Hintersteininger, M.; Pakfeifer, P.; Oufir, M.; Hamburger, M.; Erker, T.; Ecker, G. F.; Mihovilovic, M. D.; Hering, S. Efficient modulation of γ-aminobutyric acid type A receptors by piperine derivatives. *J. Med. Chem.* **2014**, *57*, 5602-5619.

164. Mohamed, T.; Gujral, S. S.; Rao, P. P. N. Tau derived hexapeptide AcPHF6 promotes Beta-Amyloid (Aβ) fibrillogenesis. *ACS Chem. Neurosci.* **2018**, *9*, 773-782.

165. Xue, C.; Lin, T. Y.; Chang, D.; Guo, Z. Thioflavin T as an amyloid dye: fibril quantification, optimal concentration and effect on aggregation. *R. Soc. Open Sci.* **2017**, *4*, 160696.

166. Lipinski, C. A.; Lombardo, F.; Dominy, B. W.; Feeney, P. J. Experimental and computational approaches to estimate solubility and permeability in drug discovery and development settings. *Adv. Drug Deliv. Rev.* **2001**, *46*, 3-26.

167. Horsley, J. R.; Jovcevski, B.; Wegener, K. L.; Yu, J.; Pukala, T. L.; Abell, A. D. Rationally designed peptide-based inhibitor of Aβ42 fibril formation and toxicity: a potential therapeutic strategy for Alzheimer's disease. *Biochem. J.* **2020**, *477*, 2039-2054.

168. Colvin, M. T.; Silvers, R.; Ni, Q. Z.; Can, T. V.; Sergeyev, I.; Rosay, M.; Donovan, K. J.; Michael, B.; Wall, J.; Linse, S.; Griffin, R. G. Atomic resolution structure of monomorphic Aβ42 amyloid fibrils. *J. Am. Chem. Soc.* **2016**, *138*, 9663-9674.

169. Bitan, G.; Kirkitadze, M. D.; Lomakin, A.; Vollers, S. S.; Benedek, G. B.; Teplow, D. B. Amyloid beta -protein (Abeta) assembly: Abeta 40 and Abeta 42 oligomerize through distinct pathways. *Proc. Natl. Acad. Sci. U. S. A.* **2003**, *100*, 330-335.

170. Wolff, M.; Zhang-Haagen, B.; Decker, C.; Barz, B.; Schneider, M.; Biehl, R.; Radulescu, A.; Strodel, B.; Willbold, D.; Nagel-Steger, L. Aβ42 pentamers/hexamers are the smallest detectable oligomers in solution. *Sci. Rep.* **2017**, *7*, 2493-3.

171. Corpetti, C.; Del Re, A.; Seguella, L.; Palenca, I.; Rurgo, S.; De Conno, B.; Pesce, M.; Sarnelli, G.; Esposito, G. Cannabidiol inhibits SARS-Cov-2 spike (S) protein-induced

cytotoxicity and inflammation through a PPARγ-dependent TLR4/NLRP3/Caspase-1 signaling suppression in Caco-2 cell line. *Phytother. Res.* **2021**, *35*, 6893-6903.

Appendix

Representative ^{1}H NMR and LC-MS data for compounds **2a, 2b** and **3b.** Under LC-MS conditions, MeOH showed absorbance and its peaks were removed when processing data.

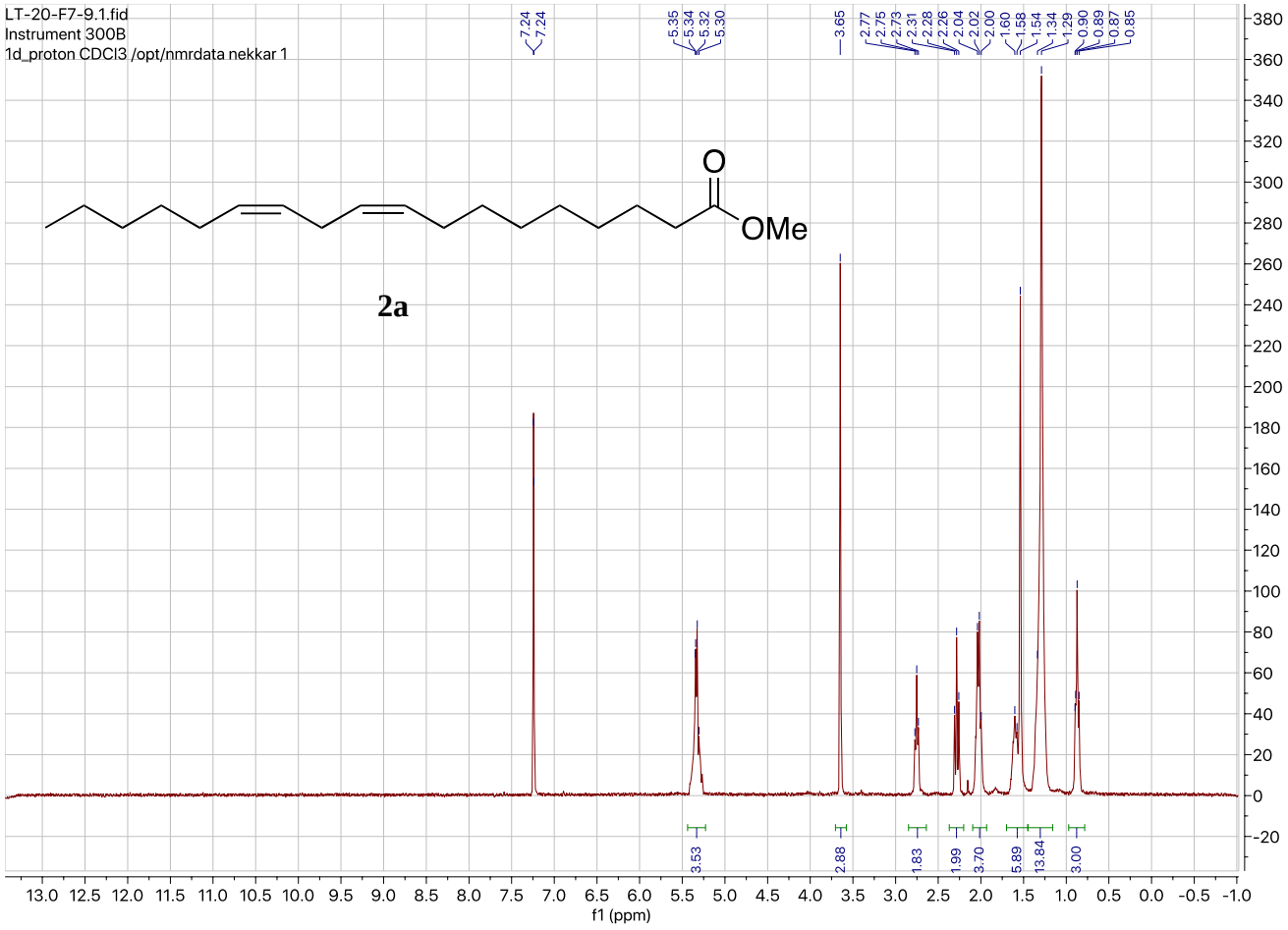

2a was not stable under LC-MS conditions.

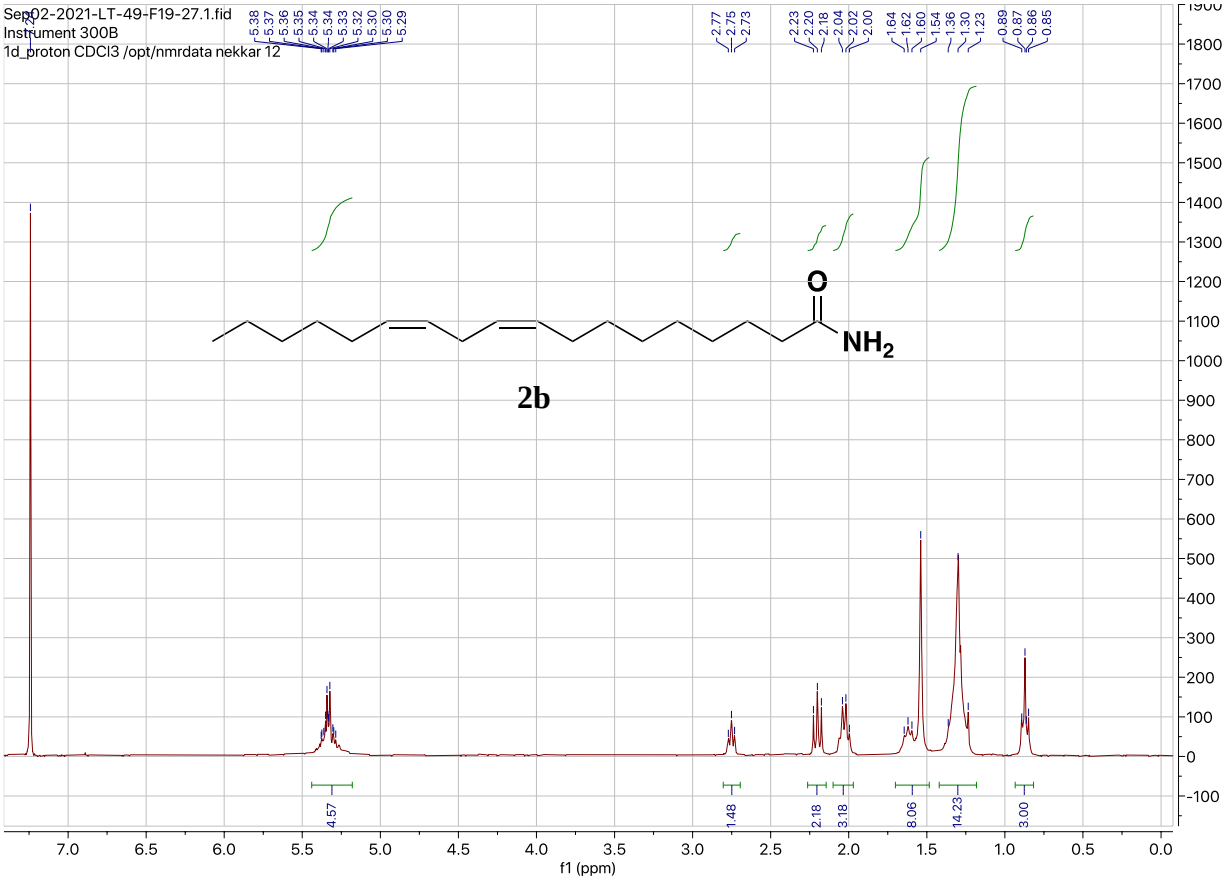

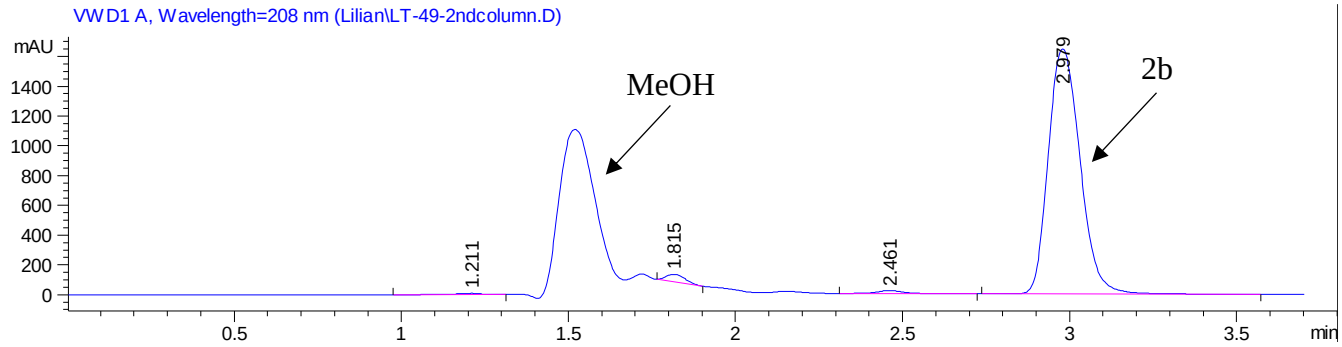

Signal 3: VWD1 A, Wavelength=208 nm

Peak #	RetTime [min]	Type	Width [min]	Area [mAU*s]	Height [mAU]	Area %
1	1.211	BB	0.0790	42.40064	7.72754	0.3767
2	1.815	BB	0.0658	204.80167	51.01274	1.8196
3	2.461	BB	0.0891	119.15310	20.12309	1.0586
4	2.979	BB	0.1052	1.08890e4	1646.37463	96.7451

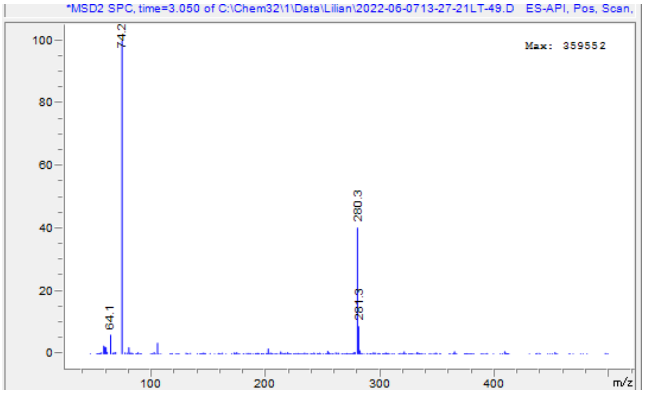

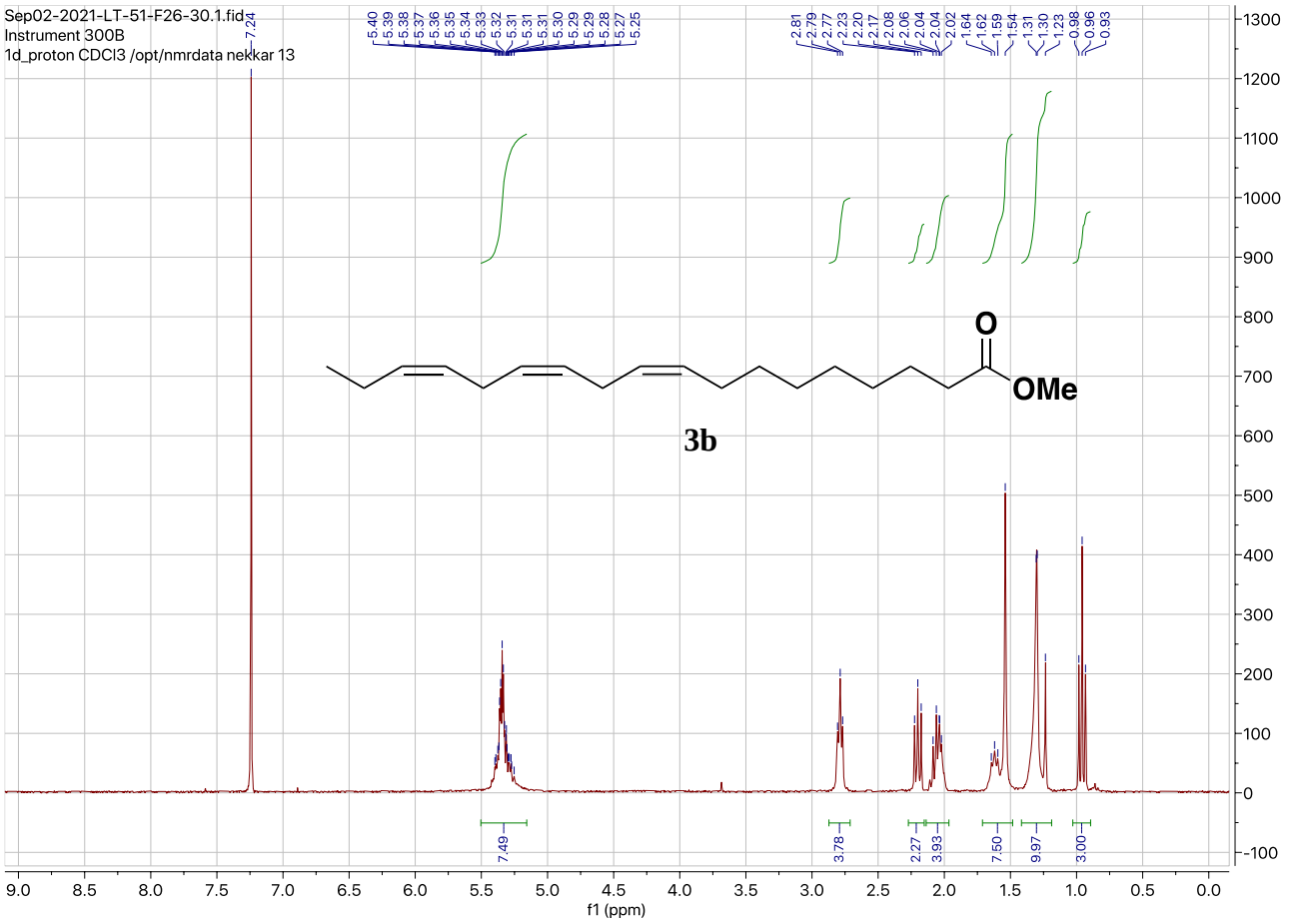

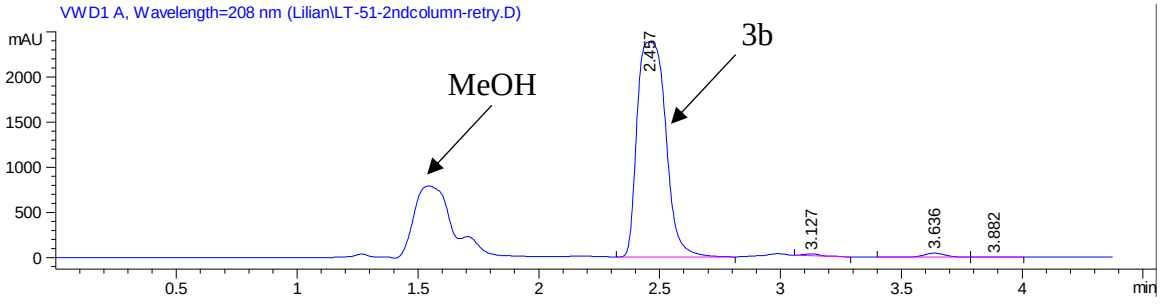

Signal 3: VWD1 A, Wavelength=208 nm

Peak #	RetTime [min]	Type	Width [min]	Area [mAU*s]	Height [mAU]	Area %
1	2.457	BB	0.1337	1.95128e4	2377.76587	98.0119
2	3.127	BB	0.0769	103.07410	20.42185	0.5177
3	3.636	BB	0.0956	272.67093	44.41516	1.3696
4	3.882	BB	0.0925	20.06251	3.46654	0.1008

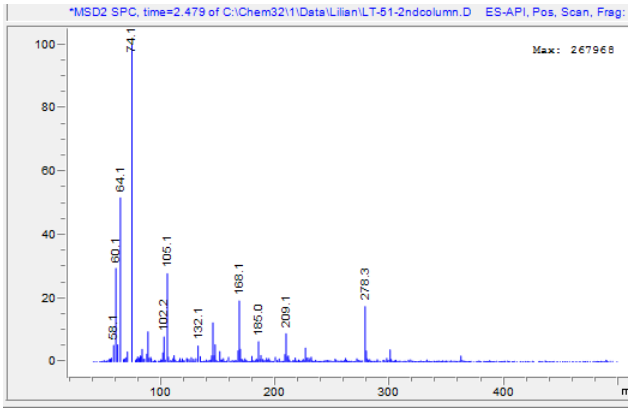

Table A: Calu-3 Cell Cytotoxicity Assay Data for Fatty Acids

Compound (25 uM)	% Cell Viability[a]
OA	100.8 ± 8.6
LNA	110.3 ± 5.8
ALA	102.3 ± 12.4
EPA	86.3 ± 15.0
DHA	94.1 ± 13.8
Quercetin	98.8 ± 16.9

[a]The percent cell viability values are based on the inhibition of absorbance values relative to untreated cells and expressed as the average ± the standard deviation of one experiment (n = 6). The values are obtained from CCK-8 assays on Calu-3 cells.

Table B: SARS-CoV-2 and ACE2 Binding Inhibition Assay Data for Fatty Acids

Compound (50 uM)	% Activity[a]
OA	112.0 ± 1.4
1a (R = OMe)	115.2 ± 14.0
1b (R = NH_2)	119.6 ± 1.4
1c (R = Piperidinyl)	121.4 ± 15.4
LNA	113.4 ± 8.3
2a (R = OMe)	113.4 ± 7.7
2b (R = NH_2)	114.4 ± 13.1
2c (R = Piperidinyl)	118.3 ± 20.5
ALA	108.5 ± 10.8
3a (R = OMe)	107.1 ± 8.0
3b (R = NH_2)	111.5 ± 6.5

[a]The percent activity values are based on the inhibition of absorbance values relative to a positive control and expressed as the average ± the standard deviation of three experiments (n = 6). The values are obtained from a SARS-CoV-2 inhibitor assay kit by Acrobio.